Wearable-based Human Activity Recognition: From a Healthcare Application to a Kinetic Energy Harvesting Approach

a dissertation presented by

José Elías Manjarrés Córdoba

presented in partial fulfillment for

the degree of Doctor in Electrical and Electronics Engineering

Advisor: Dr. Mauricio Pardo

Electrical and Electronics Engineering Department

Universidad del Norte

Barranquilla, Colombia

May, 2020

Wearable-based Human Activity Recognition: From a Healthcare Application to a Kinetic Energy Harvesting Approach

Dr. Mauricio Pardo, Advisor

Department of Electrical and Electronics Engineering

Universidad del Norte

Date Approved:

List of Publications

1. Manjarres, J.; Narvaez, P.; Gasser, K.; Percybrooks, W.; Pardo, M. Physical workload tracking using human activity recognition with wearable devices. Sensors (Switzerland) 2020, 20. **(Chapter 4)**

2. Narváez, P.; Manjarrés, J.; Percybrooks, W.; Pardo, M.; Calle, M. Assessing the Level of Physical Activity in the Workplace: A Case Study With Wearable Technology. Int. J. Interdiscip. Telecommun. Netw. 2019, 11, 44–56.

3. Manjarrés, J.; Russo, V.; Peñaranda, J.; Pardo, M. Human Activity and Heart Rate Monitoring System in a Mobile Platform. In Proceedings of the 2018 Congreso Internacional de Innovación y Tendencias en Ingenieria (CONIITI); 2018.

4. Manjarrés, J.; Dasuki, K.; Parody, H.; Gomez, O.; Pardo, M. Monitoring System for Kinetic Energy Harvesting in a Mobile Platform. In Proceedings of the 2019 IEEE International Symposium on Circuits and Systems (ISCAS); 2019.

5. Manjarres, J.; Pardo, M. An Energy Logger for Kinetic-Powered Wrist-Wearable Systems. Electronics 2020, 9, 487. **(Chapter 5)**

6. Manjarres, J.; Lan, G.; Gorlatova, M.; Pardo, M. Enhancing Kinetic Energy Harvesting-based Human Activity Recognition with Deep Learning and Data Augmentation. *Pending submission.* **(Chapter 6)**

Contents

List of Figures

List of Tables

Abstract

Wearable technology is changing society by becoming an essential component of daily life. Human activity recognition (HAR) is one of the most prominent research areas where wearable devices play a key role. HAR can achieve its biggest impact in e-health when it is combined with real-time tracking of physiological variables. The combination of these information sources enables inference of parameters of interest with applications in patient monitoring, remote therapy, occupational health, and similar fields that rely on in-situ observation of trackable variables.

The first major contribution to the field in this dissertation is a smart physical workload tracking system that combines wearable-based HAR and heart rate tracking. The proposed system employs a concept from ergonomics, the Frimat's method, to compute the physical workload from heart rate measurements within a specified time window. The HAR subsystem recognizes activities in real-time, providing in-situ information relating to the performed activity and its corresponding workload. The system is designed for cloud-powered operation, facilitating remote monitoring of workers by an occupational health expert. Tests with 20 subjects exhibit accuracies above 86% for the proposed real-time HAR system. Moreover, this dissertation includes a case of study where tracking of an individual over the course of 20 days corroborates the ability of the system to assess adaptation to an exercise routine.

On the other hand, one of the new visions of the Internet of Things (IoT) is the development of devices capable of harvesting energy from the environment. In the case of wearables, kinetic energy harvesting (KEH) technologies employed to power devices from human motion are gaining popularity. Nevertheless, there is uncertainty regarding the feasibility of using some KEH methods to obtain self-powered wearables. However, applications

utilizing KEH for both power and sensing purposes are growing, in particular for HAR. Despite the interest and usability, improvement in the classification accuracy of KEH-based HAR systems is needed to be competitive with conventional accelerometer-based HAR.

Hence, the second and third contributions of this dissertation point to KEH in wearable environments. The second contribution is an energy logger for wrist-worn systems, with the purpose of tracking energy generation in KEH systems during daily activities. Thus, it is possible to determine if the harvested energy is enough to power a conventional wearable device. The proposed system computes the harvested energy using the characteristics of the objective load, which in this case is a battery charger. I carried out experiments with multiple subjects to examine the generation capabilities of a commercial harvester under the conditions of human motion. This study provides insights of the performance and limitations of kinetic harvesters as battery chargers.

The third contribution is a KEH-based HAR system using deep learning, data augmentation and transfer learning to outperform existing classification approaches in the KEH domain. The proposed architecture comprises convolutional neural networks (CNN) and long short-term memory networks (LSTM), which has been demonstrated to outperform other architectures found in the literature. Since deep learning classifiers require large amounts of data, and KEH datasets are limited in size, this thesis also includes the proposal of three data augmentation methods to synthesize KEH signals simulating new users. Finally, transfer learning is employed to build a system that maintains performance independent of device location or the subject wearing the device.

Chapter 1

Introduction

Wearable technology has become a regular component of daily life through the popularity increasing of smartwatches/fitness trackers, smart clothes, smart glasses, among others [1]. The gap between traditional practices in medicine and contemporary options for remote patient monitoring is bridged by the adoption of wearable devices and the Internet of Things (IoT) [2]. Moreover, lifestyle changes have arisen from the impact of these devices in the technology market and in the behavior of modern society, due to the rapid decrease in the prices and the wide range of competitors developing novel wearables [3].

One of the most popular areas of wearable technology is Human Activity Recognition (HAR). A wearable-based HAR system comprises, at minimum, motion sensors and a processing unit; both components must comply with requirements of small size and low power consumption. With the first developments in the late 1990s [4], wearable-based HAR has been utilized in several scenarios including ambulatory patient monitoring [5], transportation mode detection [6], sports/fitness training [7], gaming [8], military training [9], among others.

In the area of e-health, HAR achieves high impact when it is combined with the monitoring of other physiological variables, such as the heart rate (HR) [10]. Real-time HAR and physiological tracking enable feedback and enhance the user experience in various healthcare applications [11]. Nevertheless, this potential is yet to be fully exploited. For example, studies like [12]–[14] exhibit systems that combine real-time HAR and HR tracking using on-body sensors and an integration device (commonly, a mobile phone)

to receive and display the sensors information; however, these studies stopped short of processing this information in a specific e-health problem or application. Hence, Chapter 4 helps to bridge that gap with studies combining HR tracking and HAR to compute the physical workload in real-time.

Physical workload is a key factor in ergonomics to determine the adequate length and number of breaks for a given job, helping to reduce work-related stress [15]. Thus, Chapter 4 presents the development of an automatic workload computation system, combining real-time HAR and HR tracking, and establishing a scalable framework for occupational health and for fitness-related applications. The system employs machine learning based on the motion sensor signals to determine the activity performed by a user; while simultaneously employing a concept from ergonomics, the Frimat's method, to compute the corresponding physical workload from measured HR values. Tests with 20 subjects indicate the reliability of the activity classifier, which maintains an accuracy up to 92% during real-time testing. Additionally, a case study with a single subject followed over twenty days with physical workload tracking, demonstrates the capability of the system to detect body adaptation to a custom exercise routine. The proposed system enables remote and multi-user workload monitoring, facilitating its use by experts in ergonomics and occupational health.

In addition to expanding applications for wearable-based HAR, there are challenges regarding the energy supply of wearable devices. There is a growing tendency in IoT to implement energy harvesting technologies to power small electronics systems with the conversion of light, heat and/or motion into electricity [16]. Given the exposure of wearables to human body movement, energy harvesting methods that leverage vibration and motion to generate energy, i.e., kinetic energy harvesting (KEH) schemes, are an attractive option to obtain power. KEH schemes comprise piezoelectric, electromagnetic, electrostatic and triboelectric technologies [17]–[20]; among these, piezoelectric harvesting (PEH) possesses potential for MEMS integration. This integration is suitable for small-size systems and is one of the preferred options to power wearable devices [21]. Chapter 5 contains an introduction to KEH, emphasizing on PEH.

Existing works of PEH in wearable environments are mostly focused in shoe-mounted systems, leveraging foot strikes to generate energy from the bending of piezoelectric

generators (PEG) located in the heel [22], [23]. There are other parts of the body that have been exploited for PEH such as the head [24], hip [25], elbow [26], knee [27] and wrist [28]. Nevertheless, PEH systems for these other body parts have stopped short of answering the question *"Is the harvested energy enough to build a self-powered wearable device?"* This issue is addressed in Chapter 5, emphasizing the use of commercial off-the-shelf (COTS) PEGs for experiment reproducibility.

Chapter 5 includes the assessment of a wrist-worn PEH system with a COTS PEG, to determine if the harvested energy from daily activities is sufficient to recharge the battery of a wearable HR tracker. Since PEGs are high impedance sources [29], they are expected to produce high voltages and small currents. As the authors of [30] state, PEGs typically display voltages in the order of tens of volts, while currents are in the order of microamperes. In consequence, the work developed in Chapter 5 presents a research contribution with the study of the input characteristics of the battery charger in a wearable device to estimate the voltage and current from the PEG. Additionally, this system includes a Bluetooth Low Energy (BLE) link to store data in a mobile device and release the limited memory of the wearable device from storage responsibilities. This study provides insights on the feasibility and limitations of using COTS PEGs to power wrist-worn wearables, which are common in the field of commercially available wearable devices.

Besides functioning as supplementary or primary energy sources, PEGs in wearable environments can also provide information about their context. In consequence, there is a growing interest in the literature surrounding KEH-based sensing, where kinetic harvesters are attached to different parts of the body to generate power for wearable devices and serve as sensors through their energy generation patterns [31]. The goal behind this idea is to reduce energy consumption of wearable systems by replacing sensors with energy harvesters as information sources to develop energy-efficient systems [32]. This tendency was initiated in [33] with the substitution of the accelerometer in a conventional HAR system with a COTS PEG showing the potential of using PEH to recognize activities and reduce the power requirements of the wearable device.

Nonetheless, the recognition accuracy gap between using accelerometry and KEH signals for HAR goes up to 37%, leaving room for significant improvement in KEH-based

HAR. This performance gap is due to the substantial differences between accelerometry and KEH signals. Human activities are characterized by signals with very low frequency components ($\geq$ 10 Hz) [34]. Accelerometers exhibit a low-frequency sensitivity that KEH signals do not have, due to the narrowband behavior in higher frequencies ($\geq$ 1 kHz) of PEGs [20], [29]. Therefore, KEH signals tend to be more noisy than the accelerometer output, which makes KEH-based HAR more challenging than conventional HAR.

KEH-based HAR systems in the literature rely on traditional machine learning approaches, mapping signals into representations based on a set of handcrafted features. This methodology limits the performance of classifiers, since the suitability of a feature set may change with scenarios, devices or datasets. On the other hand, artificial neural networks (ANN) offer automatic feature extraction with higher abstraction at the cost of more computational requirements and larger datasets [35]. ANN-based and different deep learning approaches have shown higher performance over traditional machine learning algorithms in several disciplines [36]. Consequently, a deep learning-based approach for KEH-based HAR is a promising alternative to enclose the gap with conventional HAR.

Thus, Chapter 6 shows the design and implementation of a deep learning architecture for KEH-based HAR that improves classification accuracy of traditional approaches by at least 17%. To supply the necessary amounts of data for the training of the ANN, three data augmentation methods for KEH signals are proposed. These methods take a pre-existing dataset and create synthetic data resembling new users performing the same activities from the dataset. In this study, the impact of these augmentation methods is assessed to show how they can create data that does not create additional confusion in the classification algorithm. Moreover, since KEH signals may change depending on the on-body location of the wearable device or on the subject that is wearing it, there are location-dependency and subject-dependency in KEH-based HAR. Hence, in the study described in Chapter 6, the employment of transfer learning to solve these issues is evaluated. In this case, the deep learning classifier is pre-trained with data from a location or a set of subjects; and then, the acquired knowledge is transferred to a new version of the architecture to classify data from the new location or subject, respectively. The combination of these transfer learning approaches with the proposed data augmentation methods provides an improvement on clas-

sification accuracy of up to 44% when the system is adapting to new locations or subjects.

To summarize, this dissertation begins addressing conventional wearable-based human activity recognition and presents a novel healthcare application, combining HAR and HR tracking. The research then focuses on the potential of kinetic energy harvesting to power wearable devices, by presenting a technical study using commercial harvesters as supplemental energy source for a wrist-worn wearable. Finally, the last set of experiments presented herein points to the challenges of using kinetic harvesters as sensors for HAR. Additionally, it describes a solution based on deep learning to improve classification performance compared to the existing approaches described in the literature.

The rest of this document is organized in the following manner. Chapter 2 contains the literature reviews regarding each research contributions of this thesis. Chapter 3 introduces human activity recognition with wearable devices, briefly explaining the basic components of a system in this area, and forming a preamble for Chapter 4. Chapter 4 exhibits the development of a solution for a specific healthcare application combining human activity recognition and heart rate tracking. Chapter 5 presents the fundamentals of kinetic energy harvesting and its role in wearable technology. Additionally, Chapter 5 shows the results of a study with a commercial harvester in a wearable environment, providing insights on the feasibility of obtaining self-powered systems from the selected harvester. Chapter 6 describes the design and development of a kinetic energy-based human activity recognition system using deep learning, data augmentation and transfer learning. Finally, Chapter 7 contains the conclusions and future work.

Chapter 2

Related Work

This chapter presents the literature review for each of the research problems addressed in this dissertation. Each section corresponds to the contributions mentioned in Chapter 1.

2.1 Physical Workload Computation

A common element among the physical effort assessment systems is HR tracking. HR has a well-known relationship with mental stress, as evidenced in [37]–[40]. The methods to obtain information about heart activity must be reliable and must allow their implementation using non-invasive devices to be relevant in practice. In [41], a comparison of HR signals coming from an ECG and a photoplethysmography (PPG) sensor establishes the reliability of PPG to obtain HR information. Additionally, the authors of [42] validate the use of a commercial HR monitor which employs PPG to track HR waveforms during rest. A similar conclusion is found in [43] with a smartwatch. This validation of PPG-based HR tracking has led to developments that seek to strengthen HR monitoring on environments where sensor signals can be corrupted by body movements [44]. Despite possible corruption, other systems have been built with PPG sensors under movement conditions and have not displayed performance issues [45]–[47]. Hence, the system in Chapter 4 also employs PPG-based HR tracking.

Several methods for continuous tracking of the physical effort can be found in the literature where qualitative data are not provided. For example, in [5], Jovanov et al. use a Wireless Body Area Network (WBAN) to monitor motion from an on-body accelerometer

and electrocardiography (ECG) sensors. This system tracks physical activity and health status with non-invasive technology. Other studies [48]–[51] propose manually-initiated recording of activities with data from HR trackers to measure the physical workload of a given population. Such methods are tested in [48]–[51] with salsa dancers, dockers, nurses and porters, respectively. In related studies, Jovanov et al. introduce real-time HR monitoring and step counting to track the work stress in nurses in [40].

The hybrid tracking of motion and physiological signals enhances the user experience in healthcare applications [11]. An automatic recognition of activities can help to relate HR levels to a particular task, allowing a deeper study of physical or mental performance in sports and occupational health. Thus, some studies have shown efforts to achieve this integration. For example, [12]–[14] present systems that combine HR tracking and online HAR using on-body sensors and an integration device to receive and display the sensors information. The integration device, typically a smartphone, can also take the place of a movement sensor [52]. Accordingly, [53]–[55] describe smartphone-based HAR systems along with corresponding challenges regarding feature extraction and selection. However, these systems are highly dependent on the on-body location of the smartphone. On the other hand, accelerometer-based HAR architectures present robust performance regardless of the sensor location and enable the system to distinguish among a wider range of activities compared to smartphone-based systems [12], [56]–[58].

The robustness and reliability of HAR with accelerometers are reflected in the variety of the e-health applications where it is applied. For example, [59] employs accelerometer-based HAR for posture recognition which helps to monitor falls in elderly people. Such approach is also present in [60]–[62], which demonstrates the popularity of this application. Moreover, some developments related to sports and fitness complemented with HAR are shown in [7], [10].

Thus, following the studies from [7], [10], [59]–[62], it can be concluded that accelerometer-based HAR is suitable as a key component for workload tracking. However, development of implementations that integrate HR and HAR tracking with qualitative workload assessments remains an open problem from an ergonomics point-of-view. Hence, Chapter 4 bridges that gap by employing the Frimat criteria in a system with online HAR and

HR tracking using wearable devices.

2.2 Piezoelectric Energy Harvesting in Wearable Devices

Several developments in literature show tests of PEGs in different body locations. Since the harvesting technology that leverages footsteps is very mature (see Section 5.4), only works for other parts of the body are considered. Moreover, the system presented in Section 5.5 refers to a wrist-worn piezoelectric harvester with a cantilevered configuration, whose harvesting mechanism differs from systems placed on shoes where energy is generated by pressure, not vibration. Hence, here I consider systems with vibration-induced energy harvesting. Additionally, it is of special interest to examine works with COTS generators because they keep focus on the system performance as well as I do in Chapter 5.

Authors of [63] introduce a novel curved piezoelectric structure and test it at a shoe and a wristwatch. Tests presented in [63] include a battery management circuit, and its voltage output shows the capabilities of the system to reach a charging voltage after 15 seconds of tapping on the structure. However, the fact of using a custom-made generator implies high costs and difficulties for reproducibility. A similar case is presented in [64] with a piezoelectric shell structure to scavenge energy from arm bending and stretching motions. Additionally, results in [64] are presented only in open circuit condition. Another structure for finger-motion kinetic harvesting is reported in [65], but this structure is tested only with resistive loads to characterize the voltage output. Same situation with harvesters for knees and head but with limited testing can be found in [66], [67] and [24], respectively. Instead, the work in Chapter 5 presents reproducible experiments due to the employment of COTS devices and the results are not attached to only one kind of activities as in [63], [64].

Other works do not propose structures but instead they show applications or studies using COTS PEGs. For example, [25] explores the average power generation using a COTS PEG module with a fixed resistive load and placing it in different parts of the body during walking, running and cycling. Authors also show the hypothetical additional time that a battery would last with the average power of each activity, while the battery

powers an activity tracker. On the other hand, the systems presented in [28], [68] employ commercially available PEGs to exploit the arm movements with wrist-worn harvesters and show their results by using a fixed resistive load without going further on the application of their devices. In the case of my study, the load is a battery charger to show the performance on a more realistic scenario. Considering an application, the work in [69] proposes a self-powered PEG-based activity tracker. Such system uses the charge in a capacitor to power a BLE beacon sender and then leverages the power of the transmitted signal to identify the activity being performed by the user. The harvester for this case is a hand-held box with a COTS PEG which has a fixed resistive load for harvesting power estimation; however, this hand-held device differs from the wearable set-up examined in Chapter 5, which changes the nature of induced vibrations on the PEG.

While systems with custom-made PEGs show promising harvesting results, the reproducibility of such systems is constrained by the technologies used in each case. In fact, the harvesting capabilities of COTS PEGs in a wearable environment are presented only with resistive loads, setting a challenge for other situations where the PEGs supply nonlinear loads. Hence, as can be noticed in cited literature, the scenario proposed in Chapter 5 where a COTS PEG is employed as battery charger and its performance is assessed in terms of transferred energy is still pending. Also, the details of the performance of the PEG with a nonlinear load, which are used here to estimate transferred power to the battery, constitute an approach that has not been presented in previous works.

2.3 KEH-based HAR

Chapter 6 is related to KEH-based context sensing and deep learning-based HAR. Literature of deep learning-based HAR provides several approaches for system design including handcrafted features and CNN, LSTM, and hybrids of CNN and LSTM. The combination of handcrafted statistical features and CNN is proposed by Ignatov in [70] to achieve real-time classification, ultimately in mobile devices; this approach outperforms traditional algorithms like Random Forest and k-Nearest Neighbors in the public UCI and WISDM datasets. The authors of [71] propose a HAR system where the signals from an accelerometer and a gyroscope are stacked to form *activity images*; then, the Discrete

Fourier Transform of these images is used for classification with a 2D-CNN architecture. Results with the UCI, USC and SHO datasets show superior performance compared to Support Vector Machines.

The work in [72] compares the performance of three popular deep learning architectures (Deep feed-forward networks, CNN and LSTM) with three public datasets (Opportunity, PAMAP2 and Daphnet Gait) to study the effect of hyperparameter values for each architecture. Results in [72] show how bi-directional LSTM outperforms other architectures in activities which exhibit short duration and sequences of ordered steps; while CNN are more suitable for repetitive and prolonged activities such as walking and running. The architecture introduced in [73] combines four convolutional layers with two recurrent LSTM layers and a dense layer to leverage the feature extraction from the CNN and the sequence interpretation from LSTM. Tests in [73] show how this architecture improves classification performance over CNN-only architectures with the Opportunity and Skoda public datasets.

Peng et al. propose an architecture where activities labeled as *simple* are classified with a CNN, and those labeled as *complex* are segmented into simpler activities and then classified with a CNN followed by a LSTM. Such architecture is tested with the Opportunity and the Ubicomp 08 datasets, showing higher classification accuracy than using CNN and LSTM independently and similar results to the architecture presented in [73]. In [74], Guan and Plötz propose an ensemble of LSTM to achieve a low bias (error between prediction and ground truth) and low variance (variability of predictions) classifier. Results on the Opportunity, Skoda and PAMAP2 datasets show how this proposal achieves higher accuracy than the works in [73] and [72].

Nevertheless, deep learning-based architectures in the literature require large datasets to avoid overfitting and have an effective learning process, and in some cases the dataset size is limited and obtaining more data is not feasible. Thus, some data augmentation methods have been proposed for accelerometer signals in [75] and for other types of time series in [76]. The work in [75] proposes several data augmentation methods for accelerometer signals in a dataset taken from users with Parkinson's disease; this dataset exhibits a limited amount of data. The results in [75] show how some of their methods can help to improve the performance of a CNN-based classifier, by increasing the training

dataset size. The authors of [76] propose a time warping method based on weighted averaging to augment datasets of time series. However, further study of the effectiveness of this method in [77] suggest that the improvements are significant in datasets with small training size (e.g. 16 and 57 in [77]), and can cause overfitting in some datasets, too.

Chapter 6 proposes a deep learning architecture for KEH-based HAR, aided by data augmentation methods designed for KEH signals, to increase the size of the training dataset and, hence, improve the generalization capabilities of the classifier.

Finally, transfer learning has been employed in the context of HAR with traditional machine learning algorithms [78], CNN [79] and CNN with LSTM [80], [81]. The work in [78] presents a *plug and learn* framework for multi-sensor scenarios, where a new sensor in a HAR system learns from the labels predicted by previously trained sensors. The approach in [78] is based on handcrafted features for classification. On the other hand, transfer learning with deep learning architectures is performed by training the ANN, and then retraining only a portion of the network by maintaining the weights (or "freezing") obtained in the first training process on the rest of the network.

The authors of [79] show results of this practice with a CNN, by maintaining the weights on the convolutional layers and retraining a dense layer to transfer knowledge across different users, sensors, and sensor placements. In [80], authors recall the architecture of four CNN, one LSTM and one fully connected (or dense) layer shown in [73] and display the results of transfer learning between users and between datasets using the Opportunity and Skoda datasets. The work in [80] presents two approaches for transfer learning: one freezing the outer convolutional layers and retraining the inner layer along with the LSTM and a dense layer, and other where only the LSTM and a dense are retrained; the first scenario exhibits better results than the second one. The approach presented in [81] includes an architecture with two CNN, one LSTM and two dense layers. In this case, the knowledge is transferred only by retraining the last dense layer, which is called an *adaptation layer*. The results in [81] comprise three public datasets where the knowledge is transferred across different sensor locations.

Although some of the cited approaches seek to build subject-independent or location-independent models, the application of transfer learning in Chapter 6 suits the context

of KEH-based sensing through feature learning transfer and data augmentation, which differs from the approaches using accelerometer data where augmentation is not required nor considered.

Chapter 3

Principles of Wearable-based Human Activity Recognition

HAR is the research area where the signals from sensors that track human body motion are processed with inference algorithms to determine the action performed by a subject [52]. This area has been gaining attention since the late 1990s in the field of computer vision [82] and pervasive computing [83]. However, approaches from computer vision are subject to privacy issues, due to the necessary video tracking in the application field, and require increased computation resources versus inertial sensor-based approaches [9]. Moreover, inertial sensors and microcontroller units (MCU) have rapidly become smaller, more powerful, and significantly more energy efficient, making them suitable for long-term functioning in battery-powered wearable systems. Hence, wearable-based HAR is now a strong pillar of Ubiquitous and Pervasive Computing, where the objective is to obtain context awareness from subject-specific information.

Additionally, developments in wearable-based HAR enabled the remote monitoring of patients in physical rehabilitation or the detection of abnormal activities in elder or mentally ill patients [84], [85]. Other applications for HAR systems include fitness tracking, entertainment, and military surveillance [10], [11], [86].

Following the models proposed by [9] and [57], let us consider the following components in wearable-based HAR system: sensors, activity data, preprocessing methods, feature extraction, and classification algorithm. The flow of these components to detect

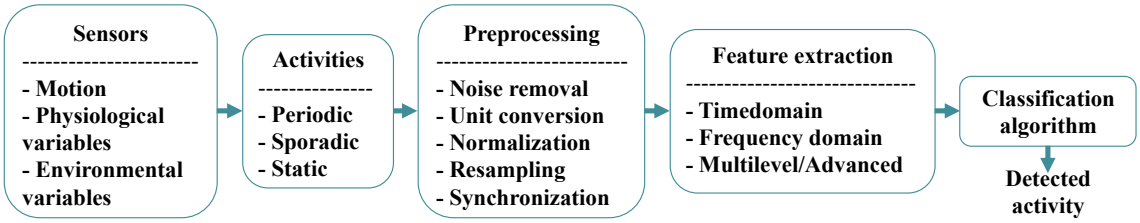

Figure 3.1: Basic components of a wearable-based human activity recognition system.

an activity is depicted in Figure 3.1.

Sensors for wearable-based HAR can measure motion (accelerometers and gyroscopes), physiological variables (heart rate, breathing rate, oxygen saturation in blood, skin temperature), and environment (location, light intensity, air pressure, sounds surrounding the subject) [9]. Motion sensors are the most common type and are present on a vast majority of HAR systems. Physiological sensors can be used to obtain complementary information in contexts such as physical rehabilitation, sports and military training. Finally, these systems can include environment descriptors through location tracking from a GPS (Global Positioning System) in addition to other sensors to determine if the activity is being performed outdoors or indoors.

The selected activities can be periodic, sporadic or static [57]. Periodic activities, as the name states, exhibit periodicity such as walking, running, biking, etc; and data can be divided using sliding windows for such activities. Sporadic are those activities that occur interspersed with other tasks, and are usually specific to applications like gaming or healthcare; in this case segmentation is crucial to isolate the data segments of interest. Static activities imply the detection of postures of specific body parts like the back or the arms; such detection requires careful segmentation to detect changes of posture.

Raw sensor data represented by time series are often noisy and can result in mistakes in the classification algorithms. Noise sources vary from motion distortion to sensor malfunction and electromagnetic interference [57]. Hence, the need for noise removal methods, such as filtering, is almost mandatory in this context. Moreover, other preprocessing schemes might include unit conversion, normalization, synchronization, and resampling [87]. However, the main goal is to preserve relevant information embedded in the signal characteristics [57].

The preprocessed sensor data, separated by observation windows (periodic activities) or by segments of interest (sporadic and static activities), must be encoded or transformed into a representation that eases discrimination for classifiers [9], [57].

Feature extraction has been traditionally carried out in a handcrafted approach, using feature engineering with three main categories: time domain, frequency domain, and multilevel or advanced feature extraction methods. Time domain features are mainly statistical signal-oriented parameters; these are the most popular in the literature due to their low computation requirements and high performance in different scenarios [57], [88]. Frequency domain analysis for feature extraction can be found using Fourier Transform [89] or Discrete Cosine Transform [90]; these methods are usually complemented with time domain features as well. Multilevel extraction methods are those where the data is first clustered, based on statistical characteristics, and then features are extracted per cluster [57]. Other advanced feature extraction methods include Principal Components Analysis, Linear Discriminant Analysis and Autoregressive Models [9].

These handcrafted feature extraction methods are necessary for traditional machine learning algorithms such as Decision Trees, k-Nearest Neighbors, Support Vector Machines, Naive Bayes, Markov Models, regression methods, ensemble methods (Random Forest, etc.), among others [9], [57], [91]–[94]. However, the performance of this combination of feature set and algorithms may depend highly on the subjects, dataset, device location or the selected activities; whenever a system of this kind is exposed to new conditions (e.g. subject, location, etc.), the classification accuracy may drop significantly due to the overfitting of the feature set to the original training dataset.

On the other hand, recent advances in mobile computing to increase the computation capacity of devices are encouraging the employment of artificial neural networks (ANN) and deep learning algorithms in wearable-based HAR systems [95]. Deep learning is an area of machine learning where the algorithms seek to discover representations of data, often at multiple levels, describing higher-level features in terms of lower-level features [96]. Hence, instead of obtaining handcrafted features as an input for the classifiers, deep learning allows an automatic inference of the characteristics that differentiate each class; this ability has helped deep learning classifiers to outperform traditional machine

learning algorithms [35]. The common deep learning architectures found in the literature for wearable-based HAR include, but are not limited to, Convolutional Neural Networks (CNN) [72], Long Short-term Memory Networks (LSTM) [74], Deep Belief Networks [97], Autoencoders [98], and hybrid architectures combining the aforementioned algorithms [99].

Despite the advantages of deep learning methods over traditional machine learning algorithms in terms of classification performance and feature extraction, a disadvantage is the execution time on mobile/wearable implementations [99]. This issue is an active research topic with several studies presenting advances towards a total adoption of some architectures in wearable-based HAR [70], [100]. Additionally, Chapter 6 revisits this issue, exploiting the capabilities of deep learning classifier for KEH-based HAR.

Next chapter shows a healthcare application for wearable-based HAR, where the concepts exposed in this chapter meet in a real-time HAR project. The system described in Chapter 4 shows how the fusion of HAR and physiological tracking enhances user experience in an e-health application.

Chapter 4

A Human Activity Recognition Application for e-Health

According to the World Health Organization (WHO), the amount of workload can be a hazard at the workplace that leads to work-related stress [101]. Having too much or too little to do at work is often an indication of poor time management resulting in increased mental stress [101], [102]. Workload adjustment is a key consideration in ergonomics and occupational health, helping to determine the adequate length and number of rest breaks for a given job and reducing work-related mental stress [15], [103]. However, the amount of workload is not necessarily determined by the length of a particular task, but by the quantity of energy required to complete it, which can also be reflected in the HR [104].

In consequence, works like [104] describe the importance of HR tracking in physical workload assessment. The authors of [104] perform a comparison between using Absolute Cardiac Cost (ACC) and Relative Cardiac Cost (RCC) to evaluate physical workload based on HR values during resting periods between activities. Similarly, Solé proposes in [105] a standardization for workload values based on RCC using the Chamoux [106] and Frimat [107] criteria, where the numeric workload scores are mapped into categories going from extremely hard to very light. These criteria allow a qualitative assessment of workload using only HR measurements.

My work in [47] improves the method proposed in [48], [105] by developing a mobile application to compute the workload during each activity performed by janitorial staff

using HR tracking and the Frimat criteria [107]. In the case of [47] the system is manually initiated, as in [48]–[50], and allows only local monitoring, which requires the presence of an expert next to the worker. In most real-life scenarios, having an ergonomics expert continuously present in the workplace is unfeasible.

To improve the user experience with physical tracking systems, it is necessary to address the problem of workload assessment from a real-time perspective as suggested by [11], [40]. Therefore, HR tracking must be integrated with real-time HAR or online HAR (according to [9]) to achieve workload assessment without requiring manual intervention to indicate the start and end of an activity.

This chapter presents a solution which embraces wearable technology and machine learning algorithms to compute physical workload in real-time. The solution here presented combines HAR and HR tracking to achieve a workload assessment that is linked automatically with the performed activity. This system eliminates the need of an expert next to every single user that is being tracked, due to enabling of remote and multi-user monitoring.

4.1 System Components

4.1.1 Wearable Devices for Activity Recognition and Heart Rate Tracking

The hardware for HAR comprises an Ultra-Low Power (ULP) MCU with Bluetooth Low Energy (BLE) capability, an ULP MEMS-based accelerometer and a small Li-ion battery. The HAR hardware is displayed in Figure 4.1. The selected ULP MCU is the Lilypad Simblee; the advantages of this device include small footprint (50 mm diameter), embedded BLE radio and a battery charge controller. A 100 mAh Li-ion battery powers the Lilypad Simblee and can be recharged through a USB controller module [108]. This MCU samples the signal from a tri-axial accelerometer at a 20 Hz rate, as the minimum recommended in [9], [57]. The accelerometer selection also follows the hardware used in [12], which is the ADXL335. This sensor allows to obtain information from movement and inclination with a sampling frequency up to 50 Hz and an acceleration up to 2 g [10].

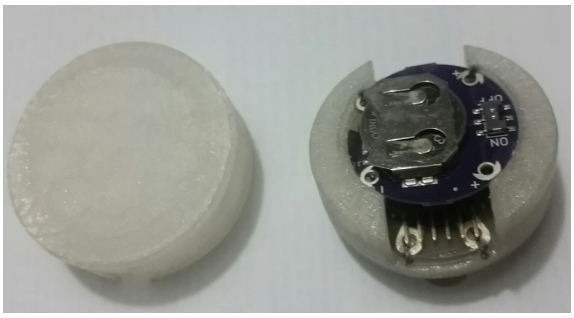

Figure 4.1: Human activity recognition hardware. The case allows the system to be worn on the hip

Figure 4.2: Microsoft Band used for heart rate tracking

For the HR tracking, a Microsoft Band (displayed in Figure 4.2) performs HR sampling with a built-in PPG sensor [109]. This wearable enables the tracking of other fitness-related variables such as sweating, arm movement, and step counting, among others [109]. This device has been validated by different authors for HR monitoring [110], [111]. For this project, only the HR sensor is required; and therefore, other sensors are deactivated to save energy. A specialized Software Development Kit (SDK) for Android devices permits the control of the Microsoft Band. This SDK can be found in [109].

4.1.2 Mobile Application

A mobile application is developed to connect automatically to both sensors and has two operating modes: Training mode and Testing mode.

In Training mode, the user interface (UI) asks for the activity that the user is going to perform from a list of predefined exercises (jogging, squatting, doing push-ups and doing crunches) and the average HR at rest to use it as a reference parameter for workload esti-

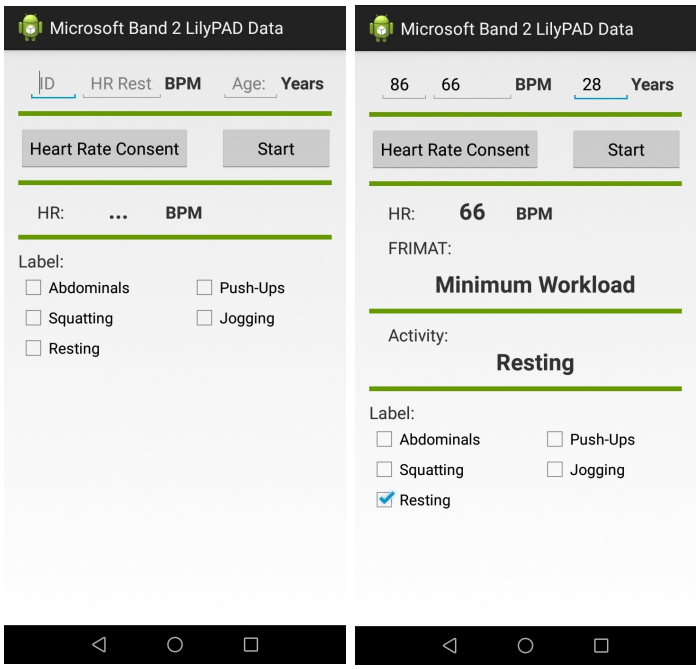

(a) Training mode (b) Testing mode

Figure 4.3: User interface of the mobile application for physical workload tracking.

mation. A 1-minute timer is used to standardize the length of the training sessions for later classification. The UI for this operation mode is displayed in Figure 4.3(a). The application stores the incoming data from both sensors in a JSON (JavaScript Object Notation) array, expecting to have 20 samples of each accelerometer axis, the average HR within one second and a label representing the activity. Every second, the JSON array containing the sensor samples is sent to a cloud server for storage in a database. After taking training samples from nine subjects, a Python script retrieves the stored data along with its corresponding activity labels and trains a classification model using the Scikit-learn library [112].

Once the classification model is validated (see Section 4.3.1), the mobile application can function in Testing mode. In this mode, the sampling process from the sensors remains the same as in Training mode; however, the UI does not have any time restriction. Therefore, a feature-computing function takes an array containing the samples from the tri-axial accelerometer. Then, the classification model detects the activity that is being performed. Finally, the detected activity and the average HR during the activity pass through a workload estimator. Figure 4.3(b) shows the UI for the Testing mode.

4.2 Physical Workload Computation

As [105] mentions, physical workload can be computed using metabolic consumption tables, oxygen consumption tables and HR measurements. However, HR measurements are the only non-invasive method which allows the integration of wearable technology. In the literature, there are two criteria to evaluate HR-based workload: Frimat's [107] and Chamoux's [106]. In one hand, the Frimat's criterion estimates workload on short work times or on specific activities; while, on the other hand, Chamoux criterion computes the workload of a full workday (at least 8 hours) [47]. In this case, the Frimat's criterion is chosen since the target comprises fitness-related activities.

The selected method requires the computation of some cardiac indicators. The first one is the Absolute Cardiac Cost (ACC) as defined by Equation 4.1:

$$ACC = HR_{activity} - HR_{rest}, \tag{4.1}$$

where $HR_{activity}$ refers to the average heart rate during the activity and HR_{rest} is the statistical mode of the HR values measured during resting periods. ACC allows the estimation of intensity for a given task. Another indicator, the Relative Cardiac Cost (RCC) is derived from the ACC as shown in Equation 4.2:

$$RCC = \frac{ACC}{HR_{\max} - HR_{rest}}; \tag{4.2}$$

RCC indicates the adaptation of the body to an activity.

In Equation 4.2, $HR_{\max}$ stands for the maximum achievable HR by a subject. The exact value of $HR_{\max}$ should be found in a stress test. However, [105] provides a theoretical definition which can have up to 5% of error compared to the actual value. Such definition for $HR_{\max}$ depends on the subject age as stated in Equation 4.3:

$$HR_{\max} = 220 - Age. \tag{4.3}$$

Frimat's criterion also needs the calculation of the cardiac acceleration (ΔHR) defined in Equation 4.4, and the mean heart rate ($\overline{HR}$) within an arbitrary time window:

$$\Delta HR = HR_{\max} - \overline{HR}. \tag{4.4}$$

Table 4.1: Relation between Frimat's Coefficients and cardiac indicators.

Frimat's	**Variable Ranges**				
Coeffs. Value	ACC **[bpm]**	RCC	$HR_{\max}$ **[bpm]**	$\overline{HR}$ **[bpm]**	ΔHR **[bpm]**
1	10 – 14	0.10 – 0.14	110 – 119	90 – 94	20 – 24
2	15 – 19	0.15 – 0.19	120 – 129	95 – 99	25 – 29
3	20 – 24	0.20 – 0.24	130 – 139	100 – 104	30 – 34
4	25 – 29	0.25 – 0.29	140 – 149	105 – 109	35 – 39
5	>30	>0.30	>150	>110	>40

Thus, once the five variables for Frimat's criterion (ACC, RCC, $HR_{\max}$, $\overline{HR}$ and ΔHR) are computed, each one of them is mapped into a corresponding Frimat's Coefficient which takes an integer value between 1 and 5. Table 4.1 details the relation between the values of each indicator and their respective Frimat's Coefficient.

Then, the method requires obtaining the Frimat's Coefficient from each input variable and adding them to obtain a Frimat's Score which ranges between 5 and 25. This score is the value that determines the level of physical workload of an activity. Following the ranking presented in [105], an activity can be ranked as shown in Table 4.2. During the implementation of the workload computation, the system takes previously measured the resting HR and compares it with the average HR within one-second time windows to compute the five cardiac indicators needed to obtain the Frimat's Score. This score is mapped to its corresponding category according to Table 4.2, accompanied with the classification of the most recent activity.

4.3 System Evaluation

4.3.1 Training and Validation of the Activity Classifier

Implementation of the online HAR subsystem requires three critical steps: data collection, training and validation. For the data collection, the activity set is a fitness routine which includes jogging, doing abdominal crunches, push-ups and squatting. These activities are among the most common exercises performed by the local population. As the workload

Table 4.2: Ranking of an activity according to its Frimat's score.

Frimat's score values	**Ranking**
25	Extremely hard
24	Very hard
22 – 23	Hard
20 – 21	Distressing
18 – 19	Bearable
14 – 17	Light
12 – 13	Very light
$\leq$10	Minimum workload

assessment tracks resting periods, standing still is also an activity taken into consideration. Additionally, to increase the system generalization capabilities, data collection must be performed from heterogeneous sources, i.e. subjects with different anatomic characteristics and different exercise styles.

Thus, nine volunteer subjects (6 men and 3 women) performed the aforementioned exercises for the same amount of time. Volunteer ages range between 19-32 years old. At least four hours before each exercise session, volunteers did not ingest substances that alter HR, such as: caffeine, alcohol, nicotine, etc. Five subjects exercise four times a week, while the other four subjects only exercise once per week. Data was collected from Monday to Friday in the evening (6 p.m. – 8 p.m.). Since exercises like push-ups and abdominal crunches are generally more physically demanding than jogging and squatting, the sessions of the experiments consists of one-minute part of exercise and three-minute part of resting. Hence, each volunteer performs at least four different sessions, one per exercise.

To avoid unexpected short pauses during the exercising part of each session, hydration needs of the subjects are attended to as required. These unexpected pauses would represent noise on the motion signals and can introduce undesired glitches in the training and validation datasets. Such glitches are unavoidable in practice, but to guarantee the correct labelling of data, subjects are asked to reduce the pauses during exercises. Hence, to overcome this issue, subjects with enhanced physical conditioning are asked

Table 4.3: Features considered for training the classifier.

Feature name	**Symbol per axis**	**Meaning**
Mean	$\bar{x}$, $\bar{y}$, $\bar{z}$	Statistical tendency of a group of samples from the same axis
Standard deviation	std(x), std(y), std(z)	Measure of variability of a group of samples from the same axis
Variance	var(x), var(y), var(z)	Measure of variability of the squares of a group of samples from their corresponding mean
Mean absolute deviation	MAD(x), MAD(y), MAD(z)	Measure of variability of a group of samples from their corresponding mean
Difference of means	$\bar{y}$-$\bar{z}$, $\bar{x}$-$\bar{y}$, $\bar{x}$-$\bar{z}$	Difference between means of two different axes

to participate in more than one experiment. By the end of collection, the dataset for training and validation contained over 118,000 three-dimensional samples taken at 20Hz from the hip-placed accelerometer.

Subsequently, the dataset is converted to a multidimensional space of features, which are summarized in Table 4.3 along with their corresponding symbol and meaning.

Each one of the 15 mentioned features must be computed from an observation window, forming a feature vector. The number of samples required to calculate a feature vector is directly related to the amount of time that the system takes to gather the samples. From the real-time implementation perspective, this time-window size is critical to determine the system latency. Hence, the selected time-window size is one second, considering

that the perception of activity changes for different users is not immediate. Thus, the minimum delay for the classifier to detect a change of activities is one second. Each feature vector is computed using 20 samples, due to the sensor 20 Hz sampling frequency, which is enough to cover the human motion signals bound to 10 Hz [34].

After setting the time-window size, the dataset is reduced to 5,900 feature vectors approximately, each one associated to their respective activity label. Next, classification algorithms to train with this dataset are needed. According to [9], [57], Random Forest and k-Nearest Neighbors (kNN) are the most common choices for online HAR applications, due to their reliability under several scenarios like the fitness activities. In this chapter, both algorithms are used to compare their performance and to select one for implementation.

Random Forest algorithm is an estimator that separates the training dataset into subsets for a custom number of decision trees. These trees decide over their respective samples; and then, the estimator averages their decisions. On the other hand, kNN algorithm maps the feature vectors into a multidimensional space and separates them according to their labels. Then, an incoming sample is compared to its closest training samples (or neighbors), determined by an internal distance measure, and the incoming sample is assigned to the class of most of its neighbors.

Collected data from the volunteers is separated by assigning 70% to a training subset and 30% for a validation subset, following a proper data randomization to avoid overfitting. Then, Random Forest estimators are trained varying the number of trees from 2 to 100, and kNN with number of neighbors from 2 to 50. These values are chosen as there is not significant improvement on overall accuracy by increasing the number of trees [113], and considering more neighbors may cause underfitting [114]; the performance stability on Random Forest is illustrated on Figure 4.6. The best results exhibit an overall accuracy of 97.7% for Random Forest with 63 trees and 95.2% for kNN with 5 neighbors. The normalized confusion matrices for both algorithms are displayed in Figure 4.4. These confusion matrices demonstrate the difference in overall accuracy by exhibiting less confusion in abdominal crunches, push-ups and squatting for the Random Forest algorithm compared to kNN. These results are obtained using the validation subset. Thus, subsequent optimization efforts are conducted towards RF.

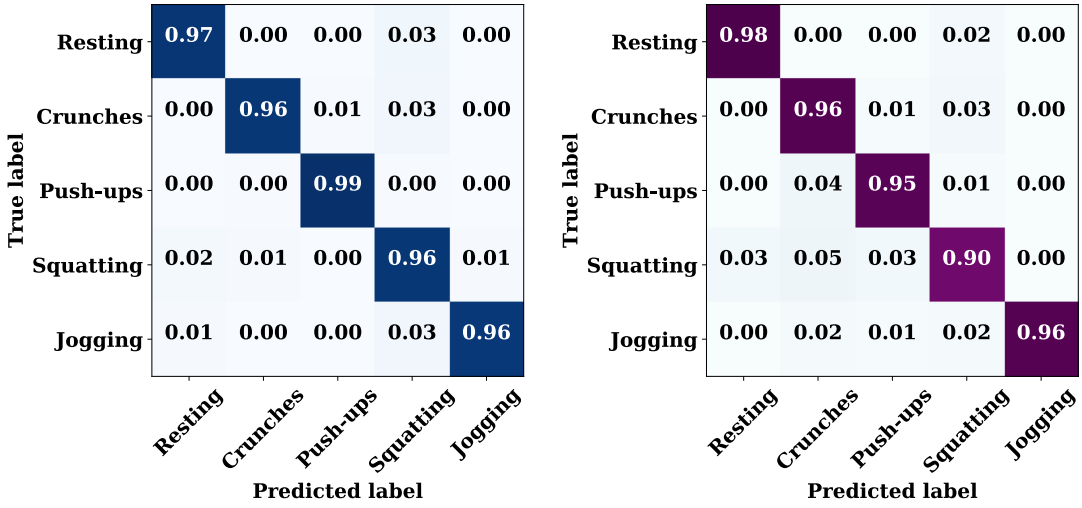

(a) Random Forest (b) kNN

Figure 4.4: Normalized confusion matrices from each classifier.

A classifier optimization process is required to reduce dimensionality and, in the case of RF, reduce the number of decision trees. After such process, validation of the optimized classifier should not show significant reduction in the performance metrics (overall accuracy and confusion matrix).

For dimensionality reduction, the level of importance that each feature has during training is analyzed. The importance levels considered here are equivalent to Gini importance, which is described in [115]. This importance is computed considering the decrease in average accuracy for the trained trees when a feature value is varied randomly. Thus, significant accuracy detriments point to the significant importance for a feature. In the case of Scikit-learn library, the feature importance levels are normalized. Figure 4.5 displays a bar graph of the feature importance. As observed, it is clear that $\bar{y}$, MAD(y), MAD(z) and $\bar{x}-\bar{y}$ are the features with the lower significance; and therefore, they are removed from the feature vectors. Even though further reduction in the number of features reduces the code size that will be embedded in the mobile application, extra reductions can also compromise the classifier performance. Thus, the new feature set comprises 11 features, which necessitates retraining the model with this new set.

Figure 4.6 shows the variation of classifier accuracy with respect to the number of trees, along with a dashed tendency line. According to the accuracy tendency line, after

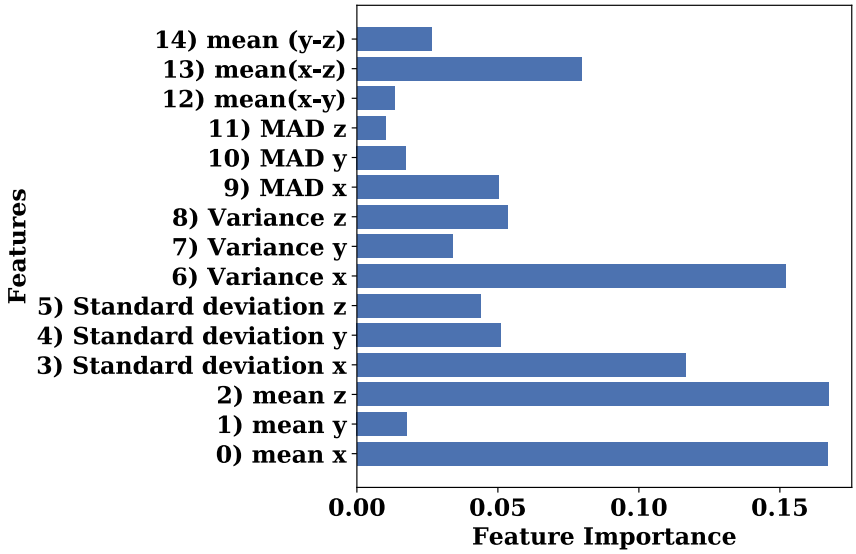

Figure 4.5: Bar graph of the importance of the features in Random Forest classifier.

20 trees, the classifier trends toward a stable behavior. Consequently, the number of trees can be reduced to a value above 20 trees without sacrificing performance. The overall accuracy with the validation subset changed from 97.7% with 63 trees to 97.5% with 24 trees, but results in a lower computational cost. Figure 4.7 shows the confusion matrix of this new model, where it can be observed that there is no performance compromise. Thus, this facilitates performing classification directly on the mobile application.

The resulting model is exported from Python to Java using the Porter tool described in [116] given the requirements of the Android environment. Thus, the model converted into a Java class contains the mathematical description of the 24 decision trees and computes the average decision among them to estimate the corresponding activity. The mobile application includes a testing mode where it reports the true label of the activity performed during the experiment and the labels detected by the model, along with a user identification number and the time stamps of the samples. Thus, this working mode is used for the remaining tests described below.

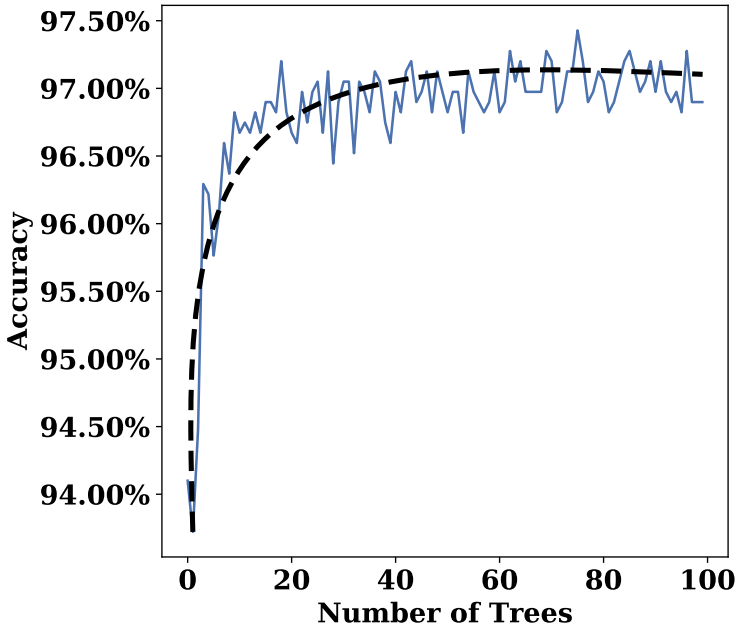

Figure 4.6: Variation of the overall accuracy with the number of trees in Random Forest classifier.

4.3.2 Online Human Activity Recognition Performance

Once the classifier model is embedded in the mobile application, the model is tested in a real-time environment. For the test, 20 people (different from the nine volunteers who participated in the training data collection) are asked to participate in a new set of experiments. This time, people register their age on the application along with the average heart rate obtained from the Microsoft Band after a preliminary 30-second resting period.

Then, they wear the HAR device on the hip and perform the following exercise routine: push-ups, resting, jogging, resting, squatting, resting, crunches, and resting. Each of these activities had a fixed duration of 30 seconds, which is set to limit physical demand and avoid unexpected resting moments. Planned, 30-second resting moments are situated between exercises to help subjects to fulfill the routine without extreme fatigue. Along with each routine, a researcher manipulates the application to set the activity label manually as the subjects shift from one activity to another. Meanwhile, the system reports to a cloud-stored database the labels obtained from the model, the labels entered manually, a system-custom user identification number and the time stamp.

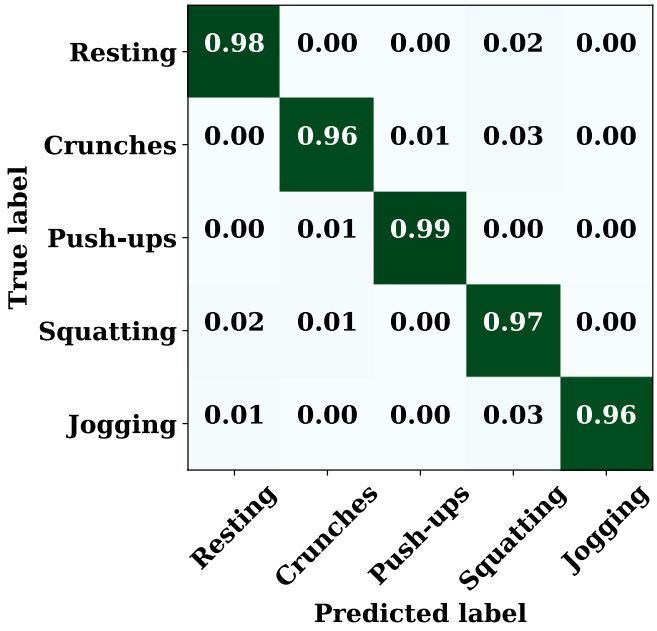

Figure 4.7: Confusion matrix of the optimized Random Forest classifier.

Table 4.4: Representative statistics of the online human activity recognition testing.

Statistical	**Accuracy percentages per activity**					
parameter	**Resting**	**Crunches**	**Push-ups**	**Squatting**	**Jogging**	**Overall**
Average	92.26%	86.11%	87.01%	86.71%	87.82%	89.53%
Standard deviation	3.34%	7.89%	4.90%	7.53%	6.47%	3.19%
Maximum	96.92%	100.00%	96.81%	98.76%	100.00%	95.13%
Minimum	84.22%	65.95%	75.24%	70.73%	76.96%	82.69%

After this data collection stage, the detected labels are compared against the manual labels to obtain the accuracy rate per activity and per user. Table 4.4 resumes the statistics of the accuracies from the testing stage. Also, Figure 4.8 shows the confusion matrix from online HAR testing. Although the validation accuracy is reported to be 97.5%, real-time tests have an average accuracy between 86% and 92% due to unexpected movements that induce noise in the classifier. Further details regarding the results of Table 4.4 and Figure 4.8 are given in the next section.

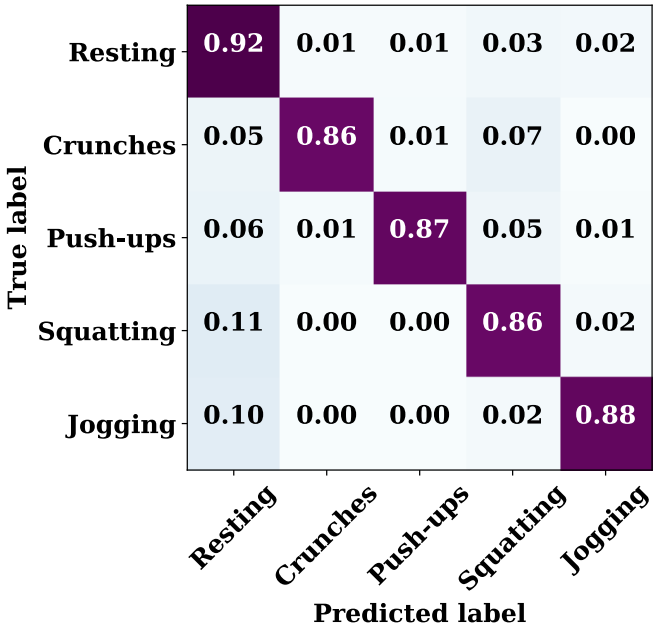

Figure 4.8: Confusion matrix from testing data.

4.3.3 Case Study: Physical Workload Evolution on an Individual

This second case study focuses on demonstrating the reliability of the workload estimator. A 27-year-old healthy male subject volunteers to participate in a twenty-day experiment. The subject performs the same exercise routine every day while its physical workload is tracked. The workload tracking is accompanied by activity recognition. Therefore, the subject must wear both devices (HAR and HR trackers) during each session. Figure 4.9 shows how the subject wears the devices and evinces that they do not represent major discomfort. Before the first session, a preliminary exercising round reveals that crunches do not represent significant physical effort for the subject. Thus, the routine for each day is defined as follows: 15 seconds of resting to find the reference HR for workload estimation, followed by 60 seconds of push-ups, 60 seconds of jogging, 60 seconds of squatting, and 60 seconds of resting. Then, the one-minute rounds are repeated three times.

The subject does not exercise regularly, which leads to the expectation of high levels of workload on the first session and a progressive decline on the physical exigency on successive sessions, as the body adjusts to the exercise routine. Additionally, the performance

Figure 4.9: Subject wearing the devices before exercising.

of the online HAR is expected to be steady along the sessions, since the system is used by the same person. Due to the methodology of workload estimation, several Frimat's scores can be obtained during a one-minute exercise round given the HR variations. However, the system maps each score to one of the eight categories, reducing information sensitivity. After each session, a Python script retrieves the classified activities, the true label of activities for HAR assessment and the workload categories for each activity. Subsequently, this script finds the statistical mode of the workload categories for an activity and sets it as the estimated physical workload.

Figure 4.10 displays the resulting mean HR for push-ups, squatting and jogging, during each daily session. Also, Figure 4.11 shows the Frimat's score values assessment during the resting rounds at the end of each session. These workload values reflect the overall perception of the body of the subject after each exercising round. Complementary, Figure 4.12 displays the online HAR performance for each session.

4.4 Discussion

This chapter introduces a system that combines real-time activity monitoring and physical workload estimation. This system enables remote tracking of workers in physically

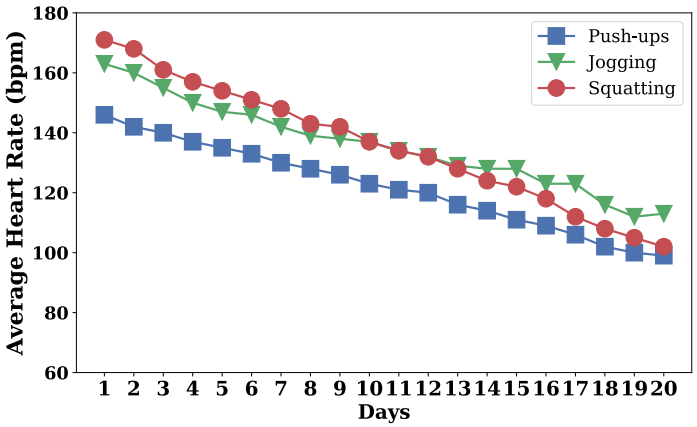

Figure 4.10: Mean heart rate results for an individual after 20 days with the same exercise routine.

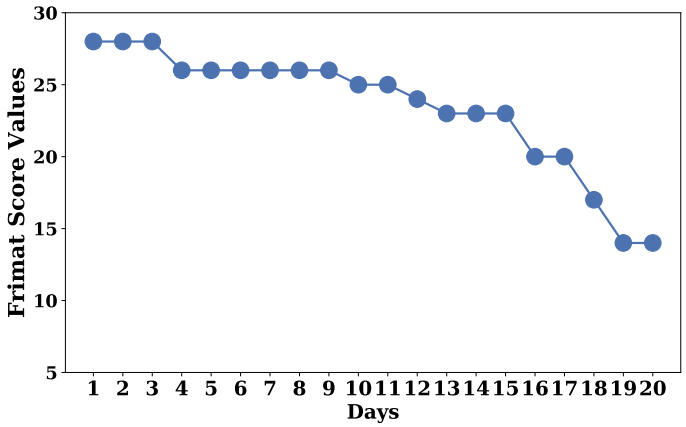

Figure 4.11: Physical workload assessment after each session.

demanding jobs for occupational health, and athletes for fitness purposes. For a comprehensive assessment of system performance, two case studies are presented. The first one embraces the training, validation and real-time testing with 20 subjects of the human activity recognition component. The second case presents the evolution of physical workload for an individual over twenty days.

The activity recognition validation accuracy stands above 95%, compared to previous studies which also employ wearable devices as shown in Table 4.5. Critical parameters regarding real-time implementation are considered for comparison such as number of sensors, number of activities and accuracy.

The comparison in Table 4.5 allows to locate the present study with an overall

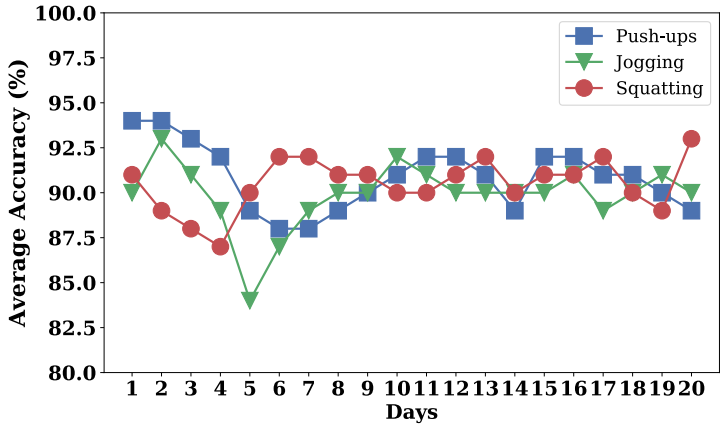

Figure 4.12: Average accuracies of online HAR for the second case study.

Table 4.5: Online HAR comparison with previous studies.

Article	No. Sensors	No. Activities	Test accuracy
[12]	1	10	98.7%
[13]	5	9	94.8%
[14]	1	5	95.7%
[53]	Smartphone	3	98.6%
[117]	1	9	94.8%
[118]	1	8	95%
This work	1	5	97.5%

accuracy that is only surpassed by a system that only considers three activities and by my work in [12]. However, the only work from Table 6 that displays results of real-time tests is [53]. There, tests are 10 seconds long, compared to the 30 seconds tests of this study. Also, [53] considers six test subjects, while this chapter considers twenty. Hence, such length and subject quantity difference can lead to errors in movement data, which makes the results shown in Figure 4.12 to stand more over related literature.

Additionally, Figures 4.12 and 4.8 evince the tendency of the system to keep a real-time accuracy above 85%. However, tests on the first case study are carried by people who do not know the system nor where intensively introduced to its use. Instead, the explanation of the experiment is held short, and they are asked to perform the exercises naturally.

Thus, there are some cases where the subjects take unexpected pauses or tremble during the exercise, introducing noise to the one-second observation windows and affecting overall accuracy. Nevertheless, by observing at the maximum values, there is also evidence of cases where classification of the embedded model shows no incorrect estimations.

On the other hand, the second case study helps to validate the reliability of the workload computation in real-time. This approach differs from other workload-related works like [48]–[51] where there is no real-time feedback. Instead, authors from [48]–[51] take activity and HR data manually and then compute the workload and categorize it. The proposed system does all this process automatically, facilitating the relationship between activity and physical effort which takes relevance at the application field. The subject considered for the twenty-day experiment of the second case study performed a physically demanding routine that is evaluated as extremely hard at the end of the first ten days, according to Frimat's criteria. However, a remarkable evolution in the perception of each activity by the subject is shown in Figure 4.10.

In the first sessions, the system evaluates that each type of exercise is extremely hard for the subject, obtaining an average HR of 150 bpm, then in the last session these activities are classified as a light workload, obtaining an average HR of 95 bpm. As expected, the first exercise of the routine (push-ups) displays the lowest workload amounts, since the body starts to adapt to the routine. But as the exercising round advances, the HR starts to increase which is reflected in higher workloads.

Another evidence of the assimilation of the exercising routine is the change from Frimat's scored values in the resting periods at the end of each session, as shown in Figure 4.11. Considering that the subject always performed the same exercise routine for twenty sessions (that is, there is no increase or variation in the load), a principle of adaptation is presented in the physical state of the subject [119]–[121]. As can be seen in Figures 4.10 and 4.11, at the beginning of the sessions, the physical capacity of the subject is not enough for the established load, but as the exercise sessions increased, the body managed to adapt to that load.

Furthermore, Figure 4.12 shows the performance stability of the online HAR component during the second case study. The accuracies stand around 90% for the three

activities, considering the fatigue effect on the subject movements. Also, it must be noticed that these experiments are longer than in the first case study and exhibited higher average accuracy; this is due to the lack of heterogeneity which leads the system to be exposed to more similar movements each session. Thus, these results confirm the reliability of the two system components for workload tracking purposes.

4.5 The Opportunity for Kinetic Harvesting in Wearable Technology

The wearables presented in this chapter rely on batteries as power supply. However, a growing tendency in the revolution of IoT suggests the use of energy harvesting technologies from human body to recharge or replace batteries.

The technologies with the greatest potential to harvest energy from human body are thermal and kinetic harvesting. Nevertheless, when harvesters are attached to the body, the kinetic generators have an advantage in terms of energy because thermal generators reduce their efficiency while human skin tries to reach thermal equilibrium with the environment [122]. Thus, kinetic harvesting technologies remain as an attractive option to power wearable devices. Among the kinetic harvesters, the literature highlights piezoelectric, electrostatic, electromagnetic and triboelectric technologies as the preferred methods. Next chapter introduces kinetic harvesting technologies, compares them, and shows a technical study of using piezoelectric harvesters to power a HR tracker.

Chapter 5

Piezoelectric Kinetic Energy Harvesting in Wearable Technology

5.1 Why Energy Harvesting for Wearables?

The growing demand for e-health and smart fashion has positioned wearable devices as a promising market for the near future with an expectation of $24bn by 2024 [123], [124]. However, wearable technologies face limited functionality due to battery lifetime and the need of battery recharging or replacing [21]. In response to this issue, energy harvesting schemes can be employed as alternative solutions by converting light, heat and/or motion into electricity [125], [16]. Moreover, the field of kinetic harvesting has shown relevant developments for the piezoelectric, electromagnetic, electrostatic and triboelectric technologies [17]–[20].

In this chapter, the principles of kinetic energy harvesting are briefly introduced. The focus is set on piezoelectric materials and the different scenarios where they have been used for kinetic energy harvesting. Finally, I introduce a technical study on the use of COTS PEGs to power wearable devices.

5.2 Principles of Kinetic Energy Harvesting

Energy harvesting (EH) refers to the process of exploiting different energy sources to obtain electricity, which is then stored and used as supply for electronic systems [29].

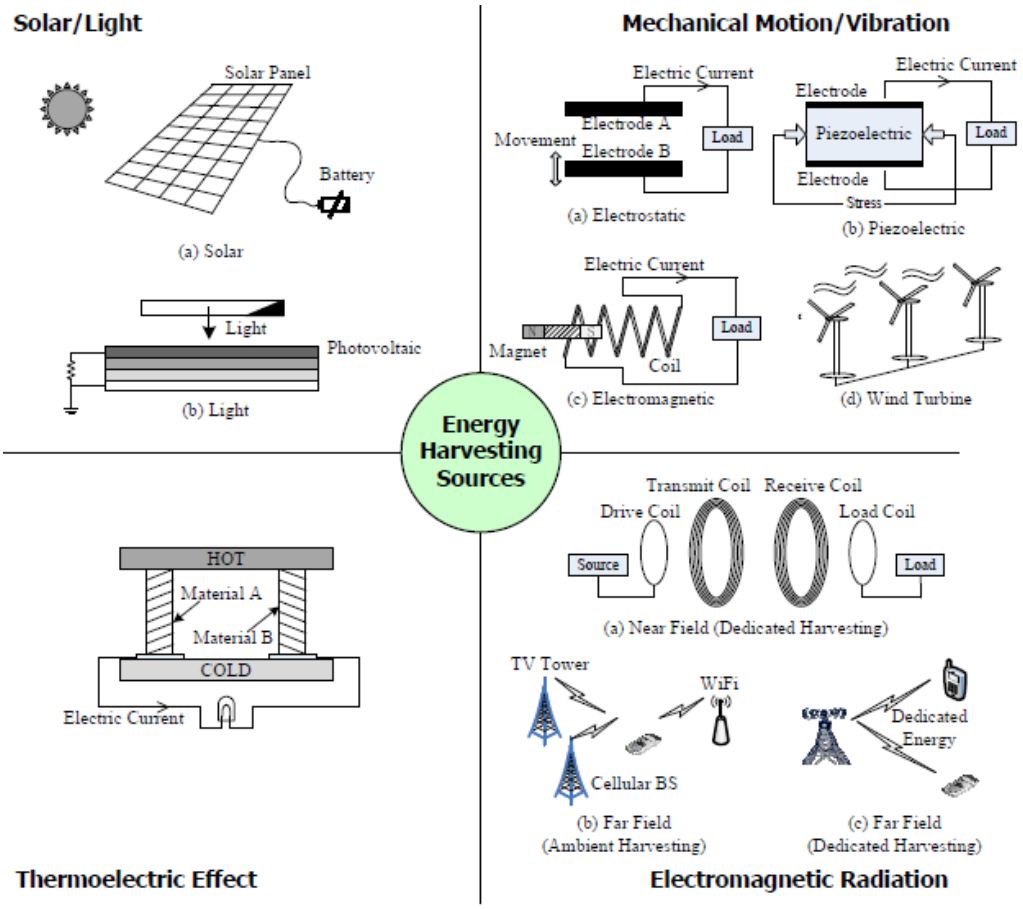

Figure 5.1: Classification of Energy Harvesting sources from [126].

The sources to exploit include solar or artificial light radiation, vibration/motion, heat, changes of temperature, and radio-frequency waves. Figure 5.1 resumes a well-known EH source classification from [126]. The four categories displayed in Figure 5.1 are light, mechanical motion/vibration, thermoelectric effect and electromagnetic radiation. The methods belonging to mechanical motion/vibration, with the exception of wind turbines, comprise KEH technologies.

KEH has attracted several researchers over the last couple of decades due to its potential to solve energy issues in fields like wireless sensor networks and wearable technology [127]. Thus, there have been successful implementations of KEH in commercial products such as the Seiko Kinetic Watch [128], whose method was later tested as energy source for pacemakers in [4] and [129], and for a wearable camera in [130].

In the field of wearable technology, piezoelectric generation and electromagnetic induction are the two most studied methods to be used as complementary energy sources

to batteries or even as battery replacement. The reason behind this interest is the compatibility of piezoelectric generators and coils with micro-electromechanical systems (MEMS), which means that these KEH technologies can be developed in a chip level, enabling their use in a wide range of wearable and implantable devices [68], [127], [131]. Although other methods such as electrostatic harvesting can be embedded into MEMS [17], they require external batteries for polarization and operation purposes, while piezoelectric and electromagnetic approaches can perform in a standalone fashion [29].

The power obtained from an electromagnetic induction harvester depends on the variation rate of the magnetic field from a magnet moving inside a coil [29]. Therefore, an electromagnetic kinetic harvester can be affected by the size of the magnet and by the speed of induced vibrations. The size issue is augmented when this technology is implemented in MEMS, since the magnet dimensions are highly restricted as well as its mobility, decreasing the achievable energy scavenging [132]. Moreover, considering the human body as vibration source, electromagnetic harvesting mechanisms may be constantly exposed to excitation levels that fall short on making the magnet to move fast enough across the coil, and hence, lead to poor harvesting performance [133].

On the other hand, PEGs do not suffer from performance detriments when implemented in MEMS, since they can be implemented with very thin films and conserve the mechanical properties that allow energy scavenging [132]. Also, the harvesting energy depends mostly on the mechanical characteristics of the materials, rather than vibration speed or magnitude [20], [133]. The major disadvantage of PEGs is the high output impedance due to the relatively high output voltage and low output current, which might represent an issue in energy transference to a load [132]. However, several works in the literature have shown significant advances to optimize the load coupling in PEG-based systems to mitigate this issue [134]. Hence, in this thesis, piezoelectric energy harvesting (PEH) is chosen as the KEH technology to study and implement in wearable devices for powering and sensing purposes.

5.3 Piezoelectric Energy Harvesting

The piezoelectric effect is a type mechanical-to-electrical energy conversion through the bending or stress of certain materials such as the Polyvinylidene Difluoride (PVDF)

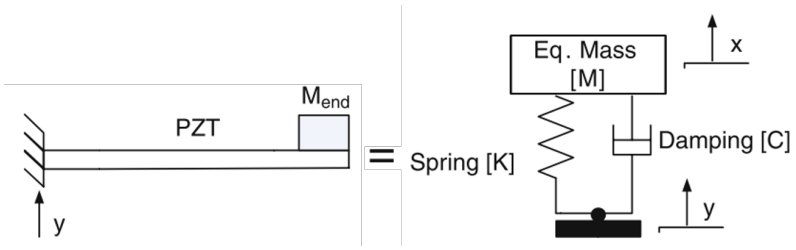

Figure 5.2: Mechanical representation of a cantilevered PEG [29].

and the Lead Zirconate Titanate (PZT-5H) [135]. A PEG is formed by one or more piezoceramic layers which are covered by plastic polymer and two electrodes.

Cantilevered structures are common for PEH in wearable set-ups, where the base is rigidly attached to the vibration source (e.g. human body) and a tip mass on the opposite end oscillates and bends the material to induce strain. Cantilevered PEGs can be modeled with the lumped spring mass representation of vibrating beams found in [136], which is later applied to PEGs in [29] as depicted in Figure 5.2. In this representation, the mass of the tip M_end and the PEG are added into an equivalent mass M, while the subtraction of system displacement x from vibration y is the mass displacement at the end of a spring with stiffness K and damping C.

After an extensive derivation from the model in Figure 5.2, which details can be found in [29], Equation 5.1 links output voltage and applied on a strain as

$$V = gE\varepsilon_{max}L_b, \tag{5.1}$$

where output voltage V depends on the piezoelectric constant g of the PEG, the elasticity modulus E of the cantilever material, the length L_b of the cantilever beam, and the strain ε that can be maximized to ε_{max} if the tip mass M_end is located at the free end of the cantilever beam.

Hence, when the PEG is exposed to dynamic strain, the piezoceramic layers generate an AC voltage output on the electrodes, which is directly proportional to the applied strain. For example, widely used materials such as the mentioned PVDF and PZT-5A exhibit piezoelectric constants around 340×10^{-3} Vm/N and 25×10^{-3} Vm/N, respectively, and can exhibit instantaneous voltage values up to 100V under strain levels which do not break the beam [29]. However, The AC voltage must be converted to DC for powering purposes, usually using a bridge rectifier and a capacitor followed by a parallel load; this

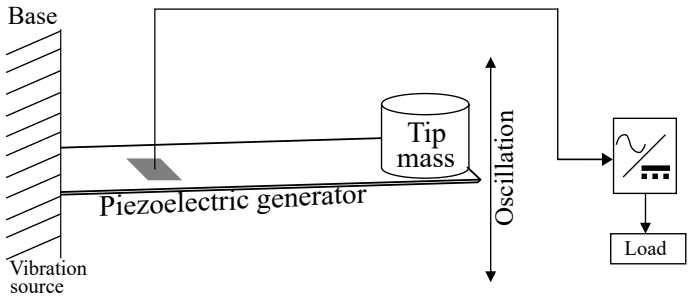

Figure 5.3: Diagram of a PEH system.

structure is pictured on Figure 5.3.

The system depicted in Figure 5.3, and other PEH configurations different from the cantilever, can be found in several works in literature into wearable set-ups, as it will be shown in the following section.

5.4 Piezoelectric Energy Harvesting in Wearable Devices

KEH wearables which rely on PEGs have evolved through the last two decades. From the early developments of an energy harvesting shoe in [22] to recent techniques to integrate piezoelectric fibers into textiles in [137], PEH has been tested in several parts of the body to assess the power generation capabilities of piezoelectric materials under vibration induced by human motion. Nevertheless, since PEH is highly affected by load coupling, due to the high output resistance of PEGs [20], [29], most of existing work exhibits tests with resistive loads matching the PEG or in open-circuit conditions.

Shenck and Paradiso develop the first shoe-mounted PEH-powered system in [22], which sends a RF beacon every time that the accumulated energy in the AC/DC converter is enough for the RF transmitter to send. The system in [22] uses custom-made PVDF and PZT transducer, while Meier et. al achieve similar harvesting results with COTS PEGs in [138], expanding the reproducibility of these developments. Kalantarian and Sarrafzadeh implement a COTS PEG in a shoe sole to power a Bluetooth beacon transmitter and use the beacon frequency to estimate footsteps in [139]. Ma et. al follow the shoe-mounted set-up and developed a system that harvests and extends the sensing

function to gait recognition, using two PEGs for powering and sensing simultaneously [140]. As it can be noticed, shoe-mounted PEH is a mature technology and has led to the development of self-powered devices. Nevertheless, wearables to other body parts are not as advanced in terms of energy harvesting assessment and powering sensors.

For example, De Pasquale et. al study how to exploit the motion of body joints like elbows and knees using flexible piezoelectric patches in [141]. However, the system in [141] is only tested with a 1 MΩ resistive load, which is not representative of real-world sensors or wearable loads. A similar idea with limitation of the resistive load is exhibited in [66]. Mokhtari et. al developed an advanced method to integrate piezoelectric fibers into textiles, being able to harvest energy from parts of the clothing that are exposed to frequent bending as the knees [137]. The work of Jung et. al in [63] proposes a curved PEG to be placed in shoes and wristwatches shows promising harvesting results, but their custom-made proposal is yet to be followed. Also, the shell structured proposed by Yang et. al in [64], which is made to be worn on the forearm, suffers from lack of potential for reproducibility. In contrast to the works of shoe-mounted PEH, developments in [63], [64], [66], [141] show promising results on specific situations or lab-controlled environments, and they are bound to custom-made PEGs which are expensive to fabricate.

On the other hand, systems with COTS harvesters and placed on the hand/wrist or the neck have shown further advances. For instance, Bai et. al investigate the impact of random vibration induced by hand and head motion in a cantilevered COTS PEH system in [142]. Nevertheless, they did not power any sensor or wearable device and they only tested the system with a resistive load. Mendez-Lira et. al employ flexible COTS piezoelectric patches to examine the energy generation from finger motion in [143], although testing is limited to regular keyboard and mouse usage.

Kalantarian et. al take a step towards using PEGs as sensors in [144] and [145] with a necklace to detect swallows to monitor eating habits. Similarly, Fang et. al employ flexible piezoelectric patches to monitor physiological variables such as the heart rate in [146]. Nevertheless, Most advanced works of PEH-based sensing are found in [23], [147]–[150]. For example, Khalifa et. al use a COTS PEG as a sensor to replace the accelerometer in a HAR system in [33], [147]. In [23], Lan et. al show a system for HAR but with a shoe-

mounted PEH. A similar set-up to the one in [147] works for transportation mode detection in [148]. Xu et. al also exhibit how gait recognition can be achieved with shoe-mounted PEGs in [149]. Finally, the recent development in [150] by Lin et. al shows the potential of using the generation patterns of a wearable PEH system for person authentication.

5.4.1 An Open Challenge

This section has revisited different PEH implementations in wearable environments, where the shoe-mounted systems exhibit the greatest maturity. Nevertheless, existing works on PEH for other body parts fall short on providing insights regarding the feasibility of using COTS PEGs for self-powered devices or wearable battery chargers. As it can be noticed, cited works provide tests with resistive loads, which do not represent the nonlinear and variable behavior of PEH-powered devices, or only report the open-circuit voltage. Thus, next section introduces a work which provides a significant insight on the generation capabilities of a wrist-worn COTS PEH system under vibrations induced by daily and fitness-related activities.

5.5 Monitoring Wearable Piezoelectric Harvesting in a Mobile Platform

This section presents the results of logging the energy transference from a wrist-worn piezoelectric harvester to a battery in a wearable device. Tests show that five minutes of activities that involve arm motion can provide between 1.75 mJ and 2.98 mJ of energy, which can represent between 3.6 seconds and 6.2 seconds of additional battery duration. Hence, these results provide an insight of the limitations and challenges remaining in the piezoelectric-based kinetic harvesting field for wearable devices.

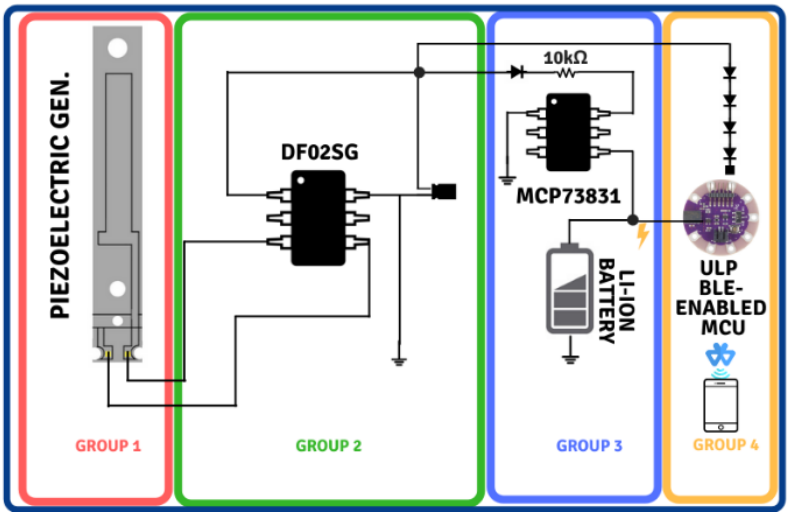

Figure 5.4: Block diagram of the system.

5.5.1 System Components

Overview

The proposed design comprises two main features: kinetic harvesting from a piezoelectric generator, and power transference tracking. For the harvesting task, the PEG shall be followed by an AC/DC converter that permits the flow of the harvested current to a battery through a controller.

For the tracking process, a device must measure the voltage and the current considering the very small currents and the low power available; and then, the information must be constantly saved for the computation of the total transferred energy. Thus, Figure 5.4 displays the diagram for this study divided into four groups.

Group 1 comprises the PEG, which is the kinetic energy scavenger. Then, the AC/DC conversion takes place within the components of Group 2. Group 3 contains a reverse-protection diode, a current-measuring series resistor, and a charge controller for a Li-ion battery. Group 4 is comprised by a series of diodes that creates a voltage reference between the harvested voltage and an ADC input pin in a BLE-enabled ULP MCU (Lilypad Simblee, as in Chapter 4).

The power monitoring system uses the MCU to read the rectified voltage from the PEG alongside with the current, and reports them to a mobile application through BLE. Following the reports, the mobile application computes the instantaneous power, and

Figure 5.5: Wrist-worn PEH-based kinetic harvester.

allows the estimation of the harvested energy specifying how much is transferred to the MCU battery during any time interval selected by the user.

Piezoelectric generator

The PEG employed in this study is a COTS device, following the tendencies from [25], [28], [147], [151]. In this case, I employ the PPA-1022 fabricated by Midé [152] for having the smallest footprint; and hence, being most compatible to wearable technologies. Since the frequency response of human activities take place below 10 Hz [34], the resonance frequency of the PPA-1022 must be adjusted to maximize the harvesting process. Thus, the resonance frequency of the PPA-1022 is trimmed to 10 Hz using a tip mass formed by two neodymium magnets corresponding to a 20-gram moving mass. Due to the magnetic force, the magnets stay attached to the PPA-1022 as shown in Figure 5.5. The device configuration is designed to keep clamped 21 mm of the cantilever leaving 32 mm free for deflections. All these conditions ensure a low resonance frequency, as explained in [152].

Energy Harvesting Circuit

As shown in Figure 5.4, following the PEG, the electronic circuitry allows processing the AC output from the PEG to the DC input in a Li-ion battery through a charge controller and the respective charge current monitoring. Thus, the first stage requires

the electronics to perform the AC/DC conversion. A compact SMD DF02S diode bridge with a 10 μF capacitor transforms the PEG output into DC voltage. The DF02S bridge rectifier offers a 1.1 V voltage drop with a 5 μA of maximum reverse current. Although other works suggest the use of Schottky rectifiers, such diodes display higher reverse currents compared to conventional rectifiers, which in a PEH-based system represents poor rectification and high losses, since the PEG emulates a very-low current source [29].

The MCU used in this study is embedded in the RFD77101 module, which is part of the Lilypad Simblee board. The Lilypad board is specially designed for wearable applications, and also contains a BLE radio and an ARM Cortex-M0 processor [108]. The overall current consumption, considering internal components, is below 10 μA in steady state. Also, this board incorporates a JST (Japan Solderless Terminal) connector for the Li-ion battery and a MCP73831 charge controller to prevent overcharge and overdischarge of the battery that supplies the board [153].

For this study, a 3.7V/110mAh single-cell Li-ion battery provides the energy for the Lilypad Simblee. The MCP73831 permits a voltage supply range from 3.75 V to 6 V [153]. Therefore, any element that intends to transfer energy to the battery must have a supply voltage of at least 3.75 V. When the charge controller is off, the internal connections of the Lilypad board can lead the battery to supply elements connected in the voltage input pin of the MCP73831 controller. In consequence, the reverse-protection diode is added to prevent the battery to charge the capacitor in the harvesting circuit as shown in Group 3 of Figure 5.4. The resistor in series with this diode stands for current measure purposes. By experimentation, I realize that the instantaneous current flowing from the AC/DC converter reaches at most 15-20 μA. Consequently, a 10 kΩ resistor in series with the charge controller helps to track the current through the voltage between its terminals, and such voltage drop falls below a maximum of 0.2V.

Energy Harvesting Tracker

To perform a proper tracking of the current flowing to the charge controller, the MCU needs measurements of the voltage in the capacitor, which is the diode-side terminal of the resistor plus the diode voltage drop, and the controller-side of the resistor. The

capacitor voltage rises to 4.3 V when the charging current is 20 μA. On the other hand, the controller-side terminal of the resistor does not change from 3.75 V, which is the minimum supply voltage for the controller. This phenomenon is due to the very-low supply current. Hence, the system must interpret the 0.55 V difference to a 20 μA charging current in this case. Since the voltage on the controller does not change under the low-current conditions of this harvesting system, the tracking of the capacitor voltage is enough to estimate the charging current. Also, the mentioned current conditions induce a low voltage drop on the reverse-protection diode of 0.35 V. Then, the 0.55 V voltage difference in this case corresponds to a 0.35V drop in the diode and 0.2 V in the resistor.

However, the MCU faces an issue in the voltage measuring process related to its analog-to-digital converter (ADC). The Lilypad Simblee provides a 3.3 V regulation for the MCU supply using a MIC5219 regulator [108]. In consequence, the ADC cannot interpret voltages above that supply. As a solution, I propose the use of a series of diodes that forces a voltage drop between the capacitor and the ADC to map the 4.3 V to 3.3 V. Thus, the capacitor must provide the energy for the battery and the voltage input for the ADC. Nevertheless, this ADC has an input resistance of 19 MΩ, which represents a neglectable current loss compared to the controller. Since the current flowing to the ADC stands below 1 μA, the voltage drop on each diode is 0.25 V approximately. Consequently, four series diodes accomplish the desired task of dropping 4.3 V to 3.3 V with neglectable losses. The MCU samples the mapped capacitor voltage periodically, every 100 ms. Then, it computes the real capacitor voltage assuming a total drop of 1 V in the diodes. After this, assuming 0.35 V fall on the reverse-protection diode, the voltage through the resistor is calculated and sent via BLE in a broadcasting event. Finally, the MCU enters in a ULP sleep state during 99 ms to save energy.

Once the Lilypad Simblee sends the current data via BLE, a custom-made mobile application for Android devices connects automatically to the Lilypad Simblee, receives data, shows current as it comes and stores it for graphical analysis and energy estimation. Figure 5.6 shows the two main views of this mobile application.

Figure 5.6(a) displays the Live tab. It contains an on/off switch that allows the automatic reception from the wearable device. When the switch is activated, it requests

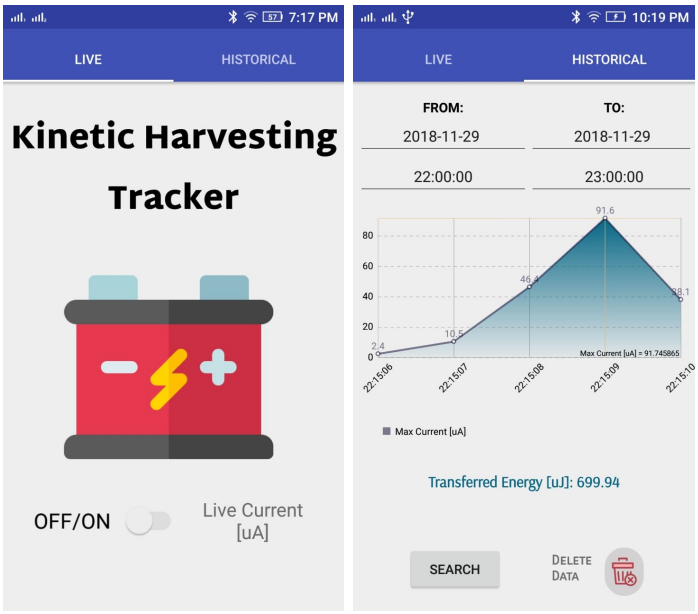

(a) Live (b) Historical

Figure 5.6: Views of the mobile applications.

the user to enable the Bluetooth connections. Internally, the app tries to catch the broadcasting signal of the pre-defined MAC address of the Lilypad Simblee. This configuration permits automatic connection and reception. According to the BLE protocol, data must be organized in different sets of features named services, which can contain different features or characteristics [154]. Each characteristic is related to data within the service. Every time the app detects a change on the value of a custom pre-defined characteristic for the voltage value, it triggers a function which immediately gets the voltage on the 10 kΩ resistor and computes the charging current. After this, the current value is stored in a local SQLite database and displayed in a label next to the switch, as seen in Figure 5.6(a).

The other main view is the Historical tab shown in Figure 5.6(b). This tab exhibits a form which asks the user for a time window. After the selection of initial and final time stamps, the user presses the Search button and the app queries the local database for the data within the selected time window. Once the data are selected, the app plots a graph of the current against time. Additionally, the current values are used to compute the instantaneous power on the input of the charge controller, assuming a 3.75 V input voltage.

According to the measuring system, when the capacitor does not have enough voltage to transfer energy, the voltage difference is negative from the system perspective. Although

there is not current flowing from the battery to the capacitor, the app computes a negative current. However, these negative values are internally related to non-charging states; and therefore, ignored in the power computation. Thus, taking all the instantaneous power values corresponding to positive current, the transferred energy from the kinetic harvester to the controller is calculated with the help of a Riemann sum as presented in Equation 5.2:

$$E = \sum_{i=2}^{n} P_i \Delta t, \tag{5.2}$$

where Δt is the length of the time window between the current sample and the previous sample, P_i is the instantaneous power of the *ith*-component in the resulting dataset, n is the number of data found, and E is transferred energy to the controller during the consulted time window. Nevertheless, the real amount of energy transferred to the battery depends on the controller efficiency under these conditions.

5.5.2 System Evaluation

Once the harvesting tracker properly reports through the app, the system is tested to validate its capabilities. Following the statements from [16], [25] about the location of on-body kinetic harvesters, the system could be placed whether in the wrist or the hip. For this study, the tests are performed with the system configured as a kinetic harvesting bracelet. The device mounted in a wrist is depicted in Figure 5.5.

Ten subjects (six men and four women) are asked to perform four different activities for 5 minutes each. All subjects carried out the activity set only one time to avoid the influence of fatigue on the results. Since the goal is to characterize the battery recharging from arm movements, the activities are selected considering the amount of arm involvement in the selected movements.

The activity set comprises clapping, jogging, dribbling a basketball, and jumping jacks. The jogging activity is performed around a college basketball court with speeds ranging from 3 km/h to 6 km/h; clapping is maintained between 1 and 2 claps per second; for the basketball dribbling, the subjects are asked to keep a pace of at least one dribble every 2 seconds, with the ball reaching the height of the hip of the subject in every bounce and without body displacement; the jumping jacks are done at rates between 20 and

Table 5.1: Energy transferred during each activity session.

Subject	**Transferred energy after activities[mJ]**			
	Jogging	*Clapping*	*Dribbling*	*Jumping*
1	2.80	2.98	2.18	2.18
2	2.36	2.75	1.94	1.88
3	1.75	2.24	1.92	1.80
4	2.16	2.29	2.07	1.97
5	1.95	2.82	1.86	1.89
6	2.07	2.59	1.94	1.77
7	1.96	2.67	1.95	1.93
8	2.25	2.46	1.79	2.21
9	2.14	2.00	1.76	1.75
10	1.83	2.63	2.00	1.84

40 jumps per minute. At the beginning of each session, authors corroborate with the subjects that they do not feel any major discomfort that conditions their performance. Then, the subjects execute each activity and they are asked to rest during at least 3 minutes. After every session, authors consult the corresponding time window in the application and tabulate the estimation of transferred energy from the kinetic harvester to the charge controller. Table 5.1 resumes the results obtained during experimentation.

Considering that the system battery charge capacity is 110 mAh, with a 3.7 V nominal voltage, the total energy available in this fully charged element is 1465.2 J, using the conversion factor of 3.6 from mWh to J. Since the results in Table 5.1 are in mJ, calculating the percentage of battery saved does not show significant values. Instead, I propose a different approach.

According to its datasheet, the RFD77101 consumes 600 nA in ULP sleep state and 8 mA while transmitting at 0dB [108]. Adding the quiescent currents of the MCP73831 and the MIC5219 regulator, the Lilypad Simblee requires a total of 50 μA during ULP sleep. Therefore, for the configuration of the kinetic harvesting tracker, the board needs 18.3 μJ for the 99 ms of ULP sleep and 29.6 μJ for the transmission events, which includes

Table 5.2: Additional working cycles obtained during activities.

Subject	**Additional working cycles after activities**			
	Jogging	*Clapping*	*Dribbling*	*Jumping*
1	58.5	62.4	45.6	45.6
2	49.4	57.5	40.6	39.4
3	36.6	46.9	40.2	37.7
4	45.2	47.9	43.2	41.2
5	40.8	59.0	38.8	39.5
6	43.3	54.2	40.6	37.1
7	41.0	55.9	40.8	40.4
8	47.0	51.5	37.5	46.1
9	44.8	41.8	36.8	36.6
10	38.2	55.0	41.8	38.5
Minimum	**36.6**	**41.8**	**36.8**	**36.6**
Average	**44.5**	**53.2**	**40.6**	**40.2**
Maximum	**58.5**	**62.4**	**45.6**	**46.1**

waking up, ADC reading, and processing of the MCU. Hence, a working cycle is defined as the process where the tracker sleeps, wakes up to measure and transmit, whose length is 100 ms, it can be stated that each cycle requires 47.9 μJ of energy.

Consequently, the impact of the kinetic harvester on the battery can be quantified in terms of additional working cycles. Thus, dividing the transferred energy by the cycle energy can provide accurate information about the capabilities of the kinetic harvesting process using PEGs. Table 5.2 shows the results in terms of additional working cycles. Additionally, Table 5.2 contains three new rows for a better understanding of the results. The average values evince the tendencies to obtain more harvested energy by jogging and clapping than dribbling a basketball and jumping jacks. These results are due to the consistent pace required by those activities. Nevertheless, clapping implies a faster movement than jogging, which leads to a rapid charging of the capacitor and more power transferred to the charge controller.

Also, it must be noted that the difference between minimum and maximum values in jogging and clapping are greater than the corresponding difference in dribbling and jumping. Although the latter reports smaller tendencies compared to the other two activities, they exhibit values that are very similar across subjects. This phenomenon is caused by the nature of these movements. Dribbling a basketball, even for people who are not experienced with such skill, forces similar deflections on the PEG among different subjects. Jumping jacks provoke such effect, as well.

In contrast, some subjects clapped harder than others, inducing larger deflections on the PEG. Also, the jogging style varied among subjects, and this determines the involvement of arm movements and consequently the amount of vibration induced in the kinetic generator. Finally, it must be noted that the harvested energy can supply at least 36 additional working cycles, which can also be interpreted as 3.6 seconds of additional battery operation. This approach for the measurement of the impact of the energy harvesting system leads to a comprehensive view of the capabilities from actual kinetic harvesters and the need to continue reducing the power requirements in wearable devices. It can be stated that this PEG cannot provide enough energy to keep the selected MCU working continuously. However, the growing tendencies of recent electronic developments towards reduction of power consumption [155] could help to extend the use of the harvested energy in a scenario similar to the presented here.

5.6 The Convergence Point of KEH and HAR

KEH has emerged as an energy-efficient technology for wearable devices, leveraging human body motion to power devices or recharge batteries [9], [18], [32], [156]. The insights on the performance of the wrist-worn piezoelectric kinetic harvester presented here can be used to determine the suitability of using off-the-shelf devices to supply self-powered systems in a wearable environment.

Furthermore, recent studies show the feasibility of using the voltage output of kinetic harvesters as sensors for context sensing, instead of accelerometers and gyroscopes, where the harvesters can work both as energy and information sources [23], [31]. In the case of KEH-based HAR, the use of approaches based on handcrafted features causes a poor

performance when it is compared to accelerometer-based HAR. Hence, next chapter presents a solution for this issue based on concepts from deep learning such as CNNs, LSTMs, data augmentation and transfer learning.

Chapter 6

Enhancing Kinetic Harvesting-based Activity Recognition with Deep Learning

KEH-based sensing replaces conventional sensors with KEH devices. The main objectives are to reduce the power consumption of the wearables due to sensors, and increase the available power by using a KEH device to provide both energy and sensing information through the generation patterns of the KEH device. The applications found in the literature for KEH-based sensing range from HAR [147] to user authentication [150]. Existing KEH-based HAR systems rely on traditional machine learning approaches, mapping signals into representations based on a set of handcrafted features [23], [31], [33], [147], [151]. This methodology limits the performance of classifiers, since the suitability of a feature set may change with scenarios, devices or datasets. On the other hand, ANN offer automatic feature extraction with higher abstraction, at the cost of more computational requirements and larger datasets [35]. ANN-based and different deep learning approaches have shown higher performance over traditional machine learning algorithms in several disciplines [36]. For the case of conventional accelerometer-based HAR, the studies in [72], [95], [99], [100], [157], [158] have shown how deep learning architectures outperform handcrafted feature-based machine learning approaches. Consequently, a deep learning-based approach for KEH-based HAR is a suitable alternative to improve existing classification performance.

Nonetheless, deep learning algorithms require large amounts of data to acquire generalization capabilities and avoid overfitting. Human activity datasets are required to have information from several subjects performing the same activities with different styles, to maximize the generalization capability of the classifiers. However, obtaining KEH data from numerous users to guarantee high motion variance might be impractical and unfeasible. Therefore, to increase the KEH dataset size the system needs data augmentation methods that generate synthetic data. This new data must resemble new users performing the same activities from existing datasets, and introduce the necessary variance to help the classifier to avoid overfitting.

Despite several efforts in the literature towards data augmentation in accelerometer-based HAR [75], [76], there are substantial differences between accelerometry and KEH signals that makes the latter a challenging object for data augmentation. These differences have origin in the frequency behavior of the sensors. Accelerometers used in wearable-based HAR have a low-frequency stable bandwidth up to at least 50 Hz [9], [57], which makes them suitable to capture human motion that is typically bound to 10 Hz [34]. On the other hand, KEH devices exhibit a narrow relatively-high frequency bandwidth, reducing their sensitivity in the band of human motion and introducing new challenges on event recognition [33], [145]. Additionally, this difference in sensor nature leads to different signal-to-noise ratios (SNR) between accelerometry and KEH signals. Voltage output of KEH devices for HAR is prone to have lower SNR than accelerometer signals due to the poor sensitivity in low frequencies and the several frequency harmonics induced by the harvesting material [29]. Therefore, activity signals from kinetic harvesters might exhibit higher interclass similarity than accelerometer signals, hardening the process of distinguishing among classes in KEH-based HAR.

Another challenge for KEH-based sensing is the dependency on the on-body position of the kinetic harvesting wearable and the dependency on the subjects who perform the activities. Handcrafted feature-based approaches perform poorly when the device position changes, or when the classifier is trained with information from few subjects and then is exposed to an unknown subject [57], [99]. In the field of deep learning, transfer learning is a well-known method to develop cross-domain algorithms where the knowledge from

a source domain (e.g., known position or set of subjects) can be transferred to a target domain [159]. However, there are no transfer learning-based works in the literature to solve the issues of position and subject dependency in KEH-based HAR.

Hence, in this chapter, I present a solution to address the challenges of introducing a deep learning architecture for KEH-based HAR, developing data augmentation for KEH signals and applying transfer learning to solve subject and position dependency.

First, I propose a deep learning architecture composed by CNN and LSTM for KEH-based HAR. This architecture is designed to be light-weight, which is critical in wearable-oriented HAR applications [99]. It is demonstrated how this architecture improves the classification accuracy compared to other approaches found in the literature for KEH-based HAR, and how this superiority remains in different scenarios were the input signals are affected by downsampling and length changes; both cases represent loss of information, and the classifier still outperforms other algorithms in such scenarios.

Second, I present three data augmentation methods for KEH signals. The methods described here are designed to augment KEH datasets by resembling new users performing the same activities of the datasets, changing the motion intensity, pace and the event location in the time series. These are the first augmentation methods proposed for KEH signals. Existing methods, such as the weighted time warping from [76], are demonstrated to be inefficient to improve the generalization capabilities of deep learning-based classifiers. The methods proposed here are conceived to introduce intraclass variance but without increasing interclass similarity. In contrast, other works found in the literature do not show how their augmentation methods may affect the intraclass variance and interclass similarity. Additionally, I study the limits of generalization improvement introduced by the augmentation methods, with experiments to show how much can a dataset be augmented before these methods induce overfitting.

Third, I apply transfer learning to solve the subject and position dependency issues in the KEH domain. To address this, I take a public KEH dataset with signals from subjects performing five activities in two different on-body positions: hand and waist. Then, I apply transfer learning between position datasets and between users of the same position. Moreover, I employ data augmentation in both source and target domains to display the

positive impact that it has on transfer learning. The inclusion of data augmentation in these approaches is what marks the difference with existing approaches in the literature, where augmentation is not considered in any domain or case study [78], [80].

6.1 Limitations of KEH-based HAR

Recent studies [23], [33], [147], [148], [160] have shown the potential of leveraging energy harvesting signals, i.e. the AC voltage output of a transducer, as an alternative to conventional motion sensors for activity sensing. This KEH-based setup for HAR eliminates the power consumption of the motion sensors and extends the battery lifetime of the wearable system simultaneously. Thus, KEH-based HAR systems have the advantage of less overall power consumption and more power available over conventional accelerometer-based HAR systems.

However, there is a significant room for improvement of the classification performance in KEH-based HAR systems. Most noticeably, owing to the low SNR of the energy harvesting signal and the lack of a multi-channel sensing input [147], [160], existing KEH-based solutions fall short of recognition accuracy when comparing with their accelerometer-based counterparts. As an example, Table 6.1 briefly summarizes the representative works in KEH-based context sensing. As shown, given different contexts, it can be noticed an accuracy gap from 5% to 37% between the KEH-based solutions and the conventional accelerometer-based approaches.

The works cited in Table 6.1 employ traditional machine learning algorithms and handcrafted feature representations, which limits the performance that can be reached with noisy signals as in the KEH domain. Handcrafted feature representation exhibits several pitfalls such as task-dependency, and they can reduce classification accuracy in the presence of high intraclass variance (caused by several styles of performing the same activity) or interclass similarity (due to activities that can exhibit similar sensor outputs) [57], [99]. In contrast, automatic feature extraction with deep learning methods has arose as an alternative to overcome the mentioned pitfalls and reduce human effort in feature engineering [35].

Nevertheless, deep learning requires large datasets for a proper learning process. A dataset for KEH-based HAR with deep learning requires hundreds of subjects to capture

Table 6.1: Performance comparison of existing HAR systems using KEH or accelerometer as the sensing modality.

Work	Context	Accuracy per sensor	
		KEH	Acc
[33]	Human Activity Recognition	64%	96%
[147]	Human Activity Recognition	70%	95%
[151]	Human Activity Recognition	53%	90%
[148]	Transportation Mode Detection	$\sim$ 90%	$\sim$ 95%
[149]	Gait-based User Authentication	$\sim$ 85%	$\sim$ 95%

high variance of motions, providing the deep learning classifier with information to reduce overfitting. Subsequently, it might be impractical and unfeasible to obtain a dataset with numerous subjects. Therefore, augmenting datasets through the generation of new samples that resemble new users can help to strengthen the generalization capability of the classifier.

Although some works have proposed data augmentation methods for accelerometer-based HAR [75], there are no methods in the literature for KEH signals. Some of the existing methods for accelerometer signals, such as the recreation of device rotations through matrix transformations [75], are specific for multi-axis signals and not compatible with KEH signals. Other methods, such as the time warping from [76] rely on weighted averages of existing time series, which limits the intraclass variance to the variance provided by the dataset and might induce classifiers to overfit, as shown in [77]. Hence, in this chapter I propose to define data augmentation methods that are suitable for KEH signals.

6.2 System Overview

Figure 6.1 shows the pipeline of the proposed system for KEH-based activity recognition. This system has two main components: a data augmentation block, and a deep learning-based classifier.

Given a dataset with activity signals from a KEH device, I split it into three subsets: training, validation, and testing. The training subset is augmented using the methods

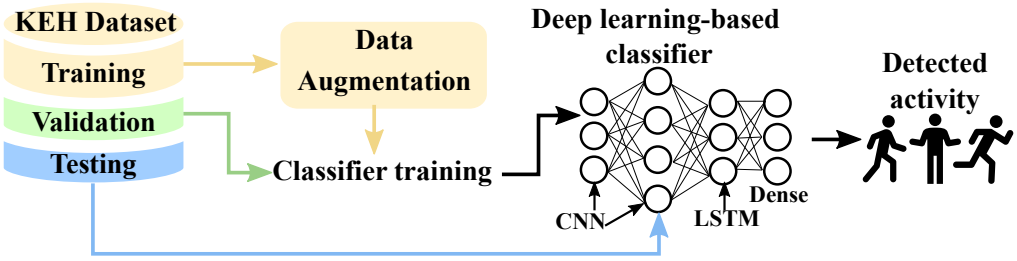

Figure 6.1: Pipeline of the proposed system.

described later in Section 6.4, generating synthetic data that resembles new users; and hence, increasing the variance of the training data. I propose three methods to augment KEH signals: time warping, magnitude warping and permutation. These methods reproduce KEH signals under changes on motion pace and intensity, which are the scenarios used to resemble new users.

The augmented training subset constitutes the input of the classifier in the training process, while the validation subset is used to tune the weights of the neural network. The proposed deep learning architecture leverages the feature extraction from one-dimensional convolutional layers and the sequence building capability of recurrent neural networks. The first layers of the architecture are CNNs, which can provide features with abstraction levels directly proportional to the number of layers, capturing local dependencies and scale variations. After the CNN, a LSTM layer learns from the time correlation of features in a the KEH signal. Including time dependencies in the classifier, instead of considering feature maps independent from each other, can help to classify signals under high interclass similarity, like in the case of KEH signals due to their low SNR. At the last part of the architecture, a fully-connected layer learns the interpret the sequence of features given the LSTM and infer the class (activity) of the incoming samples.

Once the classifier is trained, the testing subset is used to assess the classification accuracy of the system under unknown data with shared characteristics with the training and validation subsets (e.g. device position or subjects). However, when the data comes from a different device position or a new subject, classification accuracy can drop significantly. Hence, to present a position-independent and subject-independent system, I employ two transfer learning approaches for the adaptation of the deep learning classifier to new device positions and new subjects. Moreover, to overcome the limitation imposed

by restricted data availability in the new context (position or subject), I apply data augmentation in several scenarios to show its impact in the transfer learning process; this approach is explained later in Section 6.5.

6.3 Deep Learning Architecture

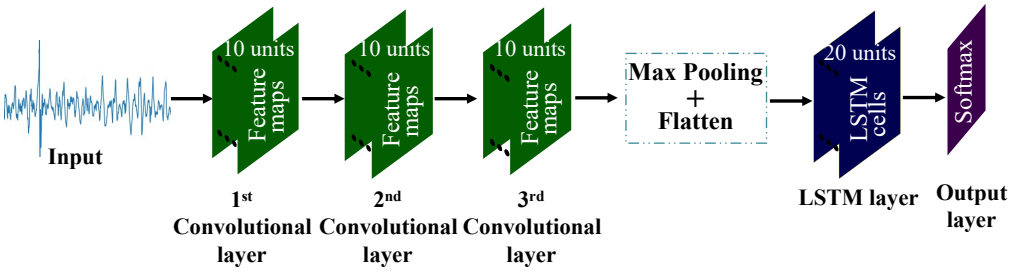

Figure 6.2: Deep learning architecture for KEH-based HAR based on CNNs and LSTMs to overcome the issues of traditional machine learning approaches.

Figure 6.2 presents the proposed deep learning architecture for KEH-based activity recognition. This architecture consists of three convolutional layers, a max pooling layer, a flatten layer, a LSTM layer and an output layer.

The first three layers are convolutional layers that provide advanced feature extraction. Each one of these layers has ten units. The units in the first layer take a portion of the input signal and compute features through convolution operations to form feature maps. The set of features from all units in a layer is hereafter referred as feature map. The activation function for the convolutional units is the ReLU, which helps to reduce the possibility of dealing with vanishing gradients during training. The following two convolutional layers increase the level of abstraction by computing feature maps over the maps from the previous layer. Hence, at the output of the third convolutional layer the system has ten feature maps with a third level of abstraction. Then, the max-pooling layer downsamples the feature maps by half, selecting the largest features and reducing dimension of the maps, and followed by a flatten layer to transform data into a sequence for the next layer.

To build a sequence of feature maps, each sample signal is divided into smaller windows which are analyzed by these first 5 layers. Subsequently, for each window a set

of feature maps are passed to the LSTM layer. Thus, the LSTM layer takes the feature maps of each window as input and discriminates among feature maps to select which features are relevant. Then, by working with all the windows in a sample signal, this layer builds a sequence of advanced features that represents the activity signal. Lastly, the output layer uses the softmax function to provide a probability for each class, depending on the sequence of features that comes from the LSTM layer. The class with the highest probability is selected as the detected activity.

6.4 Data Augmentation for KEH

Despite the improvement that the proposed architecture can offer, this is only possible if there is sufficient variance in the training data and the dataset is large enough to avoid overfitting. Since increasing the dataset size is unfeasible in most scenarios, data augmentation is employed to synthetically generate data and improve the generalization capability of classifiers.

As shown in Chapter 5, the voltage output of a KEH device is directly proportional to the applied strain, and such strain depends on human motion. In that system, the differences in motion styles among users are assumed to be motion intensity, pace and the order of events within an activity; in a KEH signal these differences are reflected in voltage magnitude, spatial distribution of samples, and the location of even-related portions of the signal, respectively. Hence, I propose three methods to augment KEH signal datasets, which simulate new users performing the same activities with different styles. Magnitude Warping resembles changes on the intensity of motions, affecting the magnitude of the voltage output from the harvester [34]. Time Warping simulates changes of pace, which is reflected on the time distribution of samples in the form of widening or tightening of waveform portions. Permutation recreates subjects with similar motion intensity and pace, but with a different observation window; this effect is similar to the window warping exhibited in [161], but without changing the length of the inputs for the classifier.

Thus, let each time series f from a KEH signal dataset be considered as the input of an operator H, i.e., augmentation method, which maps f into a new signal h belonging to the same class (activity). Both f and h have the same length L, and the indexes of

the samples of f are in $I = \{0,1,2,...,L-1\}$. Therefore, the augmentation methods are defined as follows.

- **Magnitude Warping**: This method consists of a change on the signal shape with a warping curve g. To achieve this, the operator randomly takes 10 points from a normal distribution with unitary mean and standard deviation 0.5. Then, a cubic interpolation function generates a warping curve g of the same length of the signal using the points from the distribution. Through a point-wise product, the curve and the original signal fuse to create a new signal, as depicted in Figure 6.3(a), where the warping curve resembles an envelope around the warped signal. The operator H for Magnitude Warping is defined in Equation 6.1.

$$H : f \mapsto h(i) = f(i)g(i), \forall i \in I. \tag{6.1}$$

- **Time Warping**: Similar to Magnitude Warping, a curve g is generated from a set of points taken from the same distribution. Then, the operator calculates the cumulative sum $\tilde{g}$ of the curve points, which builds a Time Warping path. Consequently, the indices in the original signal are replaced by the scaled indices in the cumulative sum, changing the temporal distribution of the samples as shown in Equation 6.2.

$$\begin{aligned} \tilde{g} &: \underset{i \in I}{i} \mapsto \sum_{j=0}^{i} g(j), \\ H &: f \mapsto h = f(\alpha \cdot \tilde{g}); \alpha = \tfrac{L-1}{\tilde{g}(L-1)}. \end{aligned} \tag{6.2}$$

  The scalar factor α keeps the values of $\tilde{g}$ between 0 and $L-1$. Figure 6.3(b) illustrates an example of this process, where a portion of the signal is temporally stretched while another section is shrunk.

- **Permutation**: In this method, the original signal f is split into blocks as an ordered tuple $(f_0, f_1, ..., f_n)$, where the length of all blocks is set to 0.5 seconds so each one can keep significant motion portions. Then, the blocks are shuffled by assigning each block to a new position in the list (e.g. $f_k \mapsto f_{j_k}$), and a new signal h_j is obtained from the reordered blocks, as shown in Equation 6.3.

$$H : f = (f_0, f_1, ..., f_n) \mapsto h_j = (f_{j_0}, f_{j_1}, ..., f_{j_n}). \tag{6.3}$$

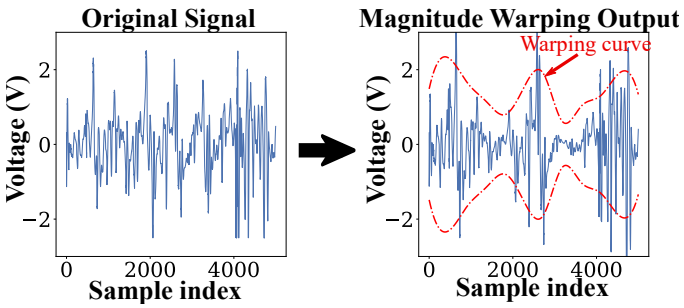

(a) Magnitude warping

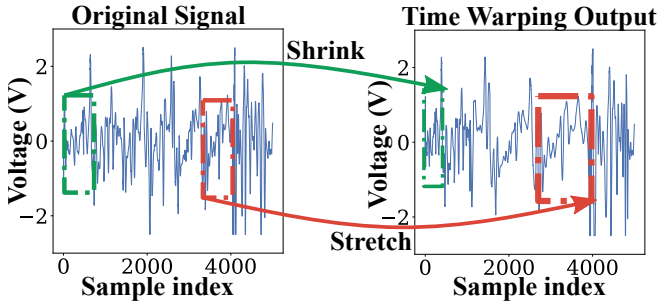

(b) Time Warping

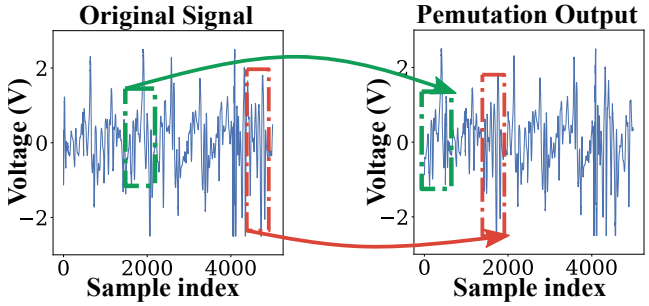

(c) Permutation

Figure 6.3: Examples of the three data augmentation methods to resemble new users performing the same activities with the same device.

In this case, the j subscript indicates that these indices might change if the operator H is applied again. An example of Permutation can be found on Figure 6.3(c), where the re-positioning of two signals blocks is highlighted.

6.5 Transfer Learning for KEH-based HAR

The input waveforms of KEH-based HAR can be affected by changes on the harvester, the subject, or the on-body position. A change of harvester implies different harvesting

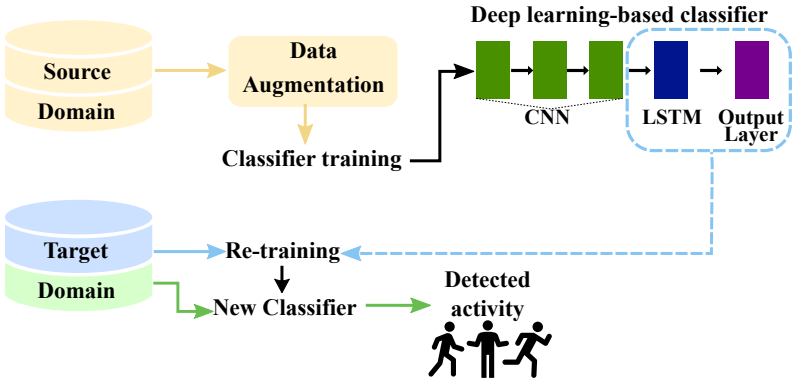

Figure 6.4: Transfer learning pipeline to adapt the proposed architecture to new sensing scenarios.

parameter values such as elasticity, dimensions, and piezoelectric constant. These changes in KEH devices are studied and modeled in [34]. However, a change of subject or device positions can produce waveforms that induce feature values which are outside the expected ranges of the classifier.

Therefore, classifiers may easily overfit to specific scenarios and perform poorly when the KEH device is placed in a different part of the body or is worn by new subjects. This issue has not been previously studied in KEH-based HAR. Thus, I employ transfer learning to help the classifier to adapt to new device positions and new subjects.

Figure 6.4 shows the pipeline of the transfer learning process. The source domain refers to the KEH dataset which is used by the classifier to learn how to detect activities from KEH signals. This domain can contain waveforms from a single device position or a set of subjects whose data are going to be known by the classifier. Before the classifier training, data augmentation is applied on the source domain to increase the variance on the training data and the generalization capability of the classifier. After the training, the convolutional layers of the proposed architectures are frozen by keeping the resulting weights from the training. The other two layers are set to be re-trained with new data. The purpose of freezing the convolutional layers is to maintain the advanced feature extraction learned from the augmented source domain, but leaving the possibility open for the classifier to learn new sequence of features in the LSTM layer.

Then, when the target domain (e.g. a KEH dataset taken from a new device position or a new subject) is considered, the LSTM and the output layer are re-trained with the

half of the data from this domain. This process ensures the use of the pre-trained CNNs for feature extraction and a new sequence-of-features learning for the last two layers. The employment of data augmentation for re-training is also considered in the System Evaluation section. Finally, after the re-training, the architecture with the new weights is assessed with the remaining half of the target domain. This assessment helps to measure the effectiveness of the transfer learning process.

6.6 System Evaluation

This section shows the impact of data augmentation on the traditional algorithms and the proposed architectures. Then, it discusses the effects of changing the default window size and the sampling frequency in both position datasets. Finally, this section includes the evaluation of the transfer learning in subject-wise and position-wise scenarios.

6.6.1 KEH Dataset

I use the public KEH dataset [147] for evaluation. It comprises five activities, which are Running, Going Downstairs, Going Upstairs, Walking and Standing Still. The KEH transducer is a PEH Volture V25W from Midé Technology. [1] This PEH is sensitive to vibrations between 40 Hz and 120 Hz; since human motion exhibits frequencies around 10 Hz and below [9], a tip mass of 7 g is attached to the PEH to increase the sensitivity at lower frequencies. An Arduino Uno equipped with a 128 GB SD card records the AC voltage output of the PEH at a 1 kHz sampling rate.

A total of ten subjects (four male and six female) participated in the experiments. Their ages, weight and height range between 26 and 35, 58 and 91 kg, 154 and 185 cm, respectively. Each subject performs the five activities at least once holding the device on one hand and another time placing it in their waist. The data collected while the device is on the hand constitutes the Hand dataset, and the data collected from the waist of the subjects account for the Waist dataset.

The duration of each experiment varies per subject due to physical conditions and

[1] https://www.mide.com/

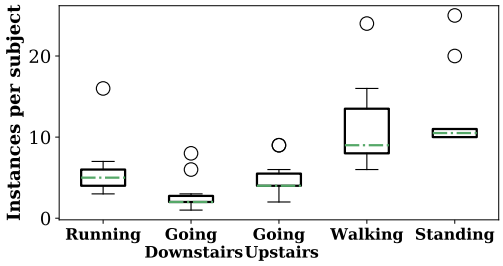

Figure 6.5: Box and wishkers diagrams of instances per class among all subjects in the datasets.

availability, and some subjects performed some experiments more than once, which can introduce bias towards the classes (activities) with more instances. Figure 6.5 illustrates this issue by showing a box and whiskers diagram of the number of instances per class among all subjects. The Walking and Standing activities have a greater average of instances per subject, while Going downstairs is the activity with less information available.

Thus, I take this distribution of instances per class into account to propose the evaluation scenarios and the corresponding metrics in the following subsection.

6.6.2 Evaluation Setup

I propose two evaluation scenarios to assess the classification performance of the system. The first scenario is hereafter referred as *leave-one-position-out*. In this scenario, the data from the subjects in each device position is combined and the number of instances per class is truncated to the size of the class with less instance, resulting in 50 and 52 instances per class in the Hand and Waist datasets, respectively. The second scenario is called *leave-one-subject-out*. In that case, the number of instances per class is kept in the amounts that generate Figure 6.5, ranging from five to 16 instances per class per subject. Then, data is separated by subjects and device positions, resulting in two position-related datasets (Hand and Waist) containing data from ten subjects each one, and evaluating each dataset separately.

For the leave-one-position-out and leave-one-subject-out experiments I consider four different classifiers. The first two are k-Nearest Neighbors (kNN) and Random Forest. These are handcrafted features-based machine learning algorithms, which are used in previous works on KEH-based HAR [69]. The other two classifiers are deep learning archi-

tectures: the one presented in Figure 6.2, hereafter referred as CNN+LSTM architecture; and a different version of it where the LSTM layer is replaced by a dense (fully-connected) layer with the same amount of units, hereafter referred as CNN architecture. Hence, the CNN architecture considers feature maps to be independent from each other, while CNN+LSTM process the feature maps in correlated sequences. The comparison of these two architectures allows to highlight the importance of combining feature extraction with time dependencies in KEH-based HAR.

I employ cross-validation (five-fold for leave-one-position-out and ten-fold for leave-one-subject-out) and compute the average testing accuracy for each algorithm. In each case of cross-validation, there are training, validation and testing subsets. For the leave-one-position-out experiments there are three folds for training, one for validation and one for testing. This process is iterated until all five folds are used for testing. Similarly, the leave-one-subject-out experiments include eight folds for training, one for validation and one for testing; and the iteration process is also done until each of the ten folds is used for testing. In the leave-one-subject-out experiments, each fold corresponds to the data from a subject.

For each experiment, I tune the number of neighbors for kNN and the number of trees for Random Forest according to the validation accuracy induced by each parameter value; the number of neighbors is varied between two a 50 and the number of trees between two and 100. Hence, for each experiment there is a different parameter value for kNN and Random Forest. According to Chapter 4, classification performance in these algorithms does not change significantly when the number of neighbors and the number of trees vary above the mentioned ranges.

In the case of the deep learning architectures, the validation accuracy is used in the training process to determine when the neural network starts to overfit the training subset, and then stop the training.If there is no early stoppage, the number of training epochs is set to 200. The batch size is 32; the optimization algorithm for the learning process is Adam [162] with a learning rate of 1×10^{-3}.

The performance of the algorithms is shown in both scenarios. In the leave-one-position-out scenario the metric is the accuracy, since the number of instances per class is the same for all activities; and hence, the results are not affected by any bias. On the

other hand, in the case of leave-one-position-out the performance metric are the average F1 score or F-score [163], to avoid bias towards classes with more instances, and the accuracy to compare results with the leave-one-position-out experiments.

The deep learning architectures are deployed using Keras 2.3 on top of the Tensorflow 2.0 framework. The testing process is carried out in a desktop with an Intel i7-8700 CPU and a Nvidia GTX 1080 GPU.

6.6.3 Validation of Data Augmentation Methods

This experiment demonstrates that the proposed methods can simulate new users and do not introduce distortion that changes the class of the KEH signal, i.e., they do not increase interclass similarity. For this purpose, I use the euclidean distance from Dynamic Time Warping (DTW) to measure similarities between signals from different classes, subjects and signals synthetically generated from data augmentation. I employ the API from [164] to apply DTW in Python and obtain the euclidean distance between waveforms.

First, I compute the average euclidean distance between the signals of any two classes. This measure helps to understand the level of similarity among classes. Then, I calculate the average euclidean distance among the subjects of each class. Since the data augmentation methods synthesize waveforms simulating new subjects and not new activities, I corroborate this by measuring the distances between each signal and its corresponding Magnitude Warping, Time Warping and Permutation output. The expectation for these average distances is to be less or equal than the distance among intraclass subjects and less than the distance to other classes. Figure 6.6 displays the results of this experiment.

Results for Running show the strong distinction between its waveforms and other classes, while Going Downstairs exhibits very similar distances to Going Upstairs and Walking. Regarding the augmentation methods, for each class, Time Warping and Magnitude Warping show average distances smaller than the average distance between intraclass subjects, while Permutation exhibits distances close to the intraclass limit but does not overpass it. For all classes, the distances from augmentation methods to the original signal meet the expectations of being below the intraclass subjects distance. Hence, it can be concluded that these methods can simulate new subjects without introducing

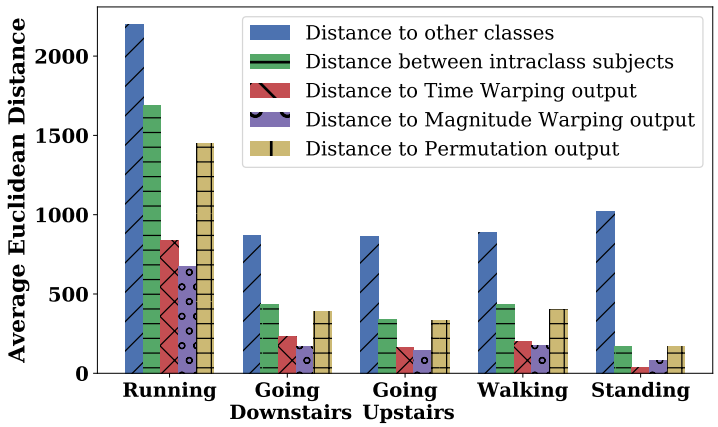

Figure 6.6: Average euclidean distances between signals from different classes, subjects of the same class, and respect to each augmentation method.

distortion that could change the class of the signal.

6.6.4 Impact of Data Augmentation Methods

Following the validation of the data augmentation methods, I investigate the impact that each one and the combinations of them have in the classification performance. Thus, I take the Hand dataset and run a five-fold cross-validation over it with the CNN+LSTM architecture. For each testing fold, the four remaining folds are taken as the input of the augmentation methods for training and validation, applying 20 times each method separately and only for training. This process is iterated until each one of the five folds has been used for testing.

As it can be seen in Figure 6.7, Time Warping (TW) increases the average accuracy of the system up to 81%, while Magnitude Warping (MW) and Permutation (Perm) alone cannot help to improve above 74%. Then, I combine the effects of Time Warping with Permutation and later with Magnitude Warping to assess which combination provides a positive effect in the accuracy.

Results in Figure 6.7 exhibit that combining the contributions of Time Warping, Permutation and applying Permutation over Time Warping output in a composed set-up, is a suitable augmentation option for this dataset, having reached the highest accuracy compared to applying one method only or the combination of the three of them. Therefore,

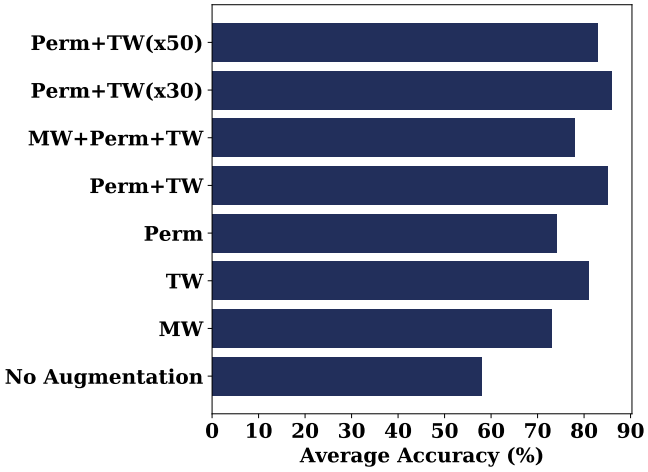

Figure 6.7: Comparison of augmentation methods in the improvement of classification performance. Time Warping combined with Permutation induce the highest improvement. Magnitude Warping has least positive impact on classification accuracy.

I study the limits of performance improvement with this augmentation methodology by increasing the amounts of application to 30 and 50 times.

The application of Time Warping and Permutation by 30 times and 50 times induces accuracy shifts to 86% and 83%, respectively. The detriment in the step from applying augmentation 30 times to 50 times is due to the limited intraclass variance (evidenced by the distances in Figure 6.6) that can be obtained from the original dataset. This issue leads to overfitting as the new synthetic data start increasing in similarity to other instances. This phenomena is also presented in [77], where Time Warping falls short to improve datasets with large amounts of instances. Since Time Warping is among the selected methods, this phenomena of limited intraclass variance is expected. However, the combination of Time Warping, Permutation and their respective composition, applied 30 times, is the selected augmentation methodology for this dataset.

6.6.5 Leave-one-position-out Experiments

Now, for the leave-one-position-out scenario, I consider the Hand and Waist datasets separately. In this case, the performance metric is the average testing accuracy from a five-fold cross-validation. With a sampling frequency of 1 kHz and a window size of five

seconds, the Hand dataset has 50 instances per class, while the Waist dataset has 52 instances per class; each instance is 5000 samples long. During the pre-processing, the instances are taken with an overlap of 50% from the dataset time series.

To observe the effect of data augmentation in each classifier, the experiments consider the classification performance with and without augmenting the training datasets on each iteration of the cross-validation. Figure 6.8 shows the impact of implementing data augmentation in both datasets to improve classification accuracy.

In the Hand dataset, kNN and Random Forest exhibit small accuracy variations before and after augmentation; improvements achieve only 4% for kNN and 1% for Random Forest with data augmentation. On the other hand, deep learning architectures show a notable benefit from augmentation; CNN architecture accuracy comes from 47% to 68%, and the proposed CNN+LSTM improves from 57% to 86%, outperforming all algorithms by at least 13%.

In the Waist dataset, kNN improves from 65% to 70% and Random Forest enhances from 78% to 79%. In the proposed architectures, CNN blasts from 47% to 77%, and CNN+LSTM rises from 70% to 87%, keeping a difference of at least 8% with other algorithms.

Therefore, the combination of the selected augmentation methods and the CNN+LSTM architecture outperforms other classifiers in an scenario with equal number of instances per classes, avoiding the bias towards activities with more instances. Now, next experiments examine how the two parameters that characterize the time series in this dataset (the window size and the sampling frequency) can affect the performance of the classifiers in this experiment after augmenting the respective training sets.

Effect of Window Size

I take the position datasets from the leave-one-position-out experiments and change the size of each observation window to obtain instances of four, three, two and one second; the overlap is maintained at 50% for all cases. Then, I run five-fold cross-validation experiments similar to leave-one-position-out and plot the results for each algorithm in Figure 6.9.

In both cases of Figures 6.9(a) and 6.9(b) the average accuracy increases with the obser-

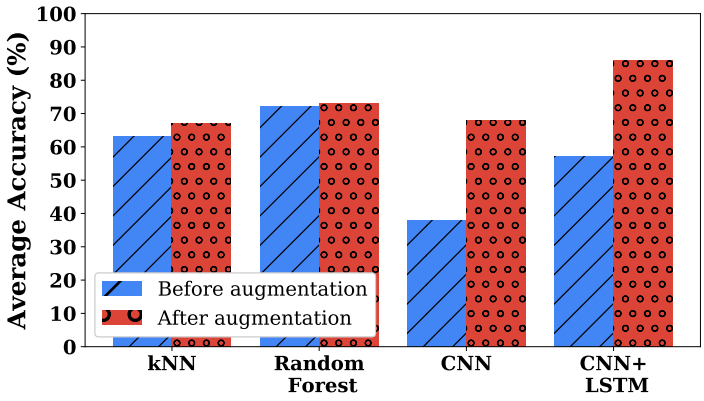

(a) Hand dataset

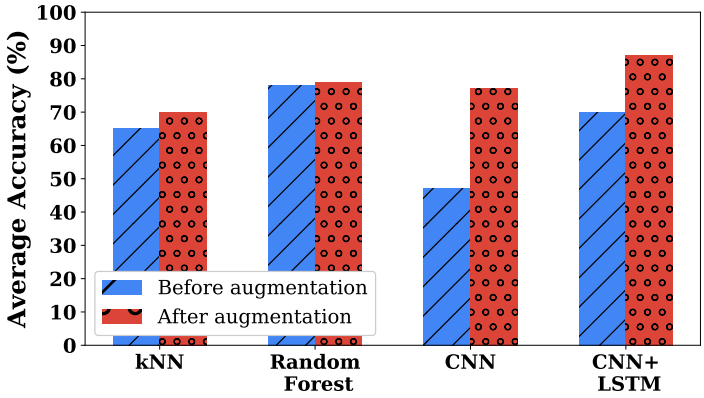

(b) Waist dataset

Figure 6.8: Average accuracy before and after applying data augmentation on the training set of each position dataset. The proposed CNN+LSTM architecture takes the highest benefit of data augmentation and outperforms other algorithms when the device is located on the hand and on the waist.

vation window size. The results exhibited in Figure 6.9(a) show how CNN+LSTM keeps a difference of at least 10% with window sizes ranging from two seconds to five seconds, for the Hand dataset. Even when the window size is one second, the CNN+LSTM outperforms CNN, kNN and Random Forest, with a margin of at least 8%. Even with larger window sizes, kNN and Random Forest maintain an accuracy below 70%. In the Waist dataset, Figure 6.9(b) confirms that CNN+LSTM exhibits higher average accuracy than the other algorithms by 2% with the smallest window size and by 8% with the largest one. In all cases, the proposed architecture keeps a superior performance over other approaches.

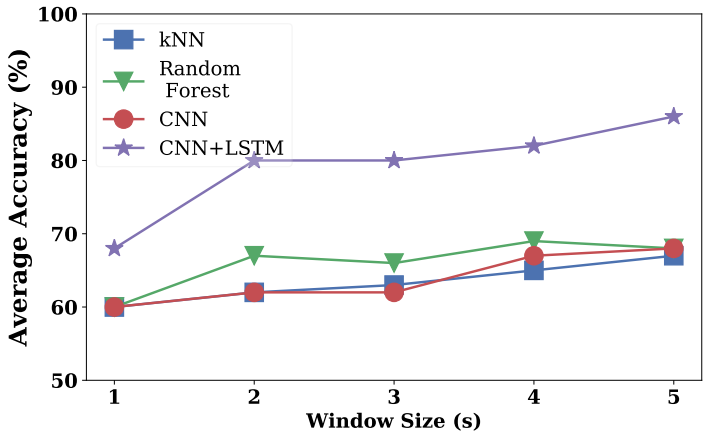

(a) Hand dataset

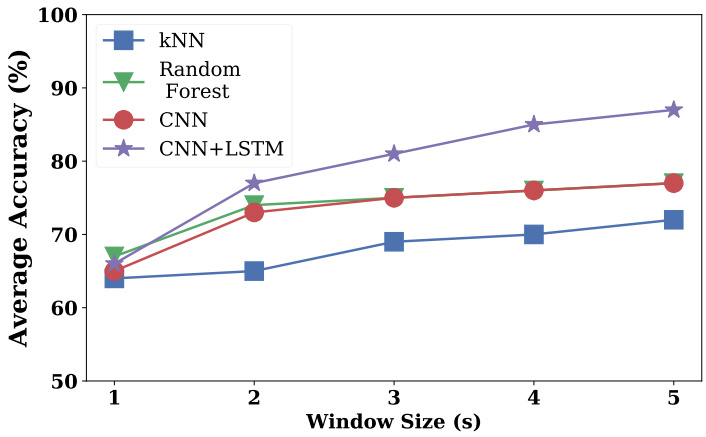

(b) Waist dataset

Figure 6.9: Averaged accuracy of the four classifiers given different window sizes. Regardless of the classifier, the recognition accuracy increases with the window size. The proposed CNN+LSTM model outperforms the other classifiers in each device position.

Effect of Sampling Frequency

Now, I downsample the signals from the leave-one-position-out experiments with new sampling frequencies: 500 Hz, 100 Hz, 50 Hz, and 10 Hz. The respective results of a five-fold cross-validation for all classifiers are plotted in Figures 6.10.

For the Hand dataset (Figure 6.10(a)), it can be observed a severe accuracy drop from 86% to 72% in CNN+LSTM; and even though, this architecture remains with the highest average accuracy for all cases. For the Waist dataset (Figure 6.10(b)), the accuracy drop

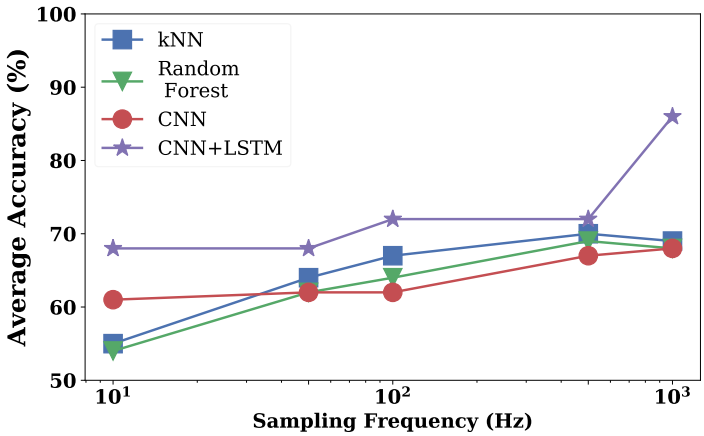

(a) Hand dataset

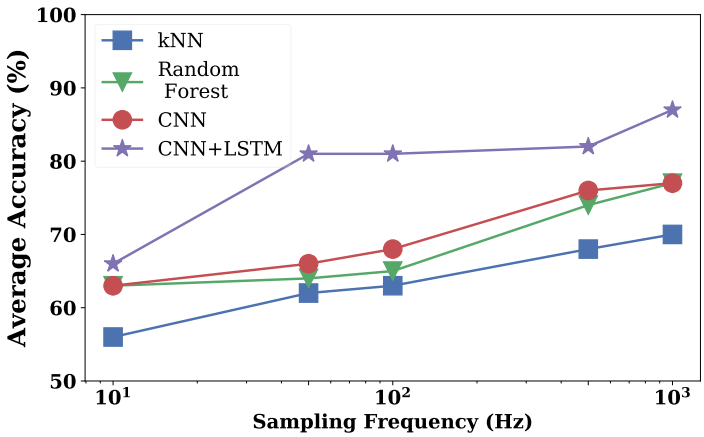

(b) Waist dataset

Figure 6.10: Average accuracies of the four classifiers with different sampling frequencies on the signals of each position dataset. Regardless of the sampling frequency, the accuracy increases with the sampling frequency and the proposed CNN+LSTM architecture outperforms other classifiers in both device positions.

is only 6%, keeping the difference of at least 10% with the other algorithms in all sampling frequencies. Performance of all algorithms decreases with sampling frequency; in particular, the accuracy of kNN and Random Forest falls below 60% in both datasets. This detriment is due to the loss of information for the calculation of handcrafted features. Nevertheless, CNN and CNN+LSTM leverage the ability of automatic feature extraction to obtain characteristics from the time series, even when the downsampling goes down to 10 Hz.

6.6.6 Leave-one-subject-out Experiments

Now, I study the performance of the classifiers when they are tested with data from an unknown subject. This scenario consists of a ten-fold cross-validation, where each fold corresponds to the data of a subject. In an iterative fashion, each subject is left out for testing, while the remaining nine are used for training (eight subjects) and validation (one subject).

Also, these experiments differ from the leave-one-position-out in the number of instances per class. In this case, the amount of instances per class is not truncated, but instead, it is left as in the original KEH dataset. However, the data is separated by the on-body device position, like in leave-one-position-out. Thus, the average F-score across subjects for the Hand and Waist datasets (before and after augmenting the training datasets) are reported in Figure 6.11. In this case, F-score takes into account the amount of instances per class; hence, the reported result are weighted averages over all classes.

Figure 6.11 corroborates the superior performance of CNN+LSTM in this approach without bias towards classes with more instances. In the Hand dataset, CNN+LSTM outperforms the other algorithms by at least 5%, while in the Hand dataset the margin is at minimum 4%. As in the leave-one-location-out experiments, kNN and Random Forest exhibit modest improvements between 1% and 7% after data augmentation is applied on the training datasets. However, CNN and CNN+LSTM leverage augmentation presenting F-score improvements of 10% and 23% in Hand, and 32% and 24% in Waist, respectively.

Although the F-score seems to exhibit a pessimist picture of the systems, it helps to assess the strength and pitfalls of the classifiers when there is no bias towards classes with more instances. When the metric is change to accuracy, the superiority of the proposed architecture is more evident, as shown in Figure 6.12.

The accuracies reported in Figures 6.12(a) and 6.12(b) are the average after taking each one of the ten subjects as testing dataset, before and after augmenting the testing dataset. The proposed CNN+LSTM architecture exhibits an average accuracy of 76% in Figure 6.12(a), which 8% above CNN and 13% above kNN and Random Forest. Similarly, Figure 6.12(b) evinces an accuracy margin of 8% between CNN+LSTM and CNN, and 18% between CNN+LSTM and conventional handcrafted feature-based algorithms. As in the leave-one-position-out experiments, these results also show how the deep learning archi-

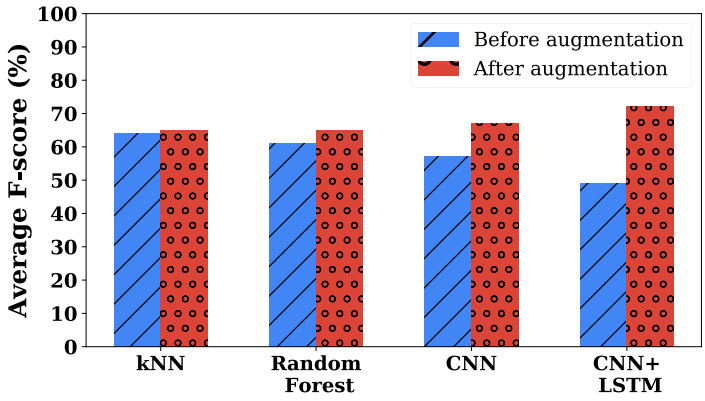

(a) Hand dataset

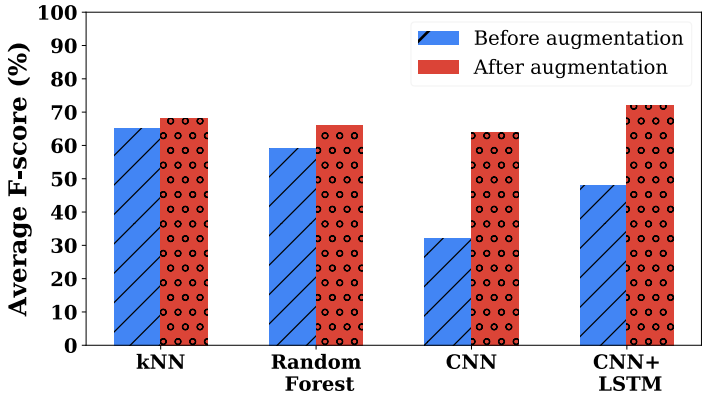

(b) Waist dataset

Figure 6.11: Average F-score for the leave-one-subject-out scenario before and after augmenting the training datasets. Without the bias towards classes with more instances, CNN+LSTM still outperforms other algorithms and takes the most benefit of data augmentation.

tectures leverage the increasing of the variance in the training datasets, while conventional algorithms cannot improve their performance significantly with data augmentation.

6.6.7 Transfer Learning Experiments

Below, I examine the performance of the proposed CNN+LSTM architecture when it is exposed to new sensing scenarios. Specifically, I consider the cases when the system is applied to a new subject and deployed at a new body position. Thus, the two scenarios are explained as follows.

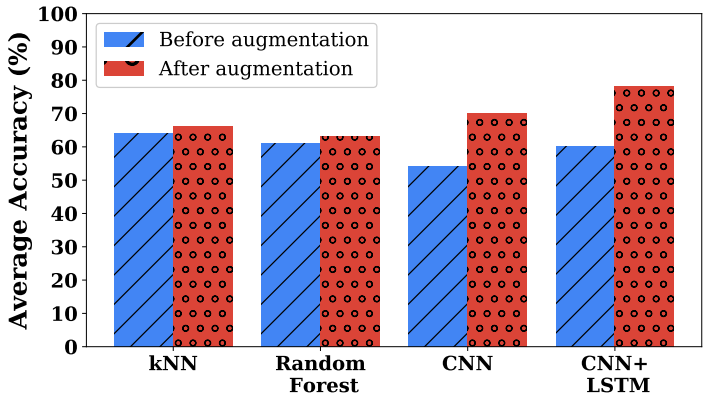

(a) Hand dataset

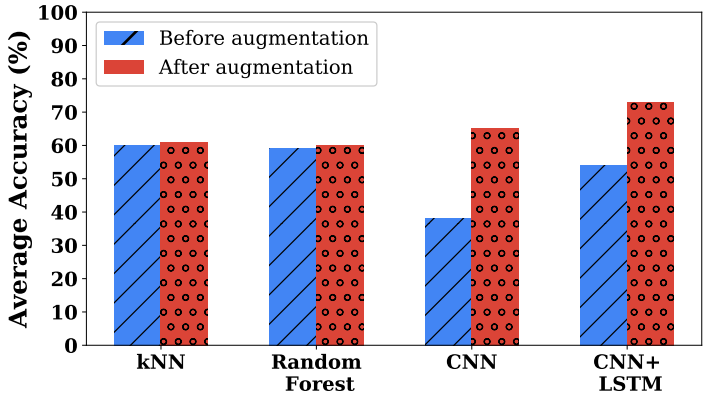

(b) Waist dataset

Figure 6.12: Average accuracy for the leave-one-subject-out scenario before and after augmenting the training datasets. These results highlight the higher performance of CNN+LSTM over the other algorithms when data augmentation is applied on the training datasets.

- **Subject-wise transfer learning**: I take a dataset and split it according to the contribution of each subject. In an iterative ten-fold cross-validation, each subject is considered as the target domain, while the remaining are considered source domain altogether. This approach reflects the capacity of the system to adapt the knowledge from previous subjects to classify data from a new subject.
- **Position-wise transfer learning**: I consider a position dataset as source domain and other as target domain. This situation provides an insight of how the system can adapt to on-body position changes.

Subject-wise Transfer Learning

Now, the following experiments discuss the ability of the CNN+LSTM architecture to transfer knowledge from nine subjects (source domain) to a new subject (target domain), in each position dataset. After a pre-training on the source domain, the weights of the convolutional layers are maintained, and the LSTM and output layer are re-trained with the half of the data from the target domain and tested with the other half. Finally, the average accuracy on each subject as target domain is computed.

To study the effects of applying transfer learning and data augmentation, six cases are considered in each dataset, contained in two sets of three cases depending whether transfer learning is applied or not. For each set, the three cases are: no augmentation, augmentation on source domain and augmentation on both source and target domain. In the case of not applying transfer learning, the first two cases coincide with the leave-one-subject-out experiments for CNN+LSTM. Thus, the six considered cases are: no transfer learning with no augmentation (No TL + No DA), no transfer learning with source domain augmentation (No TL + DA on source domain), no transfer learning with augmentation on both domains (No TL + DA on both domains), transfer learning without data augmentation (TL + No DA), transfer learning with source domain augmentation (TL + DA on source domain) and transfer learning with augmentation on both domains (TL + DA on both domains). The baseline case is No TL + No DA. Figures 6.13(a) and 6.13(b) display the results for the Hand and Waist datasets, respectively.

In both datasets the baseline performance without transfer learning and data augmentation is below 50%. Without data augmentation the system is clearly overfitted to the source domain, since its ability to classify signals from the target domain is very poor and the source domain does nit have the size and intraclass variance to effectively train a deep learning classifier. Thus, transferring knowledge without data augmentation only improves the accuracy in 12% for the Hand and 14% for the Waist dataset. Augmenting the source domain improves the generalization capabilities of the CNN+LSTM architecture, boosting the accuracy up to 77% and 73% for the Hand and Waist datasets, respectively. Transfer learning in this scenario eases the work of the classifier, which reaches accuracies of 86% in both datasets.

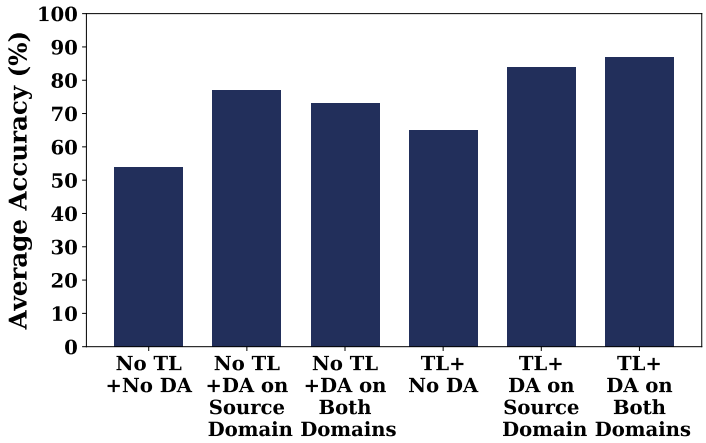

(a) Hand dataset

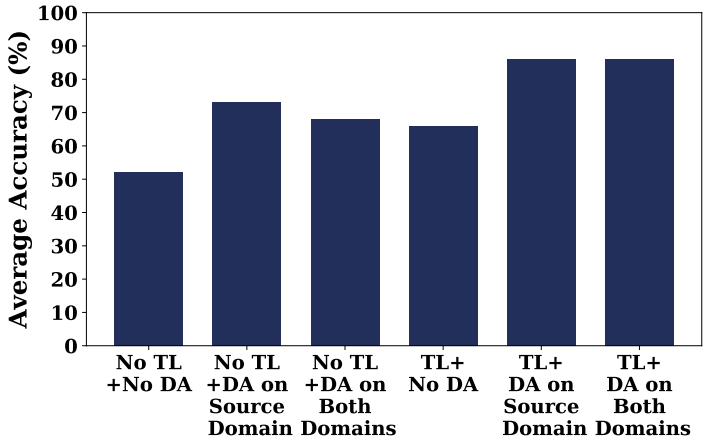

(b) Waist dataset

Figure 6.13: Average accuracy of applying transfer learning in a subject-wise scenario without data augmentation, applying it only on source domain, and applying it on both domains. The proposed transfer learning approach along with the proposed augmentation methods can boost the accuracy to classify data from unknown subjects up to 88%.

Finally, if augmentation is also applied in the target domain, increasing the intraclass variance on the testing set, the classifier exhibits a 4% accuracy detriment in the Hand dataset and 5% with the Waist dataset. However, the classifier reaches its maximum performance when, besides augmenting the target domain, there is knowledge transferred from source domain. Hence, CNN+LSTM obtains average accuracies of 88% and 87% for Hand and Waist, respectively. These results demonstrate the benefits of transfer learning and data augmentation in both domains, even with biased datasets.

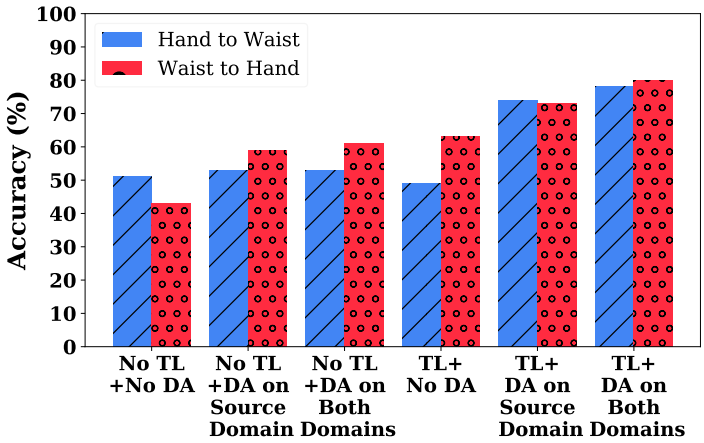

Figure 6.14: Average accuracy of applying transfer learning in a position-wise scenario without data augmentation, applying it only on source domain, and applying it on both domains. The proposed transfer learning approach along with the proposed augmentation methods can boost the accuracy to classify data from unknown positions up to 80%.

Position-wise Transfer Learning

The last set of experiments examines the system capability to adapt to different on-body positions of the device. Therefore, I consider each position dataset as source domain while the other dataset acts as target domain. To observe the effects of transfer learning and data augmentation, the same six cases of the subject-wise scenario are considered. Figure 6.14 resumes the test accuracies for each scenario before and after transfer learning.

Evaluating the classifier with data from another device position, without transfer learning or data augmentation, exhibits a poor performance of 51% training with the hand dataset and testing with waist (*Hand to Waist*), and 43% on the opposite case (*Waist to Hand*). However, data augmentation on source domain improves significantly the *Waist to Hand* case, by a 16%, while the *Hand to Waist*t does by only 2%. Without transfer learning, augmenting the target domain seems to not benefit substantially the classifier, since in *Hand to Waist* there is no change in accuracy and in *Waist to Hand* it only changes from 59% to 61%.

Nevertheless, transfer learning plays a significantly beneficial role for *Waist to Hand* in all augmentation cases: without augmentation, transfer learning induces an improvement from 43% to 63%; augmenting the source domain, the knowledge transference helps to

shift from 59% to 73%; and augmenting both domains the increasing is from 61% to 80%. However, in the case of *Hand to Waist*, the accuracy increment from transfer learning is present after introducing data augmentation: augmenting the source domain, transfer learning increases the accuracy from 53% to 74%; and augmenting both domains, the knowledge transference induces a shift from 53% to 78%. Thus, both final results show how the combination of data augmentation and transfer learning can help to build robust models with consistent performance when the on-body position is changed.

Chapter 7

Conclusion and Future Work

7.1 Research Contributions

- The development of a smart physical workload tracking system that allows health and fitness professionals to monitor several people simultaneously and remotely with a real-time activity recognition accuracy of at least 85%, which is critical in manufacturing and sport industries. To the best of my knowledge, this solution integrating the physical workload concept has not been previously explored (**Chapter 4**).

- The inclusion of a well-known concept from ergonomics (Frimat's criteria) into a real-time e-health application. This is achieved by embedding the workload computation and activity classification on a mobile application that integrates the signal from a hip-placed accelerometer and a wrist-placed photoplethysmography sensor. To the best of my knowledge, this approach has not been presented before (**Chapter 4**).

- A case study is presented regarding the physical progress of a volunteer by tracking his physical workload for twenty days while he performs the same routine. This case study evidences that Frimat's score can provide enough information to determine the level of fitness progress of a person that intends to train using physically demanding exercises (**Chapter 4**).

- A novel approach to measure the harvested power from a piezoelectric generator using the conditions of input voltage and current imposed by its load. The ab-

sence of a fixed linear load motivates this method where currents on the order of microamperes are measured by studying the behavior of the piezoelectric generator with a nonlinear load (**Chapter 5**).

- A wrist-worn piezoelectric harvesting-based battery charger for wearable applications. This prototype is tested with daily activities to assess its harvesting capabilities under human motion excitation. The results provide insights on the feasibility of using commercial piezoelectric harvesters for self-powered wearables. (**Chapter 5**).

- A deep learning architecture to improve existing classification accuracy of KEH-based activity recognition. This architecture outperforms existing approaches presented in the literature by up to 17% when the KEH device is located in the hand of the subjects, and by 10% when it is located in the waist. Moreover, the proposed classifier outperforms other algorithms with margins up to 15% of accuracy under changes of signal observation window size and sampling frequency reductions (**Chapter 6**).

- Three data augmentation methods that allow the creatation of synthetic waveforms simulating new users wearing the kinetic harvester. These methods enable the superior performance of the deep learning architecture. Chapter 6 shows how these methods do not change the signal classification but, instead, they help to increase the generalization capability of the classifier (**Chapter 6**).

- Two transfer learning approaches to obtain subject-independent and location-independent models. Additionally, the impact of combining transfer learning with data augmentation to improve classification accuracy is studied. This combination results in an improvement of 19% when the classifier is exposed to data from a unknown location or subject (**Chapter 6**).

7.2 Future Directions

- **Personalized inference of physical workload:** The healthcare application presented in Chapter 3 regarding physical workload computation can be extended to

the design of workstations. Recommendation systems are well-known in the field of machine learning for using clustering algorithms to provide suggestions based on subject preferences. Thus, the history of a subject's activity and workload data can be used to feed a predictor that models the physical exigency of certain job or workstation for the subject. Additionally, this line of work can be applied in sports to model the performance of an athlete and serve as an auxiliary mechanism to find aspects of improvement, e.g. activities of their sport were the physical demand perceived by the body has to decrease in order to be more effective. The challenges of a development for this application would be related to the design of the prediction system and the ability of the system to evolve its knowledge as the physical performance of a subject evolves.

- **Data augmentation of kinetic harvesting signals with generative adversarial networks:** In computer vision, generative adversarial networks (GANs) have been progressively used to augment image datasets in several medical applications where anomaly images are hard to obtain. Hence, GANs can be configured to augment KEH datasets. In principle, GANs learn the characteristics of each class of KEH signals and then acquire the ability to generate new waveforms that maintain those characteristics. This solution may overcome the limited intraclass variance that the proposed methods in Chapter 6 exhibit. Subsequently, GANs could be able to augment datasets more than is shown in Chapter 6 and the classification performance with deep learning architectures can be higher. Moreover, this approach might be employed to improve transfer learning by obtaining synthetic data that simulates the new device location or a new subject. However, achieving this resemblance of new conditions requires data to train the GAN, which can lead to use other data augmentation methods to facilitate this training process. Possible challenges come with network tuning and training to achieve the mentioned augmentation goals.

- **MEMS integration of multi-axis piezoelectric harvesting for context recognition:** One of the main advantages of piezoelectric harvesting over other kinetic technologies is the compatibility with MEMS. On the other hand, context sensing with kinetic harvesting signals can be improved significantly improved with

information from multi-axis sensing instead of the existing single-axis approaches. Hence, replacing tri-axial accelerometers with multi-axis piezoelectric harvesters in MEMS is a method to eliminate the power consumption by a motion sensor, have a supplementary or primary energy source in the harvester and obtain better sensing results than the existing developments in the literature. Challenges regarding the harvester durability can appear, since thin piezoelectric material can deteriorate rapidly when they are exposed to constant bending.

- **Kinetic harvesting-based motion recognition for gaming applications:** Modern virtual reality systems and gaming consoles rely on motion tracking to provide an attractive user experience. Implementing kinetic energy harvesting to enable self-powered devices, relying on KEH-based motion recognition, might be a promising application for the developments shown in this thesis. Challenges regarding the user-dependent motion intensity and device posture recognition could arise, requiring multi-axis harvesting and advanced classification techniques to allow a reliable performance. Moreover, gaming applications demand low-latency systems, setting a non-negotiable characteristic for the developments towards this area.

Bibliography

[1] Alexandro Pando, *Wearable Health Technologies And Their Impact On The Health Industry*, New York, NY, USA, May 2019. [Online]. Available: https://www.forbes.com/sites/forbestechcouncil/2019/05/02/wearable-health-technologies-and-their-impact-on-the-health-industry/%7B%5C#%7D4eac185f3af5.

[2] T. L. Hedrick, T. E. Hassinger, E. Myers, E. D. Krebs, D. Chu, A. N. Charles, S. C. Hoang, C. M. Friel, and R. H. Thiele, "Wearable Technology in the Perioperative Period: Predicting Risk of Postoperative Complications in Patients Undergoing Elective Colorectal Surgery," *Diseases of the Colon & Rectum*, vol. 63, no. 4, 2020, ISSN: 0012-3706.

[3] K. Deranek, B. Hewitt, A. Gudi, and A. McLeod, "The impact of exercise motives on adolescents' sustained use of wearable technology," *Behaviour & Information Technology*, vol. 0, no. 0, pp. 1–15, 2020. DOI: 10.1080/0144929X.2020.1720295.

[4] H. Goto, T. Sugiura, Y. Harada, and T. Kazui, "Feasibility of using the automatic generating system for quartz watches as a leadless pacemaker power source," *Medical and Biological Engineering and Computing*, vol. 37, no. 3, pp. 377–380, 1999, ISSN: 01400118. DOI: 10.1007/BF02513315.

[5] E. Jovanov, a. Milenkovic, C. Otto, P. C. de Groen, B. Johnson, S. Warren, and G. Taibi, "A WBAN System for Ambulatory Monitoring of Physical Activity and Health Status: Applications and Challenges," *27th Annual International Conference of the Engineering in Medicine and Biology Society, 2005. IEEE-EMBS 2005.*, pp. 4–7, 2005.

[6] S. Hemminki, P. Nurmi, and S. Tarkoma, "Accelerometer-based transportation mode detection on smartphones," in *Proceedings of the 11th ACM conference on embedded networked sensor systems*, 2013, pp. 1–14.

[7] A. Ahmadi, E. Mitchell, C. Richter, F. Destelle, M. Gowing, N. E. O'Connor, and K. Moran, "Toward automatic activity classification and movement assessment during a sports training session," *IEEE Internet of Things Journal*, vol. 2, no. 1, pp. 23–32, 2015, ISSN: 23274662. DOI: 10.1109/JIOT.2014.2377238.

[8] N. Jablonsky, S. McKenzie, S. Bangay, and T. Wilkin, "Evaluating sensor placement and modality for activity recognition in active games," in *Proceedings of the Australasian Computer Science Week Multiconference*, 2017, pp. 1–8.

[9] O. D. Lara and M. A. Labrador, "A survey on human activity recognition using wearable sensors.," *IEEE Communications Surveys and Tutorials*, vol. 15, no. 3, pp. 1192–1209, 2013.

[10] F. Albinali, S. Intille, W. Haskell, and M. Rosenberger, "Using wearable activity type detection to improve physical activity energy expenditure estimation," in *Proceedings of the 12th ACM international conference on Ubiquitous computing*, ACM, 2010, pp. 311–320.

[11] B. H. Dobkin and C. Martinez, "Wearable Sensors to Monitor, Enable Feedback, and Measure Outcomes of Activity and Practice," *Current Neurology and Neuroscience Reports*, 2018. DOI: 10.1007/s11910-018-0896-5.

[12] J. Manjarrés, V. Russo, J. Peñaranda, and M. Pardo, "Human Activity and Heart Rate Monitoring System in a Mobile Platform," in *2018 Congreso Internacional de Innovación y Tendencias en Ingenieria (CONIITI)*, IEEE, 2018, pp. 1–6.

[13] Z. Wang, C. Zhao, and S. Qiu, "A system of human vital signs monitoring and activity recognition based on body sensor network," *Sensor Review*, vol. 34, no. 1, pp. 42–50, 2014, ISSN: 02602288. DOI: 10.1108/SR-12-2012-735.

[14] Ó. D. Lara, A. J. Prez, M. A. Labrador, and J. D. Posada, "Centinela: A human activity recognition system based on acceleration and vital sign data," *Pervasive and Mobile Computing*, vol. 8, no. 5, pp. 717–729, 2012, ISSN: 15741192. DOI:

10.1016/j.pmcj.2011.06.004.

[15] A. J. Dababneh, N. Swanson, and R. L. Shell, "Impact of added rest breaks on the productivity and well being of workers," *Ergonomics*, vol. 44, no. 2, pp. 164–174, 2001, ISSN: 13665847. DOI: 10.1080/00140130121538.

[16] J. Selvarathinam and A. Anpalagan, "Energy Harvesting From the Human Body for Biomedical Applications," *IEEE Potentials*, vol. 35, no. 6, pp. 6–12, 2016, ISSN: 0278-6648. DOI: 10.1109/MPOT.2016.2549998.

[17] E. Blokhina and D. Galayko, "Towards autonomous microscale systems: Progress in electrostatic kinetic energy harvesting," *2016 IEEE International Conference on Electronics, Circuits and Systems, ICECS 2016*, pp. 744–747, 2017. DOI: 10.1109/ICECS.2016.7841309.

[18] M. Magno, L. Spadaro, J. Singh, and L. Benini, "Kinetic energy harvesting: Toward autonomous wearable sensing for Internet of Things," *2016 International Symposium on Power Electronics, Electrical Drives, Automation and Motion, SPEEDAM 2016*, pp. 248–254, 2016. DOI: 10.1109/SPEEDAM.2016.7525995.

[19] S. Y. Kuang, J. Chen, X. B. Cheng, G. Zhu, and Z. L. Wang, "Two-dimensional rotary triboelectric nanogenerator as a portable and wearable power source for electronics," *Pervasive Computing*, vol. 17, pp. 10–16, 2015, ISSN: 22112855. DOI: 10.1016/j.nanoen.2015.07.011. arXiv: 1307.0044.

[20] A. Erturk and D. J. Inman, *Piezoelectric Energy Harvesting*. Wiley, 2011, ISBN: 9780470682548. DOI: 10.1002/9781119991151.

[21] P. D. Mitcheson, "Energy harvesting for human wearable and implantable bio-sensors," *2010 Annual International Conference of the IEEE Engineering in Medicine and Biology Society, EMBC'10*, pp. 3432–3436, 2010, ISSN: 1557-170X. DOI: 10.1109/IEMBS.2010.5627952.

[22] N. S. Shenck and J. A. Paradiso, "Energy scavenging with shoe-mounted piezoelectrics," *IEEE Micro*, 2001, ISSN: 02721732. DOI: 10.1109/40.928763.

[23] G. Lan, D. Ma, W. Xu, M. Hassan, and W. Hu, "Capsense: Capacitor-based activity sensing for kinetic energy harvesting powered wearable devices," in *Proc. EAI*

14th Int. Conf. Mobile Ubiquitous Syst., Comput., Netw. Services (Mobiquitous), 2017, pp. 110–119, ISBN: 9781450353687. DOI: 10.475/123.

[24] A. Delnavaz and J. Voix, "Piezo-magnetic energy harvesting from movement of the head," in *Journal of Physics: Conference Series*, vol. 660, Dec. 2015, p. 012 120. DOI: 10.1088/1742-6596/660/1/012120.

[25] A. Olivares, G. Olivares, J. Gorriz, and J. Ramirez, "A study of vibration-based energy harvesting in activities of daily living," *Proceedings of the 4th International ICST Conference on Pervasive Computing Technologies for Healthcare*, 2010. DOI: 10.4108/ICST.PERVASIVEHEALTH2010.8808.

[26] M. Lee, C. Y. Chen, S. Wang, S. N. Cha, Y. J. Park, J. M. Kim, L. J. Chou, and Z. L. Wang, "A hybrid piezoelectric structure for wearable nanogenerators," *Advanced Materials*, 2012, ISSN: 15214095. DOI: 10.1002/adma.201200150.

[27] J. M. Donelan, Q. Li, V. Naing, J. A. Hoffer, D. J. Weber, and A. D. Kuo, "Biomechanical energy harvesting: Generating electricity during walking with minimal user effort," *Science*, vol. 319, no. 5864, pp. 807–810, 2008, ISSN: 00368075. DOI: 10.1126/science.1149860.

[28] M. Wahbah, M. Alhawari, B. Mohammad, H. Saleh, and M. Ismail, "Characterization of human body-based thermal and vibration energy harvesting for wearable devices," *IEEE Journal on Emerging and Selected Topics in Circuits and Systems*, vol. 4, no. 3, pp. 354–363, 2014, ISSN: 21563357. DOI: 10.1109/JETCAS.2014.2337195.

[29] S. Priya and D. J. Inman, *Energy Harvesting Technologies*, 1st ed. New York: Springer, 2009, p. 522, ISBN: 9780387764634. DOI: 10.1007/978-0-387-76464-1.

[30] E. Lefeuvre, M. Lallart, C. Richard, and D. Guyomar, "Piezoelectric Material-Based Energy Harvesting Devices: Advance of SSH Optimization Techniques (1999-2009)," *Piezoelectric Ceramics*, pp. 165–184, 2010. DOI: 10.5772/9945.

[31] M. Hassan, W. Hu, G. Lan, A. Seneviratne, S. Khalifa, and S. K. Das, "Kinetic-Powered Health Wearables: Challenges and Opportunities," *Computer*, vol. 51, no. 9, pp. 64–74, 2018, ISSN: 0018-9162 VO - 51. DOI: 10.1109/MC.2018.3620960.

[32] S. Khalifa, M. Hassan, A. Seneviratne, and S. K. Das, "Energy-Harvesting Wearables for Activity-Aware Services," *IEEE Internet Computing*, vol. 19, no. 5, pp. 8–16, 2015, ISSN: 10897801. DOI: 10.1109/MIC.2015.115.

[33] S. Khalifa, M. Hassan, and A. Seneviratne, "Pervasive self-powered human activity recognition without the accelerometer," *2015 IEEE International Conference on Pervasive Computing and Communications, PerCom 2015*, pp. 79–86, 2015. DOI: 10.1109/PERCOM.2015.7146512.

[34] M. Gorlatova, J. Sarik, G. Grebla, M. Cong, I. Kymissis, and G. Zussman, "Movers and Shakers: Kinetic Energy Harvesting for the Internet of Things," *IEEE Journal on Selected Areas in Communications*, vol. 33, no. 8, pp. 1624–1639, 2015, ISSN: 0733-8716. DOI: 10.1109/JSAC.2015.2391690.

[35] Y. Lecun, Y. Bengio, and G. Hinton, *Deep learning*, 2015. DOI: 10.1038/nature14539.

[36] I. Goodfellow, Y. Bengio, and A. Courville, *Deep Learning*. MIT Press, 2016.

[37] T. Föhr, J. Pietilä, E. Helander, T. Myllymäki, H. Lindholm, H. Rusko, and U. M. Kujala, "Physical activity, body mass index and heart rate variability-based stress and recovery in 16 275 Finnish employees: A cross-sectional study," *BMC Public Health*, vol. 16, no. 1, 2016, ISSN: 14712458. DOI: 10.1186/s12889-016-3391-4.

[38] J. Choi and G. O. Ricardo, "Using heart rate monitors to detect mental stress," in *Proceedings - 2009 6th International Workshop on Wearable and Implantable Body Sensor Networks, BSN 2009*, 2009, pp. 219–223, ISBN: 9780769536446. DOI: 10.1109/BSN.2009.13.

[39] B. M. Rosa and G. Z. Yang, "Smart wireless headphone for cardiovascular and stress monitoring," *2017 IEEE 14th International Conference on Wearable and Implantable Body Sensor Networks, BSN 2017*, pp. 75–78, 2017. DOI: 10.1109/BSN.2017.7936011.

[40] E. Jovanov, K. Frith, F. Anderson, M. Milosevic, and M. T. Shrove, "Real-time monitoring of occupational stress of nurses," *Proceedings of the Annual International Conference of the IEEE Engineering in Medicine and Biology Society, EMBS*,

pp. 3640–3643, 2011, ISSN: 1557170X. DOI: 10.1109/IEMBS.2011.6090612.

[41] M. Bolanos, H. Nazeran, and E. Haltiwanger, "Comparison of heart rate variability signal features derived from electrocardiography and photoplethysmography in healthy individuals," in *Annual International Conference of the IEEE Engineering in Medicine and Biology - Proceedings*, 2006, pp. 4289–4294, ISBN: 1424400325. DOI: 10.1109/IEMBS.2006.260607.

[42] F. X. Gamelin, S. Berthoin, and L. Bosquet, "Validity of the polar S810 Heart rate monitor to measure R-R intervals at rest," *Medicine and Science in Sports and Exercise*, vol. 38, no. 5, pp. 887–893, 2006, ISSN: 01959131. DOI: 10.1249/01.mss.0000218135.79476.9c.

[43] J. Hendrikx, L. S. Ruijs, L. G. Cox, P. M. Lemmens, E. G. Schuijers, and A. H. Goris, "Clinical Evaluation of the Measurement Performance of the Philips Health Watch: A Within-Person Comparative Study," *JMIR mHealth and uHealth*, vol. 5, no. 2, 2017, ISSN: 2291-5222. DOI: 10.2196/mhealth.6893.

[44] E. Khan, F. Al Hossain, S. Z. Uddin, S. K. Alam, and M. K. Hasan, "A Robust Heart Rate Monitoring Scheme Using Photoplethysmographic Signals Corrupted by Intense Motion Artifacts," *IEEE Transactions on Biomedical Engineering*, vol. 63, no. 3, pp. 550–562, 2016, ISSN: 15582531. DOI: 10.1109/TBME.2015.2466075.

[45] H. H. Asada, P. Shaltis, A. Reisner, S. Rhee, and R. C. Hutchinson, "Mobile Monitoring with Wearable Photoplethysmographic Biosensors," *IEEE Engineering in Medicine and Biology Magazine*, vol. 22, no. 3, pp. 28–40, 2003, ISSN: 07395175. DOI: 10.1109/MEMB.2003.1213624.

[46] M. Aileni Raluca, S. Pasca, and R. Strungaru, "Heart rate monitoring by using non-invasive wearable sensor," in *E-Health and Bioengineering Conference (EHB), 2017*, IEEE, 2017, pp. 587–590, ISBN: 9781538603581.

[47] P. Narváez, J. Manjarrés, W. Percybrooks, M. Pardo, and M. Calle, "Assessing the Level of Physical Activity in the Workplace: A Case Study With Wearable Technology," *International Journal of Interdisciplinary Telecommunications and Networking (IJITN)*, vol. 11, no. 1, pp. 44–56, 2019.

[48] J. Arana T.; Velasquez and C. R., "Determinacion de la capacidad y la carga fisica de trabajo en bailarines de una escuela de baile de la ciudad de Cali," *Ciencia & Salud*, vol. 1, no. 4, pp. 11–16, 2013.

[49] H. Zapata, G. L. Arango., and L. M. Estrada, "Valoración de carga física en estibadores de una cooperativa de trabajo asociado," *Revista Facultad Nacional de Salud Pública*, vol. 29, pp. 53–64, 2011, ISSN: 0120-386X.

[50] M. Romero, C. Fernández, and A. Ballesteros, "Evaluación de la carga física de trabajo, mediante la monitorización de la frecuencia cardíaca, en auxiliares de Enfermería de una residencia geriátrica municipal," *Revista Enfermería del Trabajo*, vol. 1, no. 4, pp. 193–202, 2011.

[51] J. A. Castillo and Á. Cubillos, "Using Pulse Rate in Estimating Workload: Evaluating a Load Mobilizing Activity," *Revista Ciencias de la Salud*, vol. 12, pp. 27–43, 2014, ISSN: 1692-7273.

[52] M. A. Labrador and O. D. Lara, *Human Activity Recognition: Using Wearable Sensors and Smartphones*, 1st. CRC Press, 2013, ISBN: 3-540-30506-8.

[53] M. Jongprasithporn, N. Yodpijit, R. Srivilai, and P. Pongsophane, "A smartphone-based real-time simple activity recognition," *2017 3rd International Conference on Control, Automation and Robotics, ICCAR 2017*, pp. 539–542, 2017. DOI: 10.1109/ICCAR.2017.7942755.

[54] O. M. Prabowo, K. Mutijarsa, and S. H. Supangkat, "Missing Data Handling using Machine Learning for Human Acitivity Recognition on Mobile Device," in *2016 International Conference on ICT For Smart Society*, 2016, pp. 20–21, ISBN: 9781509016204.

[55] J. C. Quiroz, A. Banerjee, S. M. Dascalu, and S. L. Lau, "Feature Selection for Activity Recognition from Smartphone Accelerometer Data," *Intelligent Automation and Soft Computing*, pp. 1–9, 2017, ISSN: 2326005X. DOI: 10.1080/10798587.2017.1342400.

[56] D. Yazdansepas, A. H. Niazi, J. L. Gay, F. W. Maier, L. Ramaswamy, K. Rasheed, and M. P. Buman, "A Multi-featured Approach for Wearable Sensor-Based

Human Activity Recognition," *2016 IEEE International Conference on Healthcare Informatics (ICHI)*, pp. 423–431, 2016. DOI: 10.1109/ICHI.2016.81.

[57] A. Bulling, U. Blanke, and B. Schiele, "A tutorial on human activity recognition using body-worn inertial sensors," *ACM Computing Surveys*, vol. 46, no. 3, pp. 1–33, 2014, ISSN: 03600300. DOI: 10.1145/2499621.

[58] X. L. X. Long, B. Y. B. Yin, and R. Aarts, "Single-accelerometer-based daily physical activity classification," *2009 Annual International Conference of the IEEE Engineering in Medicine and Biology Society*, pp. 6107–6110, 2009, ISSN: 1557-170X. DOI: 10.1109/IEMBS.2009.5334925.

[59] A. Babu, K. Dube, S. Mukhopadhyay, H. Ghayvat, P. S. Mukhopadhyay, H. Ghayvat, J. K. M. V, S. Mukhopadhyay, and H. Ghayvat, "Accelerometer based human activities and posture recognition," in *2016 International Conference on Data Mining and Advanced Computing (SAPIENCE)*, Mar. 2016, pp. 367–373. DOI: 10.1109/SAPIENCE.2016.7684120.

[60] X. Liu, L. Liu, S. J. Simske, and J. Liu, "Human Daily Activity Recognition for Healthcare Using Wearable and Visual Sensing Data," *... Informatics (ICHI), 2016 IEEE ...*, pp. 24–31, 2016. DOI: 10.1109/ICHI.2016.100.

[61] M. Z. Uddin and M. M. Hassan, "Activity Recognition for Cognitive Assistance Using Body Sensors Data and Deep Convolutional Neural Network," *IEEE Sensors Journal*, 2018, ISSN: 1530-437X. DOI: 10.1109/JSEN.2018.2871203.

[62] S. L. Lau, I. König, K. David, B. Parandian, C. Carius-Düssel, and M. Schultz, "Supporting patient monitoring using activity recognition with a smartphone," in *Proceedings of the 2010 7th International Symposium on Wireless Communication Systems, ISWCS'10*, 2010, pp. 810–814, ISBN: 9781424463169. DOI: 10.1109/ISWCS.2010.5624490.

[63] W. S. Jung, M. J. Lee, M. G. Kang, H. G. Moon, S. J. Yoon, S. H. Baek, and C. Y. Kang, "Powerful curved piezoelectric generator for wearable applications," *Nano Energy*, 2015, ISSN: 22112855. DOI: 10.1016/j.nanoen.2015.01.051.

[64] B. Yang and K. Yun, "Efficient energy harvesting from human motion using

wearable piezoelectric shell structures," *Solid-State Sensors, Actuators and Microsystems Conference (TRANSDUCERS), 2011 16th International*, pp. 2646–2649, 2011. DOI: 10.1109/TRANSDUCERS.2011.5969874.

[65] E. Iranmanesh, A. Rasheed, W. Li, and K. Wang, "A Wearable Piezoelectric Energy Harvester Rectified by a Dual-Gate Thin-Film Transistor," *IEEE Transactions on Electron Devices*, vol. 65, no. 2, pp. 542–546, 2018, ISSN: 00189383. DOI: 10.1109/TED.2017.2780261.

[66] M. Beyaz, "Energy Harvesting from Knee Motion Using Piezoelectric Patch Transducers," *Academic Platform Journal of Engineering and Science*, vol. 7, no. 2, pp. 255–260, May 2019. DOI: 10.21541/apjes.449102.

[67] M. Pozzi and M. Zhu, "Characterization of a rotary piezoelectric energy harvester based on plucking excitation for knee-joint wearable applications," *Smart Materials and Structures*, vol. 21, no. 5, p. 055 004, May 2012, ISSN: 0964-1726. DOI: 10.1088/0964-1726/21/5/055004.

[68] P. Pillatsch, E. M. Yeatman, and A. S. Holmes, "A wearable piezoelectric rotational energy harvester," *2013 IEEE International Conference on Body Sensor Networks, BSN 2013*, no. 1, 2013. DOI: 10.1109/BSN.2013.6575470.

[69] S. Khalifa, G. Lan, M. Hassan, and W. Hu, "A Bayesian framework for energy-neutral activity monitoring with self-powered wearable sensors," *2016 IEEE International Conference on Pervasive Computing and Communication Workshops, PerCom Workshops 2016*, pp. 1–6, 2016. DOI: 10.1109/PERCOMW.2016.7457112.

[70] A. Ignatov, "Real-time human activity recognition from accelerometer data using Convolutional Neural Networks," *Applied Soft Computing Journal*, vol. 62, pp. 915–922, 2018, ISSN: 15684946. DOI: 10.1016/j.asoc.2017.09.027.

[71] W. Jiang and Z. Yin, "Human activity recognition using wearable sensors by deep convolutional neural networks," *MM 2015 - Proceedings of the 2015 ACM Multimedia Conference*, pp. 1307–1310, 2015. DOI: 10.1145/2733373.2806333.

[72] N. Y. Hammerla, S. Halloran, and T. Plötz, "Deep, convolutional, and recurrent models for human activity recognition using wearables," *IJCAI International Joint*

Conference on Artificial Intelligence, vol. 2016-Janua, pp. 1533–1540, 2016, ISSN: 10450823. arXiv: 1604.08880.

[73] F. J. Ordóñez and D. Roggen, "Deep convolutional and LSTM recurrent neural networks for multimodal wearable activity recognition," *Sensors (Switzerland)*, vol. 16, no. 1, 2016, ISSN: 14248220. DOI: 10.3390/s16010115.

[74] Y. Guan and T. Plötz, "Ensembles of Deep LSTM Learners for Activity Recognition using Wearables," *Proceedings of the ACM on Interactive, Mobile, Wearable and Ubiquitous Technologies*, vol. 1, no. 2, pp. 1–28, 2017, ISSN: 2474-9567. DOI: 10.1145/3090076. arXiv: 1703.09370.

[75] T. T. Um, F. M. Pfister, D. Pichler, S. Endo, M. Lang, S. Hirche, U. Fietzek, and D. Kulic, "Data augmentation of wearable sensor data for Parkinson's disease monitoring using convolutional neural networks," *ICMI 2017 - Proceedings of the 19th ACM International Conference on Multimodal Interaction*, vol. 2017-Janua, pp. 216–220, 2017. DOI: 10.1145/3136755.3136817. arXiv: 1706.00527.

[76] G. Forestier, F. Petitjean, H. A. Dau, G. I. Webb, and E. Keogh, "Generating Synthetic Time Series to Augment Sparse Datasets," *IEEE International Conference on Data Mining (ICDM)*, pp. 865–870, 2017.

[77] H. Ismail Fawaz, G. Forestier, J. Weber, L. Idoumghar, and P.-A. Muller, "Data augmentation using synthetic data for time series classification with deep residual networks," in *International Workshop on Advanced Analytics and Learning on Temporal Data*, 2018.

[78] S. A. Rokni and H. Ghasemzadeh, "Autonomous Training of Activity Recognition Algorithms in Mobile Sensors: A Transfer Learning Approach in Context-Invariant Views," *IEEE Transactions on Mobile Computing*, vol. 17, no. 8, pp. 1764–1777, 2018, ISSN: 15361233. DOI: 10.1109/TMC.2018.2789890.

[79] B. Chikhaoui, F. Gouineau, and M. Sotir, "A CNN based transfer learning model for automatic activity recognition from accelerometer sensors," in *Lecture Notes in Computer Science (including subseries Lecture Notes in Artificial Intelligence and Lecture Notes in Bioinformatics)*, 2018, ISBN: 9783319961323. DOI: 10.1007/978-

3-319-96133-0_23.

[80] F. J. O. Morales and D. Roggen, "Deep convolutional feature transfer across mobile activity recognition domains, sensor modalities and locations," *International Symposium on Wearable Computers, Digest of Papers*, vol. 12-16-Sept, pp. 92–99, 2016. DOI: 10.1145/2971763.2971764.

[81] J. Wang, Y. Chen, V. W. Zheng, and M. Huang, "Deep Transfer Learning for Cross-domain Activity Recognition," *ACM International Conference Proceeding Series*, 2018. DOI: 10.1145/3265689.3265705. arXiv: 1807.07963.

[82] D. Abowd, A. K. Dey, R. Orr, and J. Brotherton, "Context-Awareness in Wearable and Ubiquitous Computing," *Virtual Reality*, 1998, ISSN: 14349957. DOI: 10.1007/BF01408562.

[83] F. Foerster, M. Smeja, and J. Fahrenberg, "Detection of posture and motion by accelerometry: a validation study in ambulatory monitoring," *Computers in Human Behavior*, 1999, ISSN: 07475632. DOI: 10.1016/S0747-5632(99)00037-0.

[84] Y. Jia, "Dietetic and exercise therapy against diabetes mellitus," in *ICINIS 2009 - Proceedings of the 2nd International Conference on Intelligent Networks and Intelligent Systems*, 2009, ISBN: 9780769538525. DOI: 10.1109/ICINIS.2009.177.

[85] J. Yin, Q. Yang, and J. J. Pan, "Sensor-based abnormal human-activity detection," in *IEEE Transactions on Knowledge and Data Engineering*, 2008. DOI: 10.1109/TKDE.2007.1042.

[86] J. Liu, L. Zhong, J. Wickramasuriya, and V. Vasudevan, "uWave: Accelerometer-based personalized gesture recognition and its applications," *Pervasive and Mobile Computing*, vol. 5, no. 6, pp. 657–675, 2009.

[87] D. Figo, P. C. Diniz, D. R. Ferreira, and J. M. Cardoso, "Preprocessing techniques for context recognition from accelerometer data," *Personal and Ubiquitous Computing*, 2010, ISSN: 16174909. DOI: 10.1007/s00779-010-0293-9.

[88] N. Ravi, N. Dandekar, P. Mysore, and M. L. Littman, "Activity recognition from accelerometer data," in *Proceedings of the National Conference on Artificial Intelligence*, 2005.

[89] L. Bao and S. S. Intille, "Activity recognition from user-annotated acceleration data," *Lecture Notes in Computer Science (including subseries Lecture Notes in Artificial Intelligence and Lecture Notes in Bioinformatics)*, 2004, ISSN: 03029743. DOI: 10.1007/978-3-540-24646-6_1.

[90] K. Altun and B. Barshan, "Human activity recognition using inertial/magnetic sensor units," in *Lecture Notes in Computer Science (including subseries Lecture Notes in Artificial Intelligence and Lecture Notes in Bioinformatics)*, 2010, ISBN: 3642147143. DOI: 10.1007/978-3-642-14715-9_5.

[91] K. Oh, H. S. Park, and S. B. Cho, "A mobile context sharing system using activity and emotion recognition with Bayesian networks," in *Proceedings - Symposia and Workshops on Ubiquitous, Autonomic and Trusted Computing in Conjunction with the UIC 2010 and ATC 2010 Conferences, UIC-ATC 2010*, 2010, ISBN: 9780769542720. DOI: 10.1109/UIC-ATC.2010.26.

[92] U. Maurer, A. Smailagic, D. P. Siewiorek, and M. Deisher, "Activity recognition and monitoring using multiple sensors on different body positions," in *Proceedings - BSN 2006: International Workshop on Wearable and Implantable Body Sensor Networks*, 2006, ISBN: 0769525474. DOI: 10.1109/BSN.2006.6.

[93] C. Zhu and W. Sheng, "Human daily activity recognition in robot-assisted living using multi-sensor fusion," in *Proceedings - IEEE International Conference on Robotics and Automation*, 2009, ISBN: 9781424427895. DOI: 10.1109/ROBOT.2009.5152756.

[94] L. C. Jatobá, U. Großmann, C. Kunze, J. Ottenbacher, and W. Stork, "Context-aware mobile health monitoring: Evaluation of different pattern recognition methods for classification of physical activity," in *Proceedings of the 30th Annual International Conference of the IEEE Engineering in Medicine and Biology Society, EMBS'08 - "Personalized Healthcare through Technology"*, 2008, ISBN: 9781424418152. DOI: 10.1109/iembs.2008.4650398.

[95] J. Wang, Y. Chen, S. Hao, X. Peng, and L. Hu, "Deep learning for sensor-based activity recognition: A survey," *Pattern Recognition Letters*, vol. 119, pp. 3–11,

2019, ISSN: 01678655. DOI: 10.1016/j.patrec.2018.02.010. arXiv: 1707.03502.

[96] Y. Bengio, "Deep Learning of Representations for Unsupervised and Transfer Learning," in *JMLR: Workshop and Conference Proceedings*, 2011, ISBN: 9780971977778.

[97] G. E. Hinton, S. Osindero, and Y. W. Teh, "A fast learning algorithm for deep belief nets," *Neural Computation*, 2006, ISSN: 08997667. DOI: 10.1162/neco.2006.18.7.1527.

[98] A. Wang, G. Chen, C. Shang, M. Zhang, and L. Liu, "Human activity recognition in a smart home environment with stacked denoising autoencoders," in *Lecture Notes in Computer Science (including subseries Lecture Notes in Artificial Intelligence and Lecture Notes in Bioinformatics)*, 2016, ISBN: 9783319471204. DOI: 10.1007/978-3-319-47121-1_3.

[99] H. F. Nweke, Y. W. Teh, M. A. Al-garadi, and U. R. Alo, "Deep learning algorithms for human activity recognition using mobile and wearable sensor networks: State of the art and research challenges," *Expert Systems with Applications*, vol. 105, pp. 233–261, 2018, ISSN: 09574174. DOI: 10.1016/j.eswa.2018.03.056.

[100] D. Ravi, C. Wong, B. Lo, and G. Z. Yang, "Deep learning for human activity recognition: A resource efficient implementation on low-power devices," *BSN 2016 - 13th Annual Body Sensor Networks Conference*, pp. 71–76, 2016. DOI: 10.1109/BSN.2016.7516235.

[101] World Health Organization, "Work organisation and Stress," *Protecting Workers Health*, no. 3, pp. 1–27, 2003, ISSN: 13665847. DOI: 92415904751729-3499.

[102] R. D. Caplan and K. W. Jones, "Effects of work load, role ambiguity, and type A personality on anxiety, depression, and heart rate.," *The Journal of applied psychology*, vol. 60, no. 6, pp. 713–719, 1975, ISSN: 0021-9010. DOI: 10.1037/0021-9010.60.6.713.

[103] J. Taelman, S. Vandeput, A. Spaepen, and S. Van Huffel, "Influence of mental stress on Heart Rate and Heart Rate Variability," in *4th European conference of the international federation for medical and biological engineering (IFMBE)*, 2008, pp. 1366–1369, ISBN: 978-3-540-89207-6. DOI: 10.1007/978-3-540-89208-3_324.

[104] A. De la Iglesia, J. Gómez, R. Sáenz, and C. Ruiz, "Carga de trabajo físico y costo cardiaco: La freuencia cardiaca de referencia," *Revista Salud y Trabajo*, vol. 106, no. 1, pp. 16–21, 1994.

[105] M. D. Solé, "NTP 295 : Valoración de la carga física mediante la monitorización de la frecuencia cardiaca," *Ministerio de Trabajo y Asuntos Sociales Espanã; Instituto Nacional de Seguridad e Higiene en el Trabajo*, 2004.

[106] P. Frimat, M. Amphoux, and A. Chamoux, "Interprétation et mesure de la fréquence cardiaque," *Revue deMedicine du Travail XV (4)*, vol. 147, p. 165, 1988.

[107] P. Frimat, D. Furon, A. Cantineau, P. Delepine, F. Six, and G. Luez, "Le travail à la chaleur (verrerie). Etude de la charge de travail par ECG dynamique. Applications de la Méthode de VOGT," *Arch. Mal. Prof*, vol. 40, no. 1-2, p. 191, 1979.

[108] Simblee Corp., "Simblee Bluetooth Smart Module RFD77101 Datasheet," Tech. Rep., 2015, pp. 1–16.

[109] Microsoft, *Microsoft Band Features*, 2017. [Online]. Available: `https://www.microsoft.com/microsoft-band/en-us/features` (visited on 08/30/2017).

[110] S. E. Stahl, H.-S. An, D. M. Dinkel, J. M. Noble, and J.-M. Lee, "How accurate are the wrist-based heart rate monitors during walking and running activities? Are they accurate enough?" *BMJ open sport & exercise medicine*, vol. 2, no. 1, e000106, 2016.

[111] A. Shcherbina, C. M. Mattsson, D. Waggott, H. Salisbury, J. W. Christle, T. Hastie, M. T. Wheeler, and E. A. Ashley, "Accuracy in wrist-worn, sensor-based measurements of heart rate and energy expenditure in a diverse cohort," *Journal of personalized medicine*, vol. 7, no. 2, p. 3, 2017.

[112] F. Pedregosa, G. Varoquaux, A. Gramfort, V. Michel, B. Thirion, O. Grisel, M. Blondel, P. Prettenhofer, R. Weiss, V. Dubourg, J. Vanderplas, A. Passos, D. Cournapeau, M. Brucher, M. Perrot, and E. Duchesnay, "Scikit-learn: Machine Learning in Python," *Journal of Machine Learning Research*, vol. 12, pp. 2825–2830, 2011.

[113] P. Probst and A. L. Boulesteix, "To tune or not to tune the number of trees in random forest," *Journal of Machine Learning Research*, vol. 18, pp. 1–8, 2018, ISSN: 15337928. arXiv: 1705.05654.

[114] S. Zhang, X. Li, M. Zong, X. Zhu, and D. Cheng, "Learning k for knn classification," *ACM Transactions on Intelligent Systems and Technology (TIST)*, vol. 8, no. 3, pp. 1–19, 2017.

[115] L. Breiman, J. Friedman, C. J. Stone, and R. A. Olshen, *Classification and Regression Trees*, ser. The Wadsworth and Brooks-Cole statistics-probability series. Taylor & Francis, 1984, ISBN: 9780412048418.

[116] D. Morawiec, *Sklearn-Porter: Transpile trained scikit-learn estimators to C, Java, JavaScript and others*. [Online]. Available: https://github.com/nok/sklearn-porter (visited on 04/02/2019).

[117] Y. Wu, S. Qi, F. Hu, S. Ma, W. Mao, and W. Li, "Recognizing activities of the elderly using wearable sensors: a comparison of ensemble algorithms based on boosting," *Sensor Review*, vol. 39, no. 6, pp. 743–751, Nov. 2019, ISSN: 02602288. DOI: 10.1108/SR-11-2018-0309.

[118] G. Bhat, Y. Tuncel, S. An, H. G. Lee, and U. Y. Ogras, "An Ultra-Low Energy Human Activity Recognition Accelerator for Wearable Health Applications," *ACM Trans. Embed. Comput. Syst.*, vol. 18, no. 5s, 49:1–49:22, Oct. 2019, ISSN: 1539-9087. DOI: 10.1145/3358175.

[119] D. C. Bellido and D. C. Bellido, "Teoría y práctica del entrenamiento deportivo," *Universidad Politecnica de Madrid*, 2006.

[120] T. O. Bompa and C. Buzzichelli, *Periodization: theory and methodology of training*. Human kinetics, 2018.

[121] J. Crossley, *Personal Training: Theory and Practice*. Routledge, 2013.

[122] V. Leonov, "Thermoelectric energy harvesting of human body heat for wearable sensors," *IEEE Sensors Journal*, vol. 13, no. 6, pp. 2284–2291, 2013, ISSN: 1530437X. DOI: 10.1109/JSEN.2013.2252526.

[123] S. Seneviratne, Y. Hu, T. Nguyen, G. Lan, S. Khalifa, K. Thilakarathna, M. Hassan, and A. Seneviratne, *A Survey of Wearable Devices and Challenges*, 2017. DOI: 10.1109/COMST.2017.2731979.

[124] J. Hayward, *Wearable Technology 2018-2028: Markets, Players, Forecasts: IDTechEx*, 2018. [Online]. Available: https://www.idtechex.com/research/reports/wearable-technology-2018-2028-markets-players-forecasts-000606.asp?viewopt=showall (visited on 10/11/2018).

[125] K. Tai and A.-R. El-Sayed, "A Survey on Recent Energy Harvesting Mechanisms," in *IEEE Canadian Conference on Electrical and Computer Engineering (CCECE)*, 2015, ISBN: 9781479979936.

[126] M.-l. Ku, W. Li, Y. Chen, and K. J. R. Liu, "Advances in Energy Harvesting Communications : Past , Present , and Future Challenges," *IEEE Communications Surveys & Tutorials*, vol. 18, no. 2, pp. 1384–1412, 2016. DOI: 10.1109/COMST.2015.2497324.

[127] P. D. Mitcheson, E. M. Yeatman, G. K. Rao, A. S. Holmes, and T. C. Green, "Energy harvesting from human and machine motion for wireless electronic devices," *Proceedings of the IEEE*, vol. 96, no. 9, pp. 1457–1486, 2008, ISSN: 00189219. DOI: 10.1109/JPROC.2008.927494.

[128] M. Hayakawa, *Electronic wristwatch with generator*, US Patent 5,001,685, Mar. 1991.

[129] A. Zurbuchen, A. Haeberlin, L. Bereuter, A. Pfenniger, S. Bosshard, M. Kernen, P. Philipp Heinisch, J. Fuhrer, and R. Vogel, "Endocardial energy harvesting by electromagnetic induction," *IEEE Transactions on Biomedical Engineering*, vol. 65, no. 2, pp. 424–430, 2018.

[130] L. Spadaro, M. Magno, and L. Benini, "KinetiSee - A Perpetual Wearable Camera Acquisition System with a Kinetic Harvester," *2016 15th ACM/IEEE International Conference on Information Processing in Sensor Networks, IPSN 2016 - Proceedings*, 2016. DOI: 10.1109/IPSN.2016.7460706.

[131] H. Yu, J. Zhou, and W. Wang, "A new hybrid piezoelectric-electromagnetic micro

vibration energy harvester," *2014 IEEE International Conference on Electron Devices and Solid-State Circuits, EDSSC 2014*, pp. 5–6, 2014. DOI: 10.1109/EDSSC.2014.7061103.

[132] T. J. Kázmierski and S. Beeby, *Energy harvesting systems: Principles, modeling and applications*. New York, NY, USA: Springer, 2011, ISBN: 9781441975652. DOI: 10.1007/978-1-4419-7566-9.

[133] S. Beeby and N. White, *Energy Harvesting for Autonomous Systems*. Norwood, USA: Artech house, 2010, ISBN: 159693719X.

[134] D. Guyomar and M. Lallart, "Recent progress in piezoelectric conversion and energy harvesting using nonlinear electronic interfaces and issues in small scale implementation," *Micromachines*, vol. 2, no. 2, pp. 274–294, 2011, ISSN: 2072666X. DOI: 10.3390/mi2020274.

[135] S. Priya, "Advances in energy harvesting using low profile piezoelectric transducers," *Journal of Electroceramics*, vol. 19, no. 1, pp. 165–182, 2007, ISSN: 13853449. DOI: 10.1007/s10832-007-9043-4.

[136] P. A. Laura, J. L. Pombo, and E. A. Susemihl, "A note on the vibrations of a clamped-free beam with a mass at the free end," *Journal of Sound and Vibration*, 1974, ISSN: 10958568. DOI: 10.1016/S0022-460X(74)80325-1.

[137] F. Mokhtari, G. M. Spinks, C. Fay, Z. Cheng, R. Raad, J. Xi, and J. Foroughi, "Wearable Electronic Textiles from Nanostructured Piezoelectric Fibers," *Advanced Materials Technologies*, vol. 1900900, pp. 1–15, 2020, ISSN: 2365709X. DOI: 10.1002/admt.201900900.

[138] R. Meier, N. Kelly, O. Almog, and P. Chiang, "A piezoelectric energy-harvesting shoe system for podiatric sensing," *2014 36th Annual International Conference of the IEEE Engineering in Medicine and Biology Society, EMBC 2014*, pp. 622–625, 2014, ISSN: 1557170X. DOI: 10.1109/EMBC.2014.6943668.

[139] H. Kalantarian and M. Sarrafzadeh, "Pedometers without batteries: An energy harvesting shoe," *IEEE Sensors Journal*, vol. 16, no. 23, pp. 8314–8321, 2016, ISSN: 1530437X. DOI: 10.1109/JSEN.2016.2591331.

[140] D. Ma, G. Lan, W. Xu, M. Hassan, and W. Hu, "SEHS: Simultaneous energy harvesting and sensing using piezoelectric energy harvester," *Proceedings - ACM/IEEE International Conference on Internet of Things Design and Implementation, IoTDI 2018*, pp. 201–212, 2018. DOI: 10.1109/IoTDI.2018.00028.

[141] G. De Pasquale and A. Soma, "Energy harvesting from human motion with piezo fibers for the body monitoring by MEMS sensors," *2013 Symposium on Design, Test, Integration and Packaging of Mems/Moems*, no. April, pp. 1–6, 2013.

[142] Y. Bai, P. Tofel, Z. Hadas, J. Smilek, P. Losak, P. Skarvada, and R. Macku, "Investigation of a cantilever structured piezoelectric energy harvester used for wearable devices with random vibration input," *Mechanical Systems and Signal Processing*, vol. 106, pp. 303–318, 2018, ISSN: 10961216. DOI: 10.1016/j.ymssp.2018.01.006.

[143] O. Méndez-Lira, E. Sifuentes, and R. González-Landaeta, "Energy Harvesting from Fingers Motions Using a Wearable System: An Experimental Analysis," *IFMBE Proceedings*, vol. 75, pp. 866–873, 2020, ISSN: 14339277. DOI: 10.1007/978-3-030-30648-9_113.

[144] H. Kalantarian, N. Alshurafa, T. Le, and M. Sarrafzadeh, "Monitoring eating habits using a piezoelectric sensor-based necklace," *Computers in Biology and Medicine*, vol. 58, pp. 46–55, 2015, ISSN: 0010-4825. DOI: 10.1016/j.compbiomed.2015.01.005.

[145] H. Kalantarian, B. Mortazavi, N. Alshurafa, C. Sideris, T. Le, and M. Sarrafzadeh, "A comparison of piezoelectric-based inertial sensing and audio-based detection of swallows," *Obesity Medicine*, vol. 1, pp. 6–14, 2016, ISSN: 24518476. DOI: 10.1016/j.obmed.2016.01.003.

[146] P. Fang, Q. Zhuo, Y. Cai, L. Tian, H. Zhang, Y. Zheng, G. Li, L. Wu, and X. Zhang, "Piezoelectrets and their applications as wearable physiological-signal sensors and energy harvesters," *2015 IEEE 12th International Conference on Wearable and Implantable Body Sensor Networks, BSN 2015*, 2015, ISSN: 2376-8886. DOI: 10.1109/BSN.2015.7299373.

[147] S. Khalifa, G. Lan, M. Hassan, A. Seneviratne, and S. Das, "HARKE: Human Activity Recognition from Kinetic Energy Harvesting Data in Wearable Devices," *IEEE Transactions on Mobile Computing*, vol. 1233, no. c, pp. 1353–1368, 2017, ISSN: 15361233. DOI: 10.1109/TMC.2017.2761744.

[148] G. Lan, W. Xu, D. Ma, S. Khalifa, M. Hassan, and W. Hu, "EnTrans: Leveraging Kinetic Energy Harvesting Signal for Transportation Mode Detection," *IEEE Transactions on Intelligent Transportation Systems*, pp. 1–12, 2019, ISSN: 1524-9050. DOI: 10.1109/tits.2019.2918642. arXiv: 1807.02268.

[149] W. Xu, G. Lan, Q. Lin, S. Khalifa, M. Hassan, N. Bergmann, and W. Hu, "KEH-Gait: Using Kinetic Energy Harvesting for Gait-based User Authentication Systems," *IEEE Transactions on Mobile Computing*, vol. 1233, no. c, pp. 1–15, 2018, ISSN: 15361233. DOI: 10.1109/TMC.2018.2828816.

[150] Q. Lin, W. Xu, G. Lan, Y. Cui, H. Jia, W. Hu, M. Hassan, and A. Seneviratne, "KEHKey: Kinetic Energy Harvester-Based Authentication and Key Generation for Body Area Network," *Proc. ACM Interact. Mob. Wearable Ubiquitous Technol.*, vol. 4, no. 1, 2020. DOI: 10.1145/3381754.

[151] L. Xiao and K. Wu, "Activity Recognition Based on Kinetic Energy Harvester and Accelerometer," *2018 IEEE International Conference on Communications (ICC)*, pp. 1–6, 2018, ISSN: 15503607. DOI: 10.1109/ICC.2018.8422998.

[152] Midé, *PPA Products Datasheet and User Manual*, 2016.

[153] Microchip Technology Inc., "MCP73831/2 Datasheet," Tech. Rep., 2014, p. 28.

[154] C. Gomez, J. Oller, and J. Paradells, "Overview and Evaluation of Bluetooth Low Energy: An Emerging Low-Power Wireless Technology," *Sensors*, vol. 12, no. 9, pp. 11 734–11 753, Aug. 2012, ISSN: 1424-8220. DOI: 10.3390/s120911734.

[155] Toshiba Corporation, "Trends in and Future Outlook for Semiconductor Devices with Enhanced Energy Efficiency," Tech. Rep., 2018, p. 9. [Online]. Available: https://toshiba.semicon-storage.com/content/dam/toshiba-ss/shared/docs/company/technical-review/technical-review-1%7B%5C_%7De.pdf.

[156] J. Manjarres and M. Pardo, "An Energy Logger for Kinetic-Powered Wrist-Wearable Systems," *Electronics*, vol. 9, no. 3, p. 487, Mar. 2020, ISSN: 2079-9292. DOI: 10.3390/electronics9030487.

[157] L. Peng, L. Chen, Z. Ye, and Y. Zhang, "AROMA: A Deep Multi-Task Learning Based Simple and Complex Human Activity Recognition Method Using Wearable Sensors," *Proceedings of the ACM on Interactive, Mobile, Wearable and Ubiquitous Technologies*, vol. 2, no. 2, pp. 1–16, 2018, ISSN: 2474-9567. DOI: 10.1145/3214277.

[158] A. Mannini and S. Intille, "Classifier Personalization for Activity Recognition using Wrist Accelerometers," *IEEE Journal of Biomedical and Health Informatics*, vol. PP, no. c, pp. 1–1, 2018, ISSN: 2168-2194. DOI: 10.1109/JBHI.2018.2869779.

[159] J. Yosinski, J. Clune, Y. Bengio, and H. Lipson, "How transferable are features in deep neural networks?" *Advances in Neural Information Processing Systems*, vol. 4, no. January, pp. 3320–3328, 2014, ISSN: 10495258. arXiv: 1411.1792. [Online]. Available: http://arxiv.org/abs/1411.1792.

[160] G. Lan, W. Xu, S. Khalifa, M. Hassan, and W. Hu, "Transportation Mode Detection Using Kinetic Energy Harvesting Wearables," *2016 IEEE International Conference on Pervasive Computing and Communications*, pp. 1–4, 2016. DOI: 10.1109/PERCOMW.2016.7457048.

[161] A. L. Guennec, S. Malinowski, and R. Tavenard, "Data Augmentation for Time Series Classification using Convolutional Neural Networks," *ECML/PKDD Workshop on Advanced Analytics and Learning on Temporal Data*, 2016.

[162] D. P. Kingma and J. Ba, "Adam: A Method for Stochastic Optimization," Dec. 2014. arXiv: 1412.6980. [Online]. Available: http://arxiv.org/abs/1412.6980.

[163] N. Chinchor and B. Sundheim, "MUC-5 evaluation metrics," Association for Computational Linguistics (ACL), 1993, p. 69. DOI: 10.3115/1072017.1072026.

[164] S. Salvador and P. Chan, "Toward accurate dynamic time warping in linear time and space," *Intelligent Data Analysis*, 2007, ISSN: 1088467X. DOI: 10.3233/ida-2007-11508.